URBAN CELLULAR WIRELESS NETWORK PLANNING WITH 3D GEOGRAPHICAL GRID STRUCTURES

by
Murat Özyurt
B.S, in Computer Engineering, Boğaziçi University, 2005
M.S, in Software Engineering, Boğaziçi University, 2008

Submitted to the Institute for Graduate Studies in
Science and Engineering in partial fulfillment of
the requirements for the degree of
Doctor of Philosophy

Graduate Program in PhD, in Computer Engineering
Boğaziçi University
2019

ACKNOWLEDGEMENTS

First of all, I would like to thank my thesis supervisor Prof. Tuna Tuğcu for his tremendous supports since 2005. This thesis would absolutely be impossible without his dedicated guidance.

I would definitely like to express my gratitude to Prof. Haluk O. Bingöl, and Assoc. Prof. Ali Emre Pusane for taking part in my thesis progress and defense juries, and for their eye-opening contributions during the thesis progress sessions. I would also like to deeply thank Assist. Prof. B. Atay Özgövde, and Assist. Prof. Ece Gelal Soyak for their contributions and for taking part in my thesis defense jury.

I would specially like to thank Assist. Prof. H. Birkan Yılmaz for his extreme guidance, and Seçkin Uluğ for his assistance.

I would also like to thank all past and present CmpE faculty members, all fellow researchers in the CmpE research laboratories, especially NETLAB, as well as the administrative and technical staff of both CmpE and Boğaziçi University for their support.

Thank you Mom and Dad for everything. Thank you my dear wife Dilek, and my dear kids Faruk, Feyza, Vera for shining into my life.

The research in this thesis has been partially supported by the Scientific and Technical Research Council of Turkey (TUBITAK) under grant number 108E101, and by the Turkish Directorate of Strategy and Budget under the TAM Project number DPT2007K120610. The author would also like to thank Telenity Inc. for partially funding the research on base station placement and providing the actual measurements and 3D maps.

ABSTRACT

URBAN CELLULAR WIRELESS NETWORK PLANNING WITH 3D GEOGRAPHICAL GRID STRUCTURES

The largest traffic on the Internet is generated by multimedia content, and the share of wireless mobile access to the multimedia content is ever increasing. The delivery process in the content depends on the type of the content, and whether it requires a strictly time sensitive live session, or it can be delivered on demand, irrespective of time of request. As a general solution in the IP networks, the delivery is taking place as multiple individual transmissions from the source to all receivers, replicating the same content at different times, or at the same time if the content is streaming live.

In this thesis, we propose an advanced collaborative multicast routing model for delivering bandwidth hungry streaming content such as IPTV to multiple users having low quality wireless connection, with the help of other nearby users having a better connection quality utilizing the wireless mesh network topology. The model reduces the amount of data replication, which causes significant overhead in the network transmissions and intermediate computations, improving the overall throughput of the wireless network. An essential issue in wireless mobile networks is where to position the base stations on the network coverage area. We also propose an alternative adaptive mixed path signal propagation estimation model for planning the base station locations in new deployment areas, based on the signal characteristics of existing networks. In doing so, we utilize digital 3D maps of urban areas and signal measurements to train the adaptive model, and to exploit local similarities in cities in order to estimate the signal channel characteristics and calculate the potential base station locations for covering the new area with a specific wireless communication technology.

ÖZET

ÜÇ BOYUTLU ŞEHİR HARİTALARI İLE KABLOSUZ HÜCRESEL AĞ PLANLAMA

İnternet trafiğinin en büyük kısmı çoklu ortam içerikleri tarafından üretilmekte ve kablosuz mobil ağlar üzerinden bu içeriğe erişim oranı günden güne artmaktadır. İçeriğin kullanıcıya ulaştırılmasında kullanılan yöntem içeriğin türüne ve gecikmeye duyarlı olarak gerçek zamanlı iletilmesine bağlıdır. Genel olarak IP ağlarında içerik kullanıcılara ayrı kopyalar olarak gönderilir. İçerik kopyaları, canlı yayın gibi gerçek zamanlı trafikte aynı anda, isteğe bağlı videoda ise farklı zamanlarda çoğaltılmaktadır.

Bu tezde baz istasyonuna düşük kaliteli bağlantısı olan kullanıcıların, kendisine yakın ve bağlantı kalitesi daha iyi olan diğer kullanıcıların yardımıyla IPTV gibi yüksek hızda gerçek zamanlı iletim gerektiren yayınları alabilmesi için kablosuz örgü topolojili ağlarda ileri düzey işbirliğine dayalı çoklu dağıtım ve yönlendirme modeli önerilmektedir. Söz konusu model, ağ kapasitesi ve iletim sistemi bilgisayarlarında ciddi bir aşırı yüke neden olan veri kopyalarının sayısını önemli oranda azaltmakta olup, bütünsel olarak kablosuz ağın verimini artırmaktadır. Kablosuz ağlarda bir diğer önemli konu da baz istasyonlarının nerelere konumlandırılacağıdır. Farklı şehirlerde mimari olarak birbirine benzerlik gösteren yerel bölgeler bulunmaktadır ve benzer yapılar sinyal yayılımı üzerinde benzer etki göstermektedir. Bu tezde ayrıca üç boyutlu şehir haritalarındaki yerel benzerliklerden ve mevcut ağ kurulumlarının sinyal ölçümlerinden yararlanılarak yeni alanlarda sinyal yayılım biçimlerini hesaplayıp baz istasyonlarının etkin şekilde yerleştirilmesini sağlayan bir çoklu yol sinyal yayılım modeli önerilmektedir.

TABLE OF CONTENTS

LIST OF FIGURES

LIST OF TABLES

LIST OF SYMBOLS

b	Base station
b_i	Base station i
B	The set of base stations
C_0	Center coordinate of a coverage area
C_i	Coordinate i
$C_{(t,n)}$	Center coordinate of tile $T_{(t,n)}$
d_i	Distance of measurement i to the corresponding base station
$d_{(b,m)}$	Distance from base station b to measurement m
G_s	Grid tile size
ℓ_2	Euclidean norm of normalized descriptor parameter vectors
m	Measurement
m_i	Measurement i
$m_{(T,b,i)}$	i^{th} measurement of base station b, located in tile T
MSS_i	Mesh subscriber station i
P_{L_0}	Path-loss at reference distance for Log-Distance propagation model
$P_{Rx,i}$	Received signal power level of a measurement i
P_{Tx}	Transmit power of a base station
R	The radius of Earth
SS_i	Subscriber station i
$T_{(0,0)}$	Center tile
$T_{(t,n)}$	Tile on a grid, having latitudinal neighboring index t and longitudinal neighboring index n with respect to the center tile $T_{(0,0)}$
$\mathbb{T}_D$	Deployment area tiles
$\mathbb{T}_T$	Training area tiles
$V_{(t,n)}$	Descriptor vector of tile $T_{(t,n)}$
v_i	A real number between 0 and 1, a descriptor value in $V_{(t,n)}$

$\Delta\lambda$	East-west longitude span of a center tile $T_{(0,0)}$
$\Delta\varphi$	North-south latitude span of a center tile $T_{(0,0)}$
γ	Path-loss exponent of Log-Distance propagation model
λ_i	Longitude value of a C_i in decimal degrees
φ_i	Latitude value of a C_i in decimal degrees
$\Omega_{(T,b,m)}$	The path between a measurement point m in tile T and base station b
$\omega_{(T,T_i,b,m)}$	The path segment of $\Omega_{(T,b,m)}$ on an intermediate tile T_i

LIST OF ACRONYMS/ABBREVIATIONS

2D	Two Dimensional
3D	Three Dimensional
3GPP	The 3rd Generation Partnership Project
ACM	Adaptive Coding and Modulation
AFR	ARQ Feedback Request
APSK	Amplitude Phase Shift Keying
BE	Best Effort
BER	Bit Error Rate
BPSK	Binary Phase Shift Keying
BS	Base Station
CA	Cumulative ACK
CAPEX	Capital Expenditures
CBR	Constant Bit Rate
CBT	Core Based Tree
CGI	Computer Generated Imagery
CID	Connection Identifier
COST	European Cooperation in Science and Technology
CR	Coding Rate
DCD	Downlink Channel Description
DL-MAP	Downlink MAP Message
DL-MAP IE	Downlink MAP Message Information Element
DRM	Digital Rights Management
DSL	Digital Subscriber Line
EM	Electromagnetic
ertPS	extended real-time Polling Service
FDD	Frequency Division Duplexing
HD	High Definition
HDTV	High Definition Television

HSDPA	High-Speed Downlink Packet Access
IEEE	Institute of Electrical and Electronics Engineers
IP	Internet Protocol
IPTV	Internet Protocol Television
ITU	International Telecommunication Union
LoS	Line of Sight
LTE	Long Term Evolution
MAC Layer	Medium Access Control Layer
MAPLE	Mixed pAth-inspired Path Loss Estimation model
MBS	Mesh Base Station
MCS	Modulation And Coding Scheme
MDC	Multiple Description Coding
MIMO	Multiple Input Multiple Output
MPEG	Moving Picture Experts Group
MSS	Mesh Subscriber Station
NACK	Negative Acknowledgement
nLoS	non-Line of Sight
NMSE	Normalized Mean Squared Error
nrtPS	non real-time Polling Service
OFDMA	Orthogonal Frequency Division Multiple Access
OPEX	Operational Expenditures
OPNET	Optimized Network Engineering Tools
PHY Layer	Physical Layer
PMP	Point to Multipoint
QAM	Quadrature Amplitude Modulation
QoS	Quality of Service
QPSK	Quadrature Phase Shift Keying
RMSE	Root Mean Squared Error
rtPS	real-time Polling Service
RS	Relay Station
SCM	Superposition Coded Multicasting

SD	Standard Definition
SDTV	Standard Definition Television
SINR	Signal to Interference Noise Ratio
SISO	Single Input Single Output
SNR	Signal to Noise Ratio
SS	Subscriber Station
TDD	Time Division Duplexing
UCD	Uplink Channel Description
UGS	Unsolicited Grant Service
UL-MAP	Uplink MAP Message
UL-MAP IE	Uplink MAP Message Information Element
VBR	Variable Bit Rate
Wi-Fi	The Standard for Wireless Fidelity
WiMAX	Worldwide Interoperability for Microwave Access
WISDoM	Wireless IPTV Service Distribution over Mesh Mode
WISDoM-Hybrid	Wireless IPTV Service Distribution over Mesh Mode Hybrid
WISDoM-SD	Wireless IPTV Service Distribution over Mesh Mode benefiting from Space Diversity
WLAN	Wireless Local Area Network
WMAN	Wireless Metropolitan Area Network
VoD	Video on Demand
VoIP	Voice over IP
WPAN	Wireless Personal Area Network

1. INTRODUCTION

Wireless networks provide ubiquitous access to all kinds of information, including the bandwidth-hungry multimedia content. The content can be delivered either as an individual point-to-point transmission or as a multicast transmission. The former method can provide time independent access to the content or parts of the content like a video-on-demand (VoD) service, while the latter method can save bandwidth and intermediate processing by synchronizing recipients on an ongoing stream of the content similar to a live broadcast session [1–3].

In the conventional wired end-to-end network systems, data can be transferred over the physically linked infrastructure devices such as routers and switches. The penetration of transmission is limited by the range of the wired devices. The congestion rate due to large content delivery over the network can be lowered down to a limited extent even when a multicast delivery is in session, since the content has to be replicated multiple times [4, 5] by the intermediate network components to be distributed over the widely used star topology [6]. Using super fast fiber connections helps reduce the latency during the transmission, however, the replication process is still a major bottleneck problem, which can only be solved by scaling up the processing power by using multiple computing devices within the network.

The delivery of multimedia content over a wireless network can eliminate the data replication process partially in a multicast service, where a data packet can be received by an unlimited number of recipients without the need for replication. In doing so, other problems arise in the process, such as the capacity of available bandwidth, or the range of wireless signals. Although the capacity is ever increasing with the use of modern modulation and transmission techniques as well as new antenna technologies, the range problem is growing bigger as high frequency bands used by the modern communication systems are by far more sensitive to distance and obstacles on the course of wireless transmission [7].

The idea of using a single base station (BS) to cover a specific area is analogous to the radio and television broadcasting systems. Considering the variety of digital services and accessibility concerns, a single BS becomes insufficient for increasing the number of mobile devices, which happen to be wandering around and between the coverage areas of different localized base stations. In order a single BS to cover a larger service area, both that BS and the mobile device have to operate with high transmission power, where the latter has to use a limited battery. On the other hand, there will be many small blind-spots where communication is not possible due to the attenuation of signals that cannot penetrate so many obstacles in between the mobile device and the BS, as can be seen in Figure 1.1.

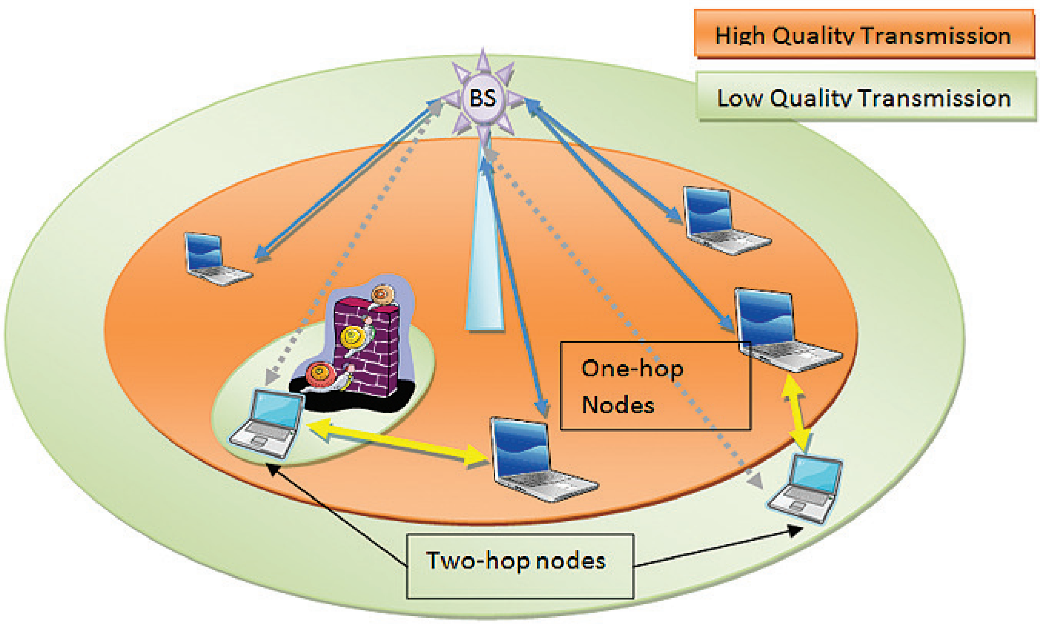

Figure 1.1. Sample WiMAX cell structure where multiple devices are connected to the base station and each other with different connection qualities.

No matter what technology is being used in a BS antenna, the overall throughput of the wireless mobile networks can be increased by using spatial diversity, i.e. increasing the number of antennas to form cells of the wireless networks. The cell formation requires a decreased transmission power per BS in order to reduce the range of transmission and eliminate the interference with other base stations in the network, where all base stations have to operate in a dedicated part of the wireless frequency spectrum. Besides, advanced modulation techniques perform better in the short range transmission, compared to the long range [7].

Using multiple base stations has other complications in terms of complexity, maintenance and cost. There has been advancements in wireless networks to extend the range of a transmission by using repeaters or relays, which are simpler wireless network components compared to the base stations. The purpose of a relay node is to re-transmit a wireless signal received from the base station (or another relay) towards an extension of the base station coverage area, by enhancing the power, modulation, or both. The positions of the relays can be adjusted to cover a relatively more crowded area such as a suburb, rather than a rural area where the expected of mobile device density is by far less than the suburbs.

Wireless networks with relay capability are also identified as wireless mesh networks, which can also be seen in Figure 1.1. The *Worldwide Interoperability for Microwave Access (WiMAX, IEEE 802.16)* [8, 9], and its updated versions, have been promising alternatives to Wi-Fi in a longer communication range. WiMAX also provides mesh access where a relay node can operate both in the infrastructure mode and the ad hoc mode simultaneously unlike the conventional Wi-Fi systems. WiMAX can be used to transmit *Voice-over-IP (VoIP)* teleconference session and *Internet Protocol Television (IPTV)* multicast services, using mobile devices capable of operating in mesh mode as relay nodes, with insignificant amount of overhead to the relay node. Being a relay comes with a variable cost to be compensated by the operator, so that users could opt to become relay nodes if their communication capacity is high enough to provide service to other users nearby, increasing the overall subscriber satisfaction.

Mesh networks can also be used as a supplementary extension for emerging satellite internet subscription services, where the possibility of successful communication with the satellites at any location indoors is low, and mesh network relay nodes can act as the intermediary solution to indoor coverage problem of such networks. Multi-hop mesh networks can also be useful for environmental monitoring systems, border security, and emergency broadcasting services.

In the first part of this thesis we have conducted the research *Utilizing WiMAX Mesh Mode For Efficient IPTV Transmission* [10], where we analyzed the capacity of the mesh network for multimedia transmission for parallel multimedia content distribution, with our own scheduler simulation application. We have extended our research further as published in the article entitled *WISDoM-SD: Wireless IPTV Service Distribution Over Mesh Mode Via Space Diversity* [11], where our technique has been thoroughly tested on the OPNET Modeler. Both studies conclude that the proposed multicasting solution over a mesh network is viable for applications requiring high bandwidth, with two-hop relaying. On the other hand, relaying more than two hops is impractical for such data demanding applications, as also shown in [12].

The second part of this thesis focuses on a more general problem in cellular communications with or without a mesh support, such as WiMAX, 3G, 4G, 5G, or beyond 5G, where the base stations should be deployed. Especially in urban deployment areas, the locations of the base stations play a crucial role in providing the highest quality-of-service (QoS) possible, so that the individual data demanding applications such as the VoD content delivery can also be served with minimum resource consumption.

Cellular network planning has many challenges including physical and legal constraints. Deployment of a single base station requires permission from land owners, leasing data links, installing auxiliary power and processing units as well as BS towers or wall mounts in various heights. Each base station has operational expenditures (OPEX) such as maintenance, rent, upgrade, personnel costs, insurance, fuel, etc., as well as the initial capital expenditures (CAPEX) like equipment costs, installation costs, etc. Therefore, mobile network operators are continuously searching for new ways to minimize the number of BS installations to an optimum amount where the network can sustain the best QoS for customer satisfaction. For that purpose, deployment plans are built on preliminary calculations on the estimated signal behavior of potential base station locations and respective transmission power levels.

In addition to the natural attenuation of electromagnetic (EM) signals, the environmental conditions such as obstacles, precipitation, humidity, temperature, water areas, or green space affect the signal power negatively on different amounts. EM signals emitted from the source will travel in omni directional paths, similar to a light bulb, unless special directional antennas are used. The coverage area of a BS is theoretically circular in shape, however, attenuation factors in urban areas prevent such circular cells in real life. Moreover, reflection, scattering, diffraction, and refraction due to the complex materials in an urban area cause the EM signals to travel in non-linear paths, which either results in blind-spots in the cells, or weak extrusions to the expected round cell boundaries. All such complex irregularities in the signal channel have been the most challenging problems in wireless network planning.

Planning wireless mobile networks for newer technologies is also getting more and more complicated as the cell sizes shrink in order to fulfill the increasing demand for data rate. It is essential for the operators to have prior knowledge on channel characteristics before the deployment in order to run pre-deployment simulations. However, no such information can be obtained precisely before the network is up and running. As there are indefinitely many possibilities for locating a BS, planning teams prioritize certain areas to be covered with higher QoS, depending on user density and capacity demand. Cell sizes are adjusted in accordance to such user segmentation.

Determining the coverage area of a cell, where the mobile devices can maintain healthy communication with the BS, requires trajectory calculations from and to the potential location of the BS. One of the common ideas for estimating the signal trajectory is ray-tracing [13–15], which in theory aims to calculate each and every possible attenuation effect of reflection, diffraction, penetration, etc., in all directions. It is clearly impossible to calculate the infinitely many alternatives that need to be considered when using the ray-tracing algorithms. However, some approximations of ray-tracing are very useful in determining the average signal behavior especially in indoor signal propagation, [13].

On the other hand, ray-tracing requires exact 3D models of the environment, including the material characteristics that reflect or allow the signal pass through at various levels, to achieve a realistic result. In addition to the precise static 3D models of the network area including the finest details like sharp corners, vegetation, water bodies, construction properties (e.g. metal/glass/concrete surfaces, roughness of the surfaces) that may cause reflection, absorption, scattering of signals, and so on [16,17], it is also important to gain knowledge on motion models in the area involving vehicles and users. The unique architecture and geography of each city requires those models to be revised continuously to predict a better deployment plan, and it will be almost impossible to provide the complete input data set.

Unfortunately, for the current state of the technology, using ray tracing on real world objects for signal propagation modeling is not a practical approach. The extreme complexity of ray-tracing has led the scientists to develop some generic mathematical, probabilistic, or empirical models that estimate the approximate received signal levels depending on certain parameters of the coverage area. The models such as *Two-Ray Ground-Reflection* [18], *Egli* [19], *Longley-Rice* [20], *ITU mixed path terrain loss* [21,22], *Young*, *Lee* [23], *Okumura radio propagation* [24], *Hata for multipath urban areas* [25], *COST-Hata/COST-231/Hata-PCS Extension* [26], and *Nakagami-m distribution* [27] have been widely used for planning cellular communications in large cities. These models mainly generate probabilistic results based on experiments and measurements. The urban characteristics like building density, building distribution, and height of the tall structures can be used as coefficients in a mathematical formulation or in a group of equations. Some of the models depend on reference signal measurements and others provide a set of equations based on physical properties in the area.

Generic models cannot estimate the actual effects of physical conditions on signals and do not result in accurate network plans. Optimization and redeployment processes are required after the deployment of the network components. Sample measurements can be taken in a deployment area by transmitting at multiple locations with nomadic base stations, which is a tedious, long, and costly process, and also subject to legal constraints. Furthermore, a long running measurement operation can compromise the confidentiality of a planning process, which has devastating effects before a spectrum auction.

Most of the previous work in the literature determine the channel parameters based on measurements in one city and use them for another. However, due to different architectures and terrain properties, no two cities are alike in terms of signal characteristics. There are local regions with distinct channel characteristics depending on the geographical and architectural structures like buildings, hills, lakes, rivers, parks, humidity, temperature, etc. Hence, some regions of a city may exhibit path loss similar to regions in other cities, while some do not. Local similarities can be exploited to utilize a simpler, cheaper, and more efficient mixed terrain path line-of-sight (LoS) propagation model to utilize vast amounts of existing network data for planning new mobile networks.

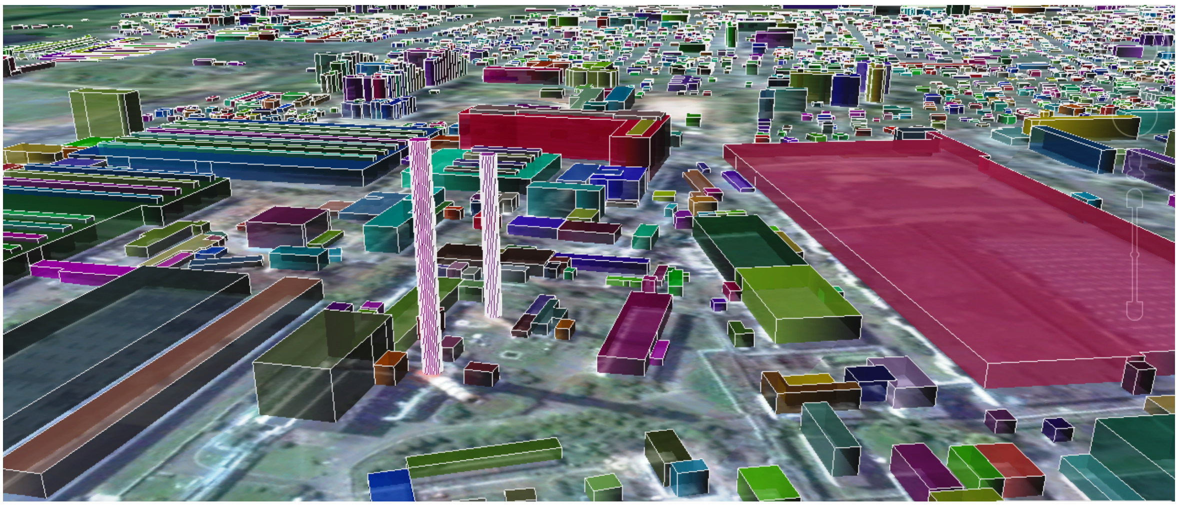

Figure 1.2. 3D city map data.

In the second part of the thesis, we have conducted a complementary research entitled *MAPLE: Mixed Path Calculation In Tile-Based 3D Maps* [28] which proposes a self-learning model for the propagation models, using signal measurements from existing mobile networks, and combining them with 3D structural map of the urban areas for determining similar areas (Figure 1.2). The model generates local regions in urban areas to estimate the signal propagation in other urban areas. Network coverage areas are divided into adjacent tiles of a geographical grid (Figure 1.3) including all 3D structures on the tiles. Each tile has a set of physical properties that are used to improve the precision of the signal propagation models locally and assign distinct propagation parameters to each tile.

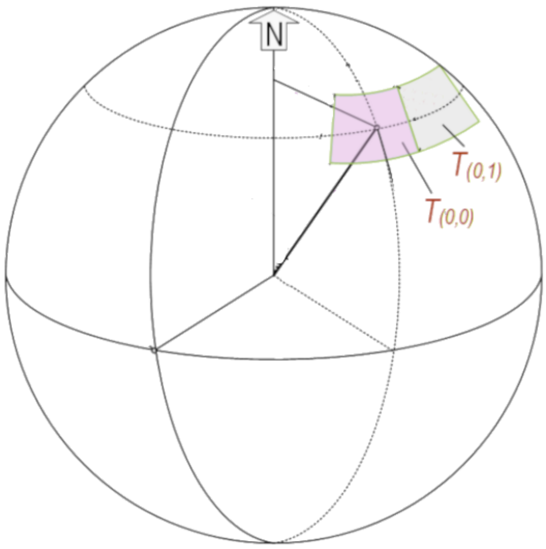

Figure 1.3. Tile positioning on the globe, showing the center tile $T_{(0,0)}$. Tiles are located on the globe with respect to their bounding latitude and longitude values.

The model can be trained with signal measurements and propagation characteristics of multiple areas having similar cellular network technologies. The similarities between physical properties of the tiles can then be used to find out potential signal propagation models of future deployment areas, and to plan the locations of base stations more effectively, reducing the planning efforts and optimization costs. The received power level at any signal measurement location is the result of a *mixed path* propagation [21, 22] penetrating tiles with different fading effects due to artificial or natural structures, vegetation, and water bodies between the measurement points and the corresponding base station locations.

MAPLE can be used as an alternative to existing propagation models, for planning base station locations to support high capacity bandwidth such as IPTV and VoD services in new deployment areas. As a practical approach, it is simpler, cheaper, and more efficient to utilize a mixed-path LoS propagation approximation model. It uses the vast amounts of already available actual measured signal data from training areas having similar wireless mobile network technology that will be deployed to the new areas.

1.1. Contribution of This Thesis

In this thesis we propose an alternative IPTV multicasting solution, *Wireless IPTV Service Distribution Over Mesh Mode Via Space Diversity (WISDoM-SD)* for obtaining more stable content distribution with less amounts of path delay fluctuations. WISDoM-SD provides an alternative parallel transmission model for distributing IPTV content on mesh networks with a more stable scheduling algorithm. To demonstrate its performance, we have developed a proof-of-concept implementation of WISDoM-SD on a simulator for the mesh mode of WiMAX (IEEE 802.16) [10, 11].

WISDoM-SD combines the multicasting option with mesh mode operation of WiMAX, utilizing a two-hop multicasting model with a single high capacity modulation at each hop, instead of a low capacity modulation in a single hop connection. The proposed model increases the efficiency of mesh mode further by using parallel transmissions at diverse locations, as we have also studied in [10] previously.

We also extend this model (independent of the mobile technology) for estimating base station locations in new deployment areas using 3D maps and actual signal measurements from existing networks. The proposed *Mixed pAth-inspired Path Loss Estimation (MAPLE)* model [28] improves the path loss estimation performance of the existing Log-Distance propagation model for new deployment areas [29]. The contributions of the proposed models can be summarized as follows:

- Providing IPTV service to users connected with poor signal quality to the base station, by relaying them over other users who have strong connectivity either to the BS, or to another relay node.

- Exploiting and improving the mesh mode relaying capability of the wireless network, by utilizing multicast service instead of bandwidth consuming point-to-point unicast architecture for IPTV streaming.
- Scheduling parallel transmissions over WiMAX relay nodes.
- Cell planning with 3D maps and existing signal measurements.
- Propagation model estimation for areas without network deployment.
- Coverage prioritization with respect to user density.

1.2. Organization of This Thesis

In the following parts of this thesis, we have briefly studied the background information and literature survey on WiMAX networks and IPTV for the WISDOM-SD model, followed by the results and outcomes of the proposed model in detail, in Chapter 2. In Chapter 3 we have introduced the details of the MAPLE model and the corresponding results following the background information and literature survey on wireless network planning and signal propagation models. The runtime performance of the algorithms has been presented in Section 3.4.3. In Chapter 4 we have provided our conclusions followed by the future work.

2. IPTV DISTRIBUTION IN WIRELESS MESH NETWORKS

Improvements in high capacity internet connection have enabled the availability of data intensive applications, such as IPTV to mass users [30, 31]. Commercial telecommunication companies have also been offering data packages that include unlimited multimedia access to certain web services. As an extension to the triple play services *(data, voice, video)*, operators have also included the *mobility* into triple play, to form the profitable quadruple play service package [31, 32].

Many wireless network technologies rely on point-to-point transmissions from a base station to multiple wireless users. The environmental effects of urban area obstacles on wireless signals cause local spots with poor connection quality. As an enhancement to network coverage, the mesh networks have been proposed to provide coverage to the users with poor connections, by relaying them over other nearby users with strong connections. The WiMAX technology (IEEE 802.16) [9] provides a realistic mesh network topology. The technical infrastructure of the alternative IEEE 802.16m is highly capable of providing multimedia content such as IPTV effectively [33]. This technology has been designed to be a wireless broadband alternative to fixed Digital Subscriber Line (DSL) services, where infrastructure investment for cabling may not be viable especially for suburban or rural areas [8, 34, 35].

As of IEEE 802.16d version of WiMAX, the wireless networks can operate in either of two modes. The first mode is named as *Point to Multipoint (PMP)* mode, where the *Subscriber Station (SS)* devices connect directly to the BS, as in IEEE 802.11 WLAN [36]. SS devices can either be mobile, or fixed (e.g. building access points), and the network scheduling is managed by the BS. The second mode is named as the *Mesh* mode, where the *Mesh Subscriber Station (MSS)* devices can additionally connect to other MSS devices in an ad hoc fashion, which can relay the network connection of the BS, in case the MSS cannot establish a high capacity wireless connection to the BS directly. This option can be exploited to provide data intensive services such as IPTV to MSS devices that have insufficient direct connection to the BS.

In many IPTV channels, the traffic can be multicast from the source to the receivers, instead of end-to-end unicast distribution of the same content being transmitted simultaneously, reducing a significant amount of overall network load [37–40]. Some users in a multicast group tuned to a specific IPTV channel may experience low quality transmission from the BS, although they reside in similar proximity to the BS as other users with high quality connection to the BS. The signal to noise ratio (SNR), which determines the transmission quality, is a highly variable factor especially in urban areas. In a single multicast group, some users may have to downgrade to a lower bit rate for a more robust modulation technique to receive transmission, which imposes additional complexity to wireless multicasting, such as having to duplicate the same traffic in multiple modulations with a trade-off of reduced network performance [32,37].

2.1. Background Information

Multiple approaches in application layer as well as the physical layer (PHY) exist in the literature to solve the channel quality diversity problem in multicast environments. As studied in [32,41], the application layer solution in *Multiple Description Coding (MDC)*, and the physical layer solution *Superposition Coded Multicasting (SCM)* can be merged in a single solution to solve the diversity problem efficiently [42, 43]. However, these solutions enforce the entire group of users in the multicast session to use the most robust modulation technique of the subscriber with lowest transmission quality, which in turn results in customer dissatisfaction for receiving Standard Definition TV (SDTV) streaming instead of the achievable High Definition TV (HDTV). Such approaches lack servicing of users that have no means of direct BS connection.

As studied in [44] and [45], retransmissions caused by multiuser transmission diversity can be avoided by a fraction. Also, the subscribers with no direct BS connection can be served by cooperation (i.e. relaying). These models assume high quality wireless links between the BS and all relay nodes, where any low quality link may degrade the overall throughput by imposing path delays which cannot be tolerated for IPTV streaming for longer periods of time, since it will require large buffers in intermediate nodes on the network. It can also be possible to utilize cooperation models between different multicast groups [44, 45], serving other IPTV channels along with the IPTV channel of the current multicast group, depending on the bandwidth conditions.

2.1.1. WiMAX

WiMAX technology has been implemented as a *Wireless Metropolitan Area Network (WMAN)* to provide long range wireless access, and it is a complementary solution to fixed line DSL. Both WiMAX and most DSL services are connection oriented. WiMAX is also a long range alternative to the Wi-Fi. However, Wi-Fi is a wireless alternative to the similarly contention based ethernet.

Due to the nature of microwaves, the initial WiMAX standard was planned to operate as a regular PMP solution in LoS environments, at frequencies between 10 GHz and 66 GHz. The WiMAX Forum was established in 2001 to manage the standardization of IEEE 802.16, and to handle the compliance of the technology for vendors all around the world. The initial range of transmission was planned to be 1.5 to 5 km, and the data rate was expected to be around 135 Mbps.

In urban areas, LoS connection can be achieved mostly on roof tops or high towers, where a nomadic user can rarely find the opportunity to establish such a connection. Therefore, the improved standard IEEE 802.16a has been introduced in 2003, with a new PHY payer to support non-line-of-sight (nLoS) connectivity and the support for mesh mode operation. On the other hand, it is more convenient to use the frequency range between 2 GHz and 11 GHz due to the diminishing effects of multipath fading in nLoS transmission, where the wireless signal has to penetrate obstacles on its path. The standard has been revised in 2004 with improved compatibility, as version IEEE 802.16d.

The standard was initially planned as a fixed line alternative, mostly for nomadic users. In 2005, IEEE 802.16e has been introduced to add mobility support to the existing standard, most commonly known as *Mobile WiMAX*. As the mobility constraints are more restrictive, the operating frequency range has been planned to be between 2 GHz and 6 GHz, and extra QoS improvements were introduced to support mobility.

Table 2.1. Bit rates for 4×4 MIMO, 2048 OFDMA, 20MHz bandwidth WiMAX.

Modulation	Coding Rate (CR)	Bit-rate (Mbps)
BPSK	1/2	33
QPSK	1/2	66
QPSK	3/4	100
16-QAM	1/2	133
16-QAM	3/4	199
64-QAM	2/3	266
64-QAM	3/4	299
64-QAM	5/6	332

The improvements IEEE 802.16j and IEEE 802.16h were released in 2009, providing support for multi-hop capable relaying and operating in license free frequency bands, respectively. In 2011 the IEEE 802.16m [46], release 2 of the mobile WiMAX has been approved, which introduces *Multiple Input Multiple Output (MIMO)* antenna support in PHY layer for enhanced data rates up to 100 Mbps for mobile, and up to 1 Gbps for nomadic services [47]. The simulations and results presented in this thesis are based on the data rates of this version of the standard given in Table 2.1, using 4×4 MIMO antenna array in OFDMA 2048 with 1728 subcarriers, and 20MHz bandwidth [48].

WiMAX transmissions take place in predefined units of time called frames. The frames contain specific units of data to negotiate the type of modulation, coding rate (CR), downlink and uplink channel structures, etc. The two operating modes of WiMAX are briefly explained in sections 2.1.1.1 and 2.1.1.2.

2.1.1.1. WiMAX PMP Operating Mode. Among the two operating modes of WiMAX, in the PMP mode of operation the network traffic scheduling is managed entirely by the BS. PMP mode contains five QoS classes, which can be ordered with respect to priority as:

- Unsolicited Grant Service (UGS): Allocates the Constant Bit Rate (CBR) to the SS whether it is used or not. (e.g. T1/E1 services)
- Extended Realtime Polling Service (ertPS): Allocates variable bandwidth with respect to utilization (e.g. VoIP services)
- Realtime Polling Service (rtPS): Allocates variable bit rate (VBR) to the subscriber (e.g. progressive video, or sound)
- Non Realtime Polling Service (nrtPS): Allocates the minimum bandwidth reserved
- Best Effort (BE): No bandwidth allocation is required. (e.g. non time critical systems)

The PMP mode supports two types of frames:

- Frequency Division Duplexing (FDD): The frames are constituted of downlink subframes originated from the BS and transmitted to the SS. The uplink subframes originated from the SS and transmitted to the BS are sent over a different frequency then the frequency of the downlink subframes. Downlink and uplink transmissions can take place simultaneously.
- Time Division Duplexing (TDD): The frames are constituted of both downlink and uplink subframes, both of which are transmitted over the same frequency at different time slots.

2.1.1.2. WiMAX Mesh Operating Mode. When the mesh mode is utilized, any MSS receiving service through another relay MSS is called a child node. Similarly the relay MSS is called the parent node. The path from the BS through parent nodes to the child nodes constitutes a centralized routing tree. All parent and child nodes may choose to establish additional ad hoc links other than the ones on the centralized tree, forming distributed links, if they are close enough to each other.

Depending on the link type between any two nodes operating in mesh mode, the transmission has to adhere to either of the two scheduling types, namely:

- Centralized Scheduling: The BS manages all the inter-node scheduling on the routing tree, similar to PMP mode.
- Distributed Scheduling: The nodes decide on the schedule, for the available slots left from the centralized scheduling.

Mesh mode supports only the TDD frame structure and the structure of the TDD frames are different than the TDD frame structure of the PMP mode. The frames contain two sub-frames, a control sub-frame and a data sub-frame. Both sub-frames contain units for centralized and distributed scheduling.

2.1.1.3. WiMAX Adaptive Performance. Depending on the wireless signal channel quality, the connection between BS and SS (or MSS), can be established using the highest capacity burst profile, or modulation and coding scheme (MCS) that is applicable. The channel quality depends on environmental conditions, distance, multipath fading, interference, and so on.

A WiMAX BS is capable of transmitting in multiple MCSs simultaneously. Depending on the data rate requirements, it is possible to downgrade user devices to lower capacity MCS even though they can use higher capacity MCS, in order to provide service to other users running applications that demand high priority QoS. This powerful procedure is called *MCS link adaptation* [49, 50], which is optional but not a part of the standard, and the implementation is left to the vendors and operators. The process is also known as adaptive coding and modulation (ACM) which is also used by mobile technologies such as HSDPA, LTE, other MIMO systems, and some of the IEEE 802.15x WPAN networks [51–55].

2.1.2. IPTV

In contrast to one way transmission in analog/digital TV broadcasting infrastructure, the IPTV offers two-way communication between the subscriber and the network operator. This enables the addition of VoD, VoIP, and multicast streaming over the IP network, at low costs. However, this functionality comes with an investment requirement both in wired and wireless infrastructures [31] as the demanded data rates are ever increasing with the improved quality of video and audio transfer during IPTV services. An SDTV session may require 1.5-to-4 Mbps of bandwidth when using H.264, or MPEG-2 compression algorithms. Similarly an HDTV would consume 6-to-19 Mbps of bandwidth with the same algorithms [56, 57].

Transmission of a single HDTV channel over IPTV requires at least 6Mbps of bandwidth. As can be seen in Table 2.1, up to five distinct HDTV channels can be supported in a single cell when using the robust BPSK with CR=1/2 MCS having a bit rate of 33 Mbps. According to the given MCSs, the total number of simultaneous HDTV channel transmissions can be more than 50 when using the 64-QAM with CR=5/6 MCS. It may also be possible to utilize the 256-QAM with CR=5/6 MCS having a capacity of 443 Mbps in very close proximity areas of the BS, to support more than 70 HDTV channels over the wireless infrastructure [58].

2.2. Literature Survey

There exist several publications in the literature regarding IPTV, IPTV transmission over wireless networks, and WiMAX. The foundations and difficulties of transmitting IPTV services and applications over WiMAX have been explained by the studies [32, 37, 41, 44, 45, 58–64] in detail. Also, the research in [60] emphasizes an IPTV delivery framework along with key features and challenges of IPTV content distribution over WiMAX, focusing on MAC and PHY layer solutions. Additionally, the study in [37] provides another framework for IPTV delivery, built on the multicasting feature of WiMAX, with a PHY layer improvement. On the other hand, both studies lack the results of simulations or sufficient experiments.

IPTV delivery over WiMAX for multiple concurrent multimedia streams is efficient only if multicasting is available. Otherwise, the solution simply transforms into unicasting, where each subscriber gets a copy of the same simultaneous transmission, overloading the network [32, 37, 60]. Multicasting can take place in a single hop transmission as in PMP mode of WiMAX [32, 40, 41, 44, 45, 61, 62, 65–68], or in ad hoc multi-hop transmissions such as mesh mode of WiMAX [39, 69–73].

For dense networks, a MAC layer multicasting solution has been proposed in [65], which suggests addition of a common multicast IP address and a common Connection Identifier (CID) for the subscriber stations to be able to easily join or leave the multicast group. This approach avoids the unicasting and data duplication, increasing throughput and decreasing packet delays. On the other hand, the model is designed for single multicast transmission and it is not resilient to multiple unicast or multicast transmissions coexisting in the network. Also, in case of reverse traffic from the SS to the BS, an additional messaging structure is required to avoid confusion due to the same IP address being used by all SSs in the multicast group. A similar shared CID model has been proposed in [69] for unicast transmissions in WiMAX mesh networks. A bandwidth efficient multicasting model with shared CID in mesh networks has been studied in [69], with modifications to the centralized routing tree. This model also considers a single multicast group, and the presence of unicast and other multicast transmissions needs further improvements as in [65].

Focusing on reliability concerns of mobile networks, the authors of [40] propose a multicasting model that schedules retransmissions in case of Negative Acknowledgement (NACK) in PMP mode. The retransmissions can be sent as a unicast message if the network load is not too high. In case several NACKs are received from different mobile users, the model may choose to multicast the retransmission to reduce the overhead. This model utilizes a distinct Core Based Tree (CBT) routing [74] for each multicast group in the network. The model also requires all routers to be capable of delivering the messages in order. Retransmissions can be initiated from the local agents, if the data can be buffered, instead of starting from the original source, eliminating multi-hop retransmissions. However, the retransmissions and NACK mechanism needs to be fine tuned to support time dependent applications like the IPTV, where delays may cause shifts in the overall transmission, and the intermediate buffers can easily become exhausted. The model also considers the handover procedure for mobile users, where the multicast group registrations are adjusted before the handover. Also, packet forwarding from the old BS to the new BS is suggestively eliminated as the new BS starts buffering the required packets in parallel to the old BS. According to the results presented, the multicast model performs well in case of high number of users, while unicasting can be selected for fewer users, where duplicate retransmissions are far less, both in regular transmission and handover.

Although multicasting solves the data replication problem partially, the same data has to be transmitted at different modulations in parallel due to the varying channel quality of each user [32]. One solution to reduce such overhead in video multicasting at WiMAX networks is to use Multiple Description Coding (MDC) [42], which encodes video packets of a layer into several packets, robustly transmitting videos in higher quality, and optimize resource allocation to reduce the delay of video packets due to retransmissions. Another alternative solution to the problem of diverse channel conditions of users in the same multicast group is to utilize the PHY layer Superposition Coded Multicasting (SCM) technique [43]. Adding multi-layer support to regular PHY layer SCM [41] allows simultaneous transmission of distinct messages to receivers by a single BS, using both a resilient modulation and a higher capacity modulation for the same transmission, so that users can receive at least the low quality video stream in case of temporary problems in the less robust but higher quality streaming modulation.

According to the results of [41], the overall received video quality is higher compared to that of [32], which simply utilizes PHY layer SCM. The purpose of both models in [32] and [41] is to provide an acceptable video quality in case of temporary channel degradation. The authors of [61] and [62] also suggest similar multi-layer encoding models. The selection procedure of high quality modulation has been studied in [68], optimizing spectral efficiency. The user expectation for high quality video cannot be addressed if any user resides in a low quality reception zone of the PMP network, for long periods of time, in any of the proposed models listed here.

As multicasting eliminates the data duplication for many users, one major problem arises in multicasting as the handling of individual reverse traffic on the uplink. The authors of [66] study the uplink messaging in PMP mode and propose saving on the usage of uplink slots by assigning two of the orthogonal CDMA codes of the WiMAX OFDMA infrastructure to each SS in order to enable simultaneous transmission of feedback messages from each SS to the BS. Both Cumulative ACK (CA) and ARQ Feedback Request (AFR) for retransmission can be sent effectively with reduced uplink traffic. Despite the significant improvements, the model has a limit on the number of users simultaneously sending uplink messages, where only 128 simultaneous transmissions are possible for the 256 OFDMA codes available. For increased number of users, rescheduling is necessary to eliminate collisions on the uplink.

With the motivation for reducing the number of retransmissions in a PMP network, the receivers may be required to be ready for the actual transmission. One way to attain such condition is to poll the client devices before the transmission as proposed in [67]. As the probability of having all receivers ready is significantly low, the research suggests the use of a Threshold-T Policy [75], where the BS holds the transmission until T out of the total M users are ready in the multicast group. Improving the throughput by reducing retransmissions using this method creates longer delays on the receiver side. The study also proposes a stability optimization algorithm for data rate by adjusting the value of T dynamically. A third contribution in this multi-layer solution is to transmit the missed packets to any user left out of the T group. To eliminate this reliability issue, the authors use a Digital Fountain [76], encoding the missed packets into the transmission of new packets, so that the missed data can be reconstructed at the receiver site. Due to the overhead of polling and encoding/decoding, the performance of the model is suitable for small groups of multicast sessions; otherwise, many users may not receive service resulting in lower QoS.

In PMP mode, cooperation can be used to recover missed or lost packets of IPTV in a multicast environment, without the need to retransmit the packets from the BS. As suggested in [44], the BS transmissions are scheduled first, followed by a period of recovery among subscriber stations. That traffic also takes place over the BS, since PMP mode does not support ad hoc mode explicitly. The model allocates cooperation groups to optimize network resources and to ensure minimum IPTV QoS requirements. The model presents better results compared to unicast error recovery. In addition to this approach, the authors of [45] propose a scheduling algorithm to solve the indifference in QoS between the multicast groups, where one group may have better overall channel condition compared to the others, or members of one group may mostly suffer from bad channel conditions. On the other hand, having a very low average transmission rate in a multicast group, the cooperation overhead may easily go off the limits, causing further delays which may not be tolerated in time sensitive IPTV. As the proposed models are based on closed loop cooperation inside the multicast groups, it may be possible to implement cooperation among different multicast groups if the retransmission requirements are lower than expected. Comparatively, our WISDoM model [11] proposes a fixed multicast tree that stabilizes the fluctuations in data rates and packet delays, for a better decision on the required modulation. Meanwhile, WISDoM-SD proposes a common period for relaying over the entire relay nodes of all multicasting groups, benefiting from proximity of user nodes in different multicast groups as well.

In WiMAX mesh solutions for multimedia distribution such as [70], the frames are delayed for distribution until the very end of the frame deadline, eliminating processing for scheduling computations. Besides the improvements, the results presented show that delays for more than two hops are intolerable for IPTV.

User expectation on regular TV channel switching delay is no more than a fraction of a second, when using a hardwired TV set. On digital systems, especially transmitted over wireless IP networks, there is a continuous two-way flow of messaging. In case of channel switching, a set of control messaging takes place for switching to a new multicast group. The research in [77] proposes to calculate a stable multicasting routing tree based on probabilistic calculations, so that minimum amount of tree modifications are necessary both for adding an MSS to a new group and relocating the MSSs that are children of a relay node that is changing its current multicast group.

Regarding concurrent transmission in mesh networks with respect to spatial diversity, interference plays a key role in distributed scheduling, which improves the throughput significantly. The authors of [39] propose an interference-aware relay node selection method for newly joining mesh subscriber stations so that minimum amount interference is encountered during simultaneous relay transmission. A broader approach presented in [71] proposes to construct the routing tree based on the interference calculation of the entire network, instead of the interference state of the potential relay node as in [39]. Both models are shown to exhibit high overall throughput with the help of interference aware routing tree construction.

One of the major issues in mobile multimedia is blocking of data packets, especially in high mobility conditions. The research in [64] proposes transmission model that employs multicasting for highly demanded streams as much as applicable, and unicasting otherwise to minimize the blocking probability. By the nature of high mobility, expected size of multicast groups is relatively small compared to nomadic users, which enforces the unicast model and increases the network load, that is in turn compensated by low quality transmission of the IPTV streams.

Another aspect in IPTV delivery in general is the content protection like Digital Rights Management (DRM). In addition to standard DRM protocols, [78] proposes protection mechanisms for attacks, and a content distribution gateway service for content providers and subscribers. As IPTV is generally a paid service, user authentication is a major issue especially in wireless environments. The research in [79] presents an authentication and key management system for secure messaging in the IPTV platform. Also the security in content delivery is another major concern, which has been addressed in [80], where the authors propose an efficient encryption management infrastructure considering the overhead of messaging during a channel switching process.

2.3. WISDoM-SD

Our proposed model is based on high capacity multicasting in mesh networks. We have implemented a model named *Wireless IPTV Service Distribution Over Mesh Mode Via Space Diversity (WISDoM-SD)*, where we use IPTV and WiMAX mesh network as the testing application and testing environment, respectively. The model is applicable to other ad hoc networks with such capability. The main purpose is to improve the overall transmission quality for users who cannot receive the wireless service directly from the BS, but have sufficiently good connection to other users in close proximity with better connection to the BS.

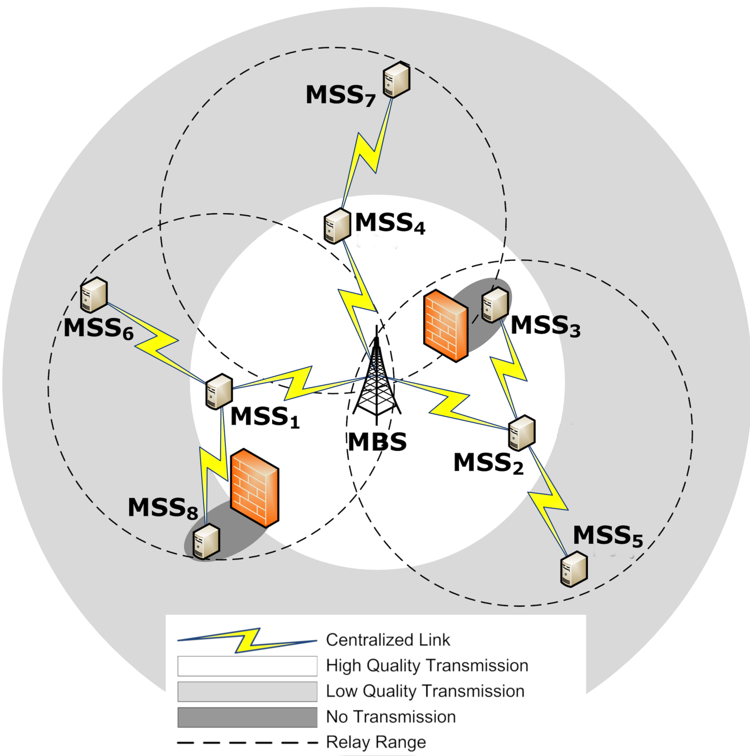

Figure 2.1. WiMAX mesh mode relaying.

As shown in Figure 2.1, users may reside in high quality transmission zones of the mesh base station (MBS), or lower quality transmission zones. Some users inside the high quality zone may even fall into a low quality transmission (or no direct connection) state due to obstacles. Any user in a low quality transmission state can establish indirect communication to MBS with higher quality transmission over a neighboring relay node, if such a node resides in close proximity. The inner circle in the figure is an example of the high quality modulation zone with MSS_1, MSS_2, and MSS_4 acting as relay nodes for MSS_3, MSS_5, MSS_6, MSS_7, and MSS_8, which either have no direct connection to the MBS or are in the more robust transmission zone of the MBS, which is less efficient in spectrum usage. Connections with more than two hops may be necessary, however, as presented in [12], the delay in packet delivery and the network overhead increases significantly for indirect connections with more than two hops, which makes such type of routing impractical for time dependent IPTV streaming. For that reason, our study focuses on at most two hop connections to the MBS.

Multicasting in wired networks have performance improvements over unicasting, but the data is still replicated on the network to be sent over the intermediate routers and switches. Multicasting in wireless networks has far more significant performance improvements in terms of overall network throughput since the data is not replicated further from the BS. Once the signal is sent, it can be received by unlimited number of users. For multi-layer wireless systems like WiMAX, the data may have to be sent over multiple modulations depending on the reception quality of users. There is also a major QoS problem causing retransmissions, which is much less in wired networks, resulting in inefficient utilization in the wireless networks.

As the demanded quality of IPTV resolution increases, the modulation to be selected to transmit the streaming media needs to be capable of carrying the load. On the other hand, the higher the modulation capacity gets, the less resilient it becomes to obstacles. To avoid retransmissions, more robust modulations can be used in widespread area, however, this causes inefficient use of the spectrum for subscriber stations which can receive higher quality transmissions. There needs to be an optimum solution between the amount of retransmissions and spectral efficiency.

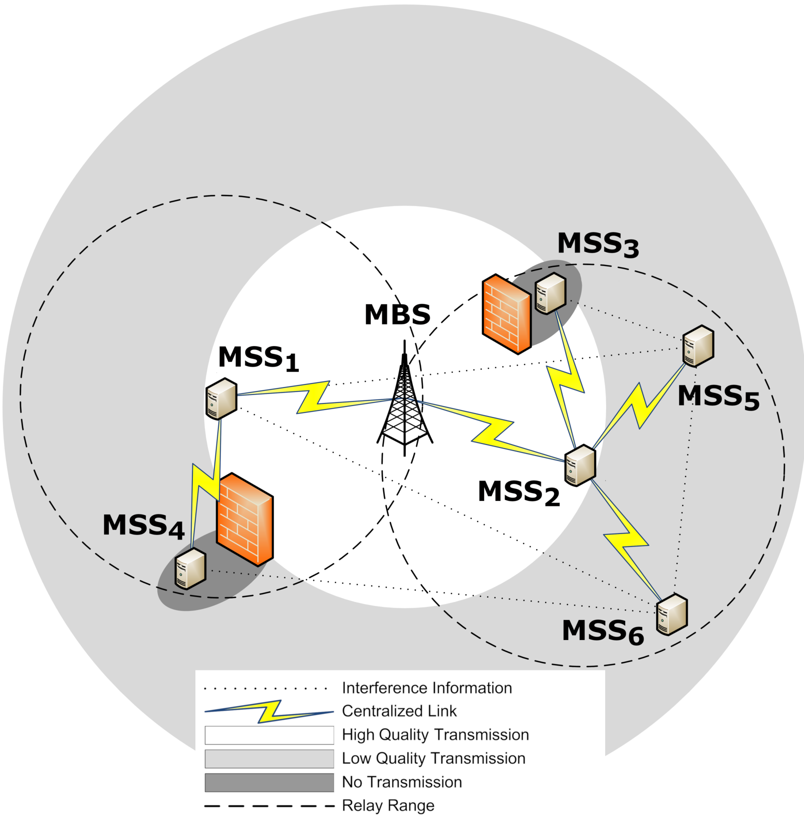

Figure 2.2. WISDoM-SD parallel transmissions.

Multimedia streaming with HDTV quality requires approximately 6 Mbps data rate [56,57]. For such higher resolutions, connecting directly to a base station with high capacity bandwidth may not be an option. However, there may be indirect connections available for such high data rate streaming. As seen in Figure 2.1, some nodes may prefer connecting over a relay node with higher capacity modulation instead of direct connection to BS at a lower data rate.

Many cooperative multicasting models have been discussed in the literature, such as [44, 45], where the cooperation takes place within the multicast group. If users of a multicast group reside on a low quality transmission zone of the BS, the overall throughput is decreased dramatically. Similarly, the cooperation links within the multicast group may also be at low transmission quality, reducing the throughput further. The WISDoM-SD model is based on WiMAX Mesh mode, which inherently supports the ad hoc cooperation capability. Also, the model allows cooperation between different multicast groups, where a relay node can supply IPTV stream to its children demanding multimedia content of another multicast group. The model also benefits from parallel distributions at distinct locations of the network coverage area, regarding interference constraints as seen in Figure 2.2, where MSS_1 and MSS_2 can relay the same content in parallel to some of their children. According to the interference information provided in the figure as dotted lines, the traffic between MSS_1 and MSS_4 can be scheduled to take part simultaneously with the traffic between MSS_2 and MSS_3.

2.3.1. Construction of the Multicast Routing Tree

As an improvement to the regular parent node selection with respect to highest SNR in WiMAX Mesh mode, WISDoM-SD considers parallel communications in the entire network to improve the throughput, adding interference conditions into the selection process. The formation of the routing tree has essential effects on the performance of the wireless network, as also shown in [39, 71]. Additionally, WISDoM-SD employs an opportunity metric for parallel transmissions, since the dynamic user behavior enforces the continuous reformation of the routing tree depending on the IPTV channel switching and selection of parent nodes.

In the parent selection process, a node MSS_i selects the MBS as its parent if it can establish direct connection with sufficient capacity. The MSS_i will select a neighboring MSS_x as its parent, if no such direct connection to the MBS can be established. If more than one neighbors are within the communication range of the MSS_i, then they are ranked according to the number of parallel transmission they can provide. For each child of any relay node MSS_y other than the potential relay node MSS_x, if the MSS_y and its child do not cause harmful interference on the communication between the MSS_i and MSS_x, then MSS_x gets a plus score on the opportunity metric. The MSS_x with highest score is selected as the parent node of the MSS_i for relaying. As shown in Figure 2.3, MSS_1, MSS_2, and MSS_3 support relaying in the respective areas bounded by the dashed circles. The interference information is provided with dotted

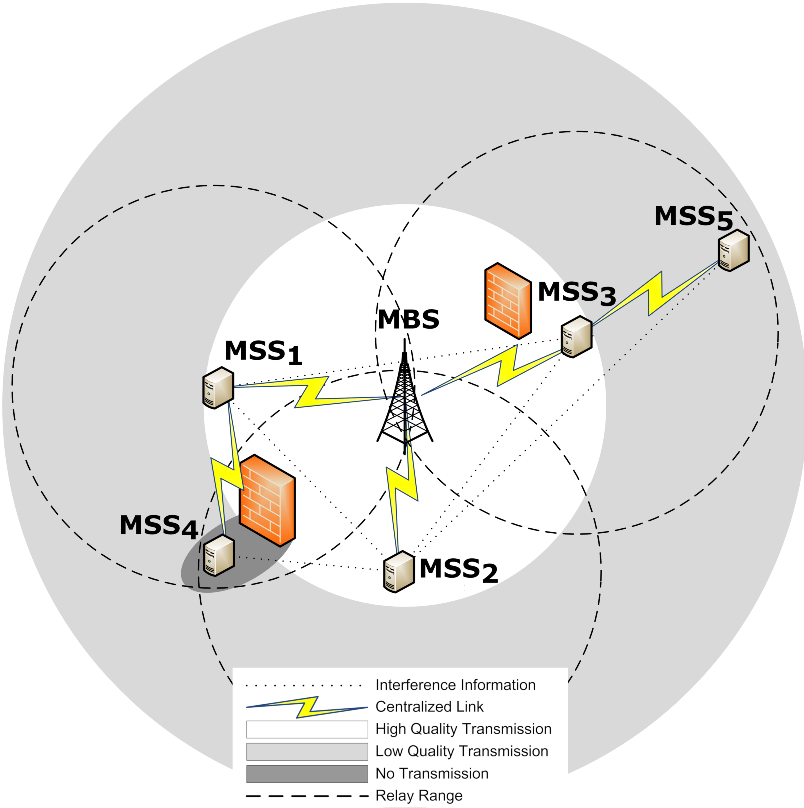

Figure 2.3. WISDoM-SD multicast routing tree formation.

lines. MSS_5 has no parent option other than MSS_3. On the other hand, MSS_4, selects MSS_1 as its parent node since the connection in between the couple has higher score for *not interfering with other nodes*.

2.3.2. Mesh Base Station (MBS) Scheduler

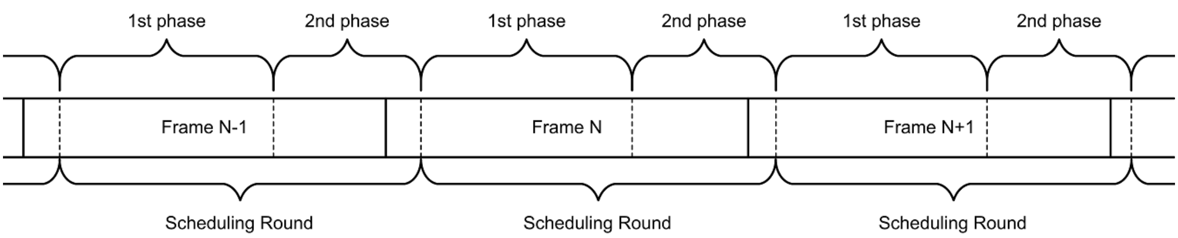

Figure 2.4. WISDoM-SD WiMAX mesh mode scheduler phase diagram.

WiMAX mesh mode allows distributed scheduling on the centralized routing tree for the relay nodes. In addition to the enhancement in parent node selection process to maximize parallel transmission opportunities, WISDoM-SD focuses on minimizing the data packet delays for two-hop nodes, which already receive a delayed sequence of data compared to the one-hop nodes, and optimize the average delay for the entire set of nodes in the cell, without affecting the overall QoS.

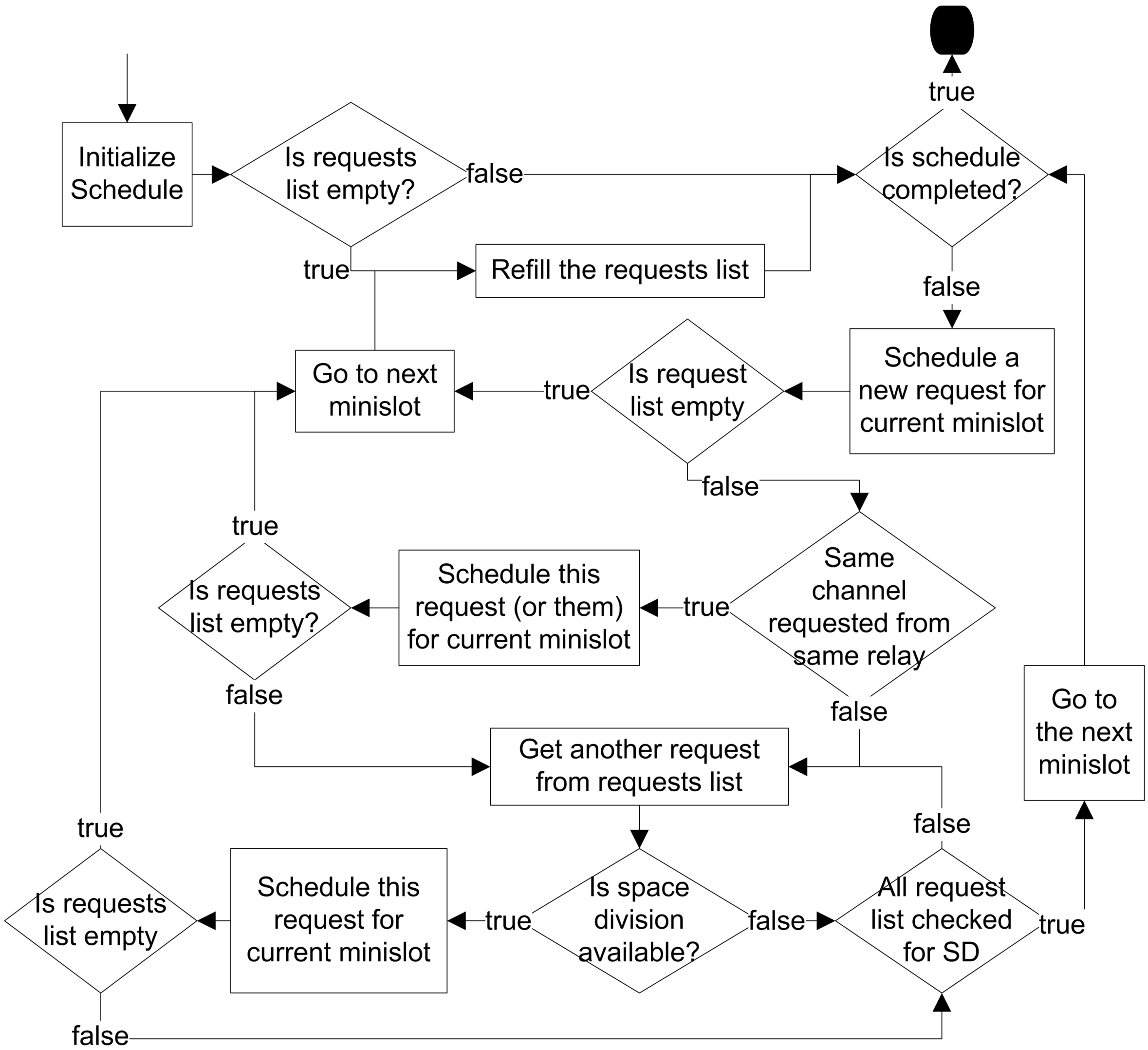

Figure 2.5. WISDoM-SD WiMAX mesh mode scheduler flowchart.

The proposed scheduling algorithm works on consecutive rounds, where each round consists of two phases, first one for the MBS, and the second for the relay nodes, as presented in Figure 2.4. The first phase is reserved for the multicasting of all IPTV channels requested in the network. Any one-hop node, including the relay nodes, receive and buffer the transmission if either required by the node itself or will be multicast to its children. Relay nodes are not allowed to transmit in this phase as they may interfere with the transmission to the other one-hop nodes in the area. The second phase is more complex compared to the first one. The duration of the second phase is divided into minislots for transmission of requested IPTV data. The order of children to be served needs to be determined according to the amount of conflicts when parallel transmission is not possible. The requested data with lowest possibility to be transmitted in a parallel minislot are scheduled first, reducing the conflicts for the remaining requests. The conflicts are calculated among different relay nodes since there is no possibility of scheduling two distinct data into one minislot in the same relay node. However, the data of at least two child nodes can be transmitted in one minislot in a multicast fashion, if they requested the same IPTV channel in the first place. The process is shown in Figure 2.5.

2.4. WISDoM-SD Performance

WISDoM-SD has been proposed as a MAC layer improvement to WiMAX mesh mode, and the results of both systems have been compared following a set of OPNET Modeler simulations. There are two phases in the simulation, namely, network initiation for deployment of nodes and establishment of links, and simulation execution.

Table 2.2. Minimum SNR for 20MHz OFDMA WiMAX [81].

Modulation	Coding Rate (CR)	Minimum SNR (dBm)
QPSK	1/2	≥ -79
16-QAM	1/2	≥ -72
16-QAM	3/4	≥ -69
64-QAM	2/3	≥ -65
64-QAM	5/6	≥ -58

2.4.1. Simulation

The simulations are based on WiMAX operation at 5GHz with 20 MHz bandwidth OFDMA, which has the SNR requirements listed in Table 2.2. The OPNET parameters for the simulation has been given in Table 2.3. The area for obstacle and node deployment has been selected to be as large as the coverage area of 64-QAM modulation, calculated as 3.8 km in radius from the MBS with respect to free space propagation, using omnidirectional antennas on both MBS and MSS.

Table 2.3. OPNET simulation and topology parameters.

Parameter	Value
Transmitter Frequency	5 GHz
Transmitter Antenna Gain	24 dBm
Receiver Antenna Gain	24 dBm
Transmit Power	23 dBi
Obstacle Penetration Loss	20 dB
Fading Factor	18 dB
Nakagami m value	2.0
Number of Nodes	50 to 300
Number of Obstacles	200
Obstacle Width (Minimum)	25 m
Obstacle Width (Maximum)	100 m

The obstacles and the MSS nodes are deployed uniformly in the network coverage area of 3.8 km in radius, according to the simulation parameter given in Table 2.3. Following the deployment, potential links are established with respect to obstacle penetration loss parameter. The centralized multicast routing tree is formed as described in Section 2.3.1, using Nakagami-m propagation model [82] as the wireless channel.

Table 2.4. WiMAX and IPTV simulation parameters.

Parameter	Value
Length of WiMAX Frame	20 msec
Data Minislot Count	256
Control Minislot Count	10
Modulation	64-QAM
Coding Rate	5/6
Number of Available IPTV Channels	100
IPTV Channel Bit Rate	6 Mbps
Length of IPTV Frame	300 Kbits
Simulation Length	600 seconds
Channel Switching Polling Interval	1 second
Channel Switching Probability	0.05

Parameters used in the simulation executions regarding WiMAX and IPTV are listed in Table 2.4. For each subscriber, a decision is made at each round of *Channel Switching Polling Interval* parameter, where the user switches the channel according to the probability value in *Channel Switching Probability* parameter.

The results of WISDoM-SD presented in the following sections are based on two different types of channel switching, which affects the network traffic and multicast routing. The first case assigns equal probability to each IPTV channel to be selected by the users (i.e. uniform distribution), and the second case assigns a selection probability to each channel according to a normal distribution to indicate the popularity of it.

2.4.2. Results

The rate of users that can receive IPTV service directly or indirectly is given in Figure 2.6, with respect to the number of total users in the network. While the PMP mode does not allow indirect communication with the BS, the overall connectivity is around 67% for that mode of operation since many users suffer from insufficient channel conditions and cannot reach the SNR margin at least as good as QPSK modulation with CR=1/2, i.e. the standard modulation for WiMAX control messaging in mesh mode [81].

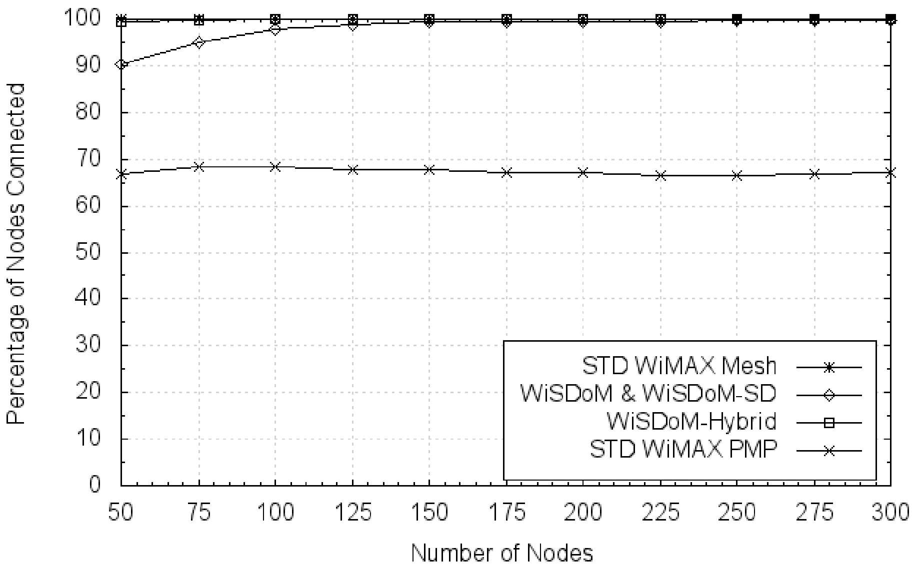

Figure 2.6. Rate of connected nodes with respect to total number of nodes.

The WiMAX mesh mode implementation provides service to all users successfully by relaying for users with bad direct channel conditions. The alternative WISDoM model considers relaying only over the links with high capacity, and does not utilize parallel transmissions. As there is a minimum capacity requirement for WISDoM and WISDoM-SD such as 64-QAM with CR=5/6, these models provide selective service to users that can reach such condition in order to provide high data rate required for IPTV. However, standard WiMAX mesh mode provides service to all users, without considering the desired QoS. Therefore, both WISDoM models slightly fall behind the WiMAX mesh mode. Both models perform significantly better than PMP mode.

The nodes and obstacles are uniformly distributed to the area with radius 3.8 km. Having at least 125 nodes in the area, the connectivity rate of WISDoM models increases above 99%. For node count less than 150, many nodes fail in finding a relay node with high capacity direct connection to both the MBS and the demanding MSS itself, due to sparse deployment in the area. To solve the connectivity problem in sparse networks, a third WISDoM model is proposed as WISDoM-Hybrid, where the modulation constraint is relaxed down to allowing 16-QAM with CR=1/2 for users that cannot establish direct or indirect connection to the MBS. The connectivity rate of WISDoM-Hybrid is almost as good as WiMAX mesh mode, with better QoS. As the PMP mode does not perform anywhere close to the mesh mode alternatives, we will focus only on these models in the following sections.

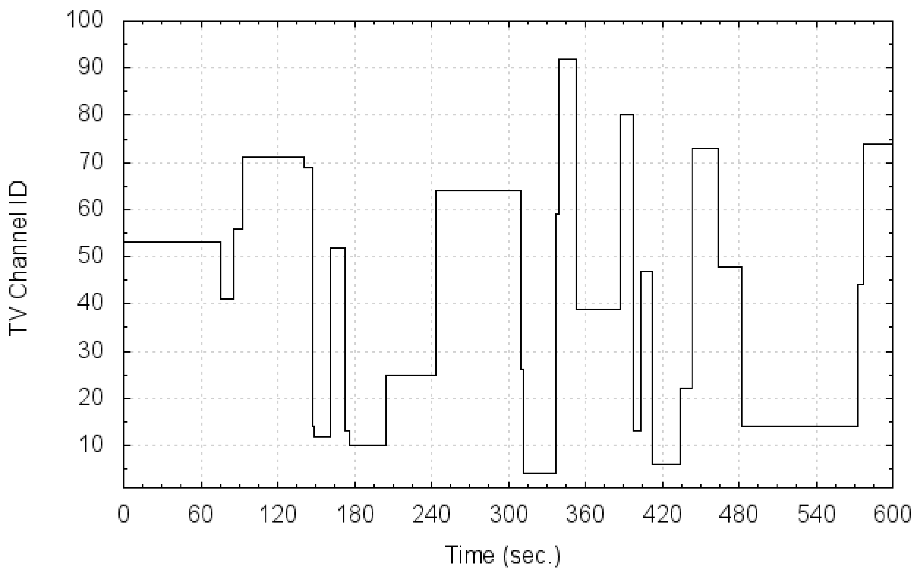

Figure 2.7. IPTV channel switching behavior over time, using uniform distribution of channel selection probability.

2.4.2.1. IPTV Channel Switching Using Uniform Distribution. A user may decide to select any channel with equal probability, where in the long run, all channels will have almost equal number of audience. For each set of user deployments, the simulations are performed with 30 repetitions, each one lasting 600 seconds. A sample plot of user behavior for channel switching is provided in Figure 2.7 for one sample set of execution. Users decide on switching to any channel with equal probability due to uniform distribution.

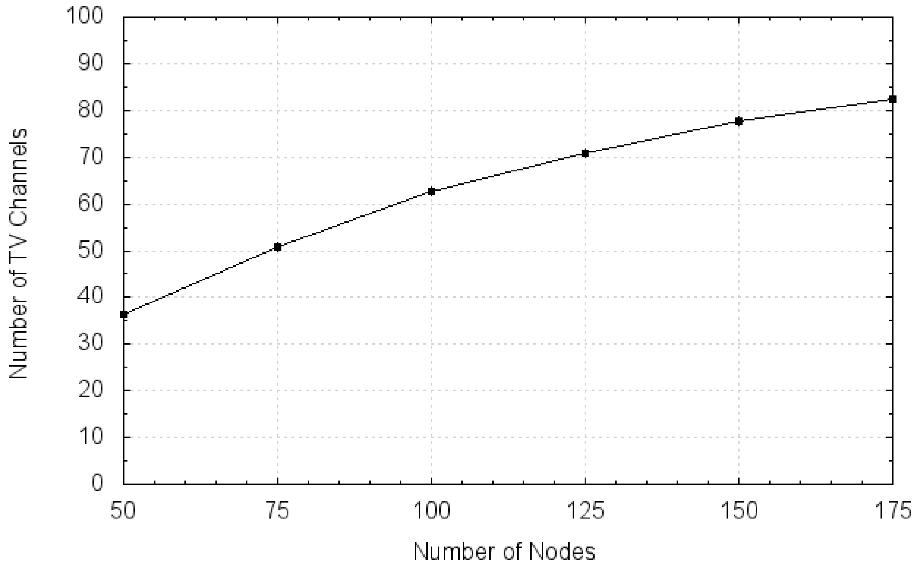

Figure 2.8. Average number of requested distinct IPTV channels using uniform distribution of channel selection probability.

In accordance with the pigeon hole principle, the average number of requested distinct IPTV channels increases up to a certain value, and the rate of increase slows down with the addition of extra users to the network, as shown in Figure 2.8. With respect to the increasing trend with the number of users, the limited number of 100 channels are equally likely to be selected by more users.

The average number of transmitted IPTV data frames for each one of the two-hop transmissions are shown in Figure 2.9. As the number of subscribers increase, the second hop transmissions also converge to the first hop transmissions, increasing the user satisfaction who would not be served so well in a PMP transmission network.

The parallel transmissions approach with the proposed multicast routing tree formation method decreases the number of retransmissions significantly. At each round of transmission scheduling, the number of parallel transmissions of IPTV frames is shown in Figure 2.10. With respect to different number of users receiving parallel

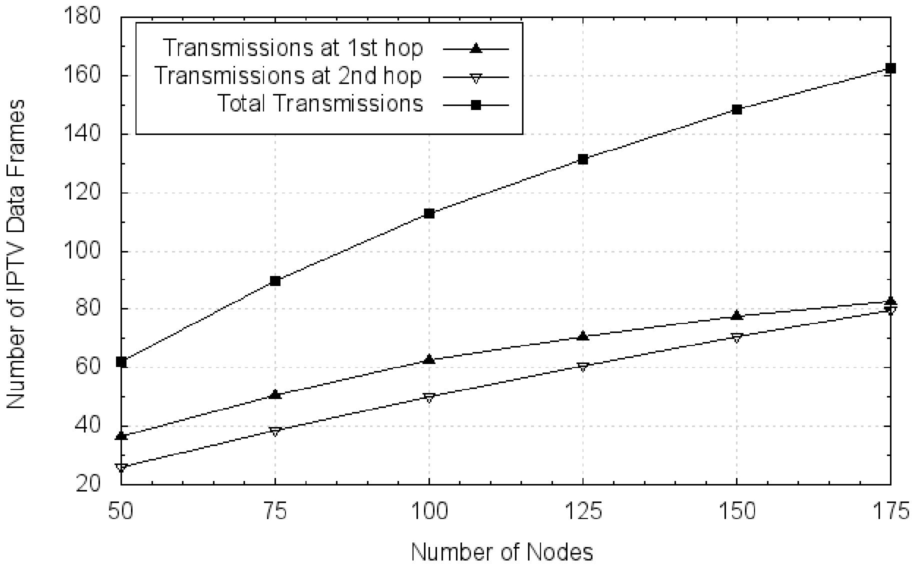

Figure 2.9. Average number of IPTV data frame transmissions in a scheduling round using uniform distribution of channel selection probability.

transmission in the simulations, the total number of IPTV data frame transmissions has been reduced by almost 20% compared to the non-parallel transmissions case in the alternative WISDoM model.

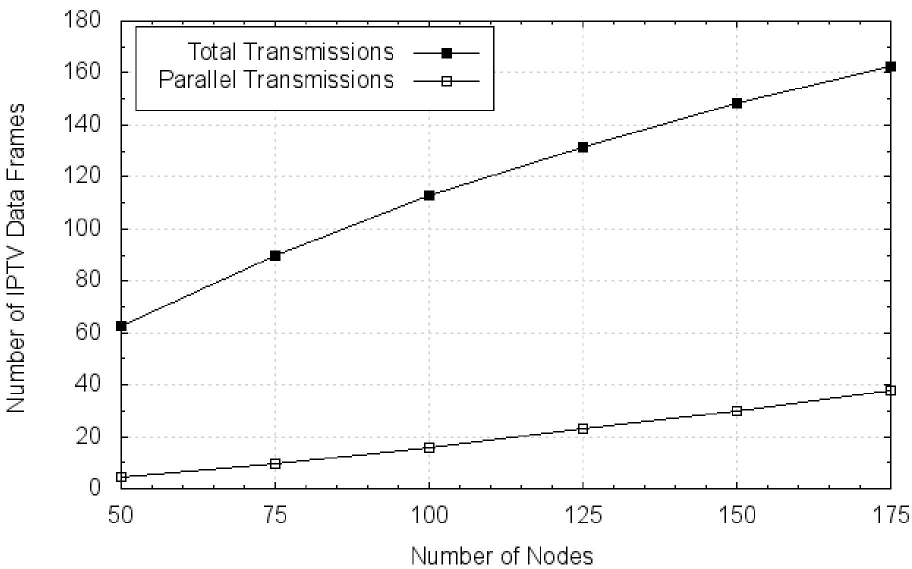

Figure 2.10. Average number of parallel IPTV data frame transmissions in a scheduling round using uniform distribution of channel selection probability.

One of the most critical performance metric in IPTV transmission and other time sensitive services such as VoIP is the amount of delays faced by the data frames. In a 330 Mbps wireless network, 50 IPTV channels with each one requiring 6 Mbps of data rate can be delivered over direct links from the BS with no delays. On a regular mesh mode operation with two hops, due to the scheduling round required for the second hop transmissions, the total number of MBS streamed channels is reduced to less than that of the PMP case. On the other hand, relaxing the *no delay* policy to allow delays up to 100 milliseconds, which does not cause discomfort at the audience [83], our simulations can achieve more number of IPTV channels to be transmitted over the network.

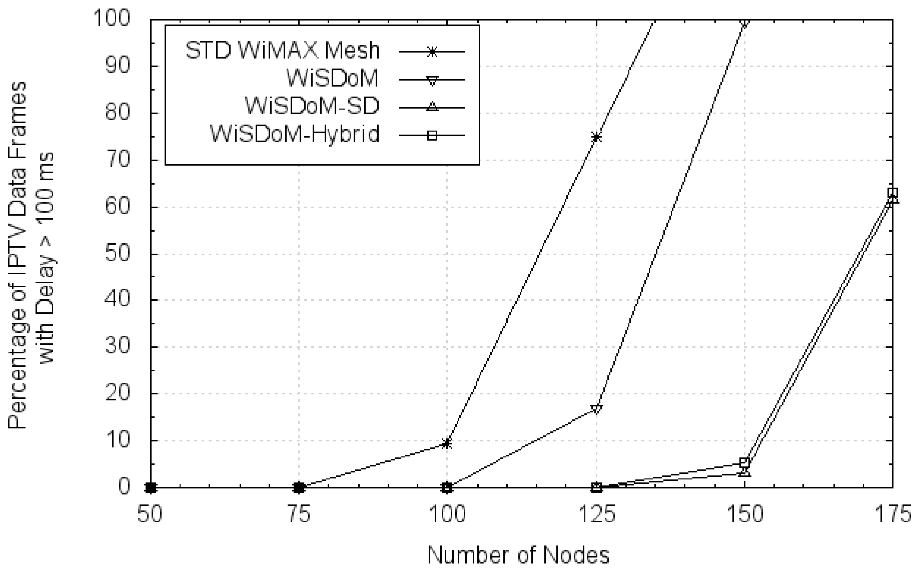

Figure 2.11. Percentage of IPTV data frames delayed more than 100 milliseconds using uniform distribution of channel selection probability.

Figure 2.11 shows the percentage of frames experiencing delays more than 100 milliseconds, with respect to increase in the number of users, for WiMAX Mesh, WISDoM, WISDoM-Hybrid, and WISDoM-SD solutions. Allowing the percentage of packets delayed more than 100 milliseconds to be at most 1%, WiMAX Mesh mode can support up to 77 users given the WiMAX and IPTV simulation parameters in Table 2.4. For WISDoM model that relays over high capacity links and does not allow the parallel transmissions, the number of users that can be served increases to 98, with a 27% improvement over the WiMAX Mesh mode.

For the WISDoM-Hybrid model, the number of users that can be served increases to 128, providing a 66% improvement over the WiMAX mesh mode, although some of the users have to use low capacity modulation in the simulations. Finally, the WISDoM-SD model serves up to 130 users with the help of parallel transmissions, with a 69% improvement over the WiMAX Mesh mode.

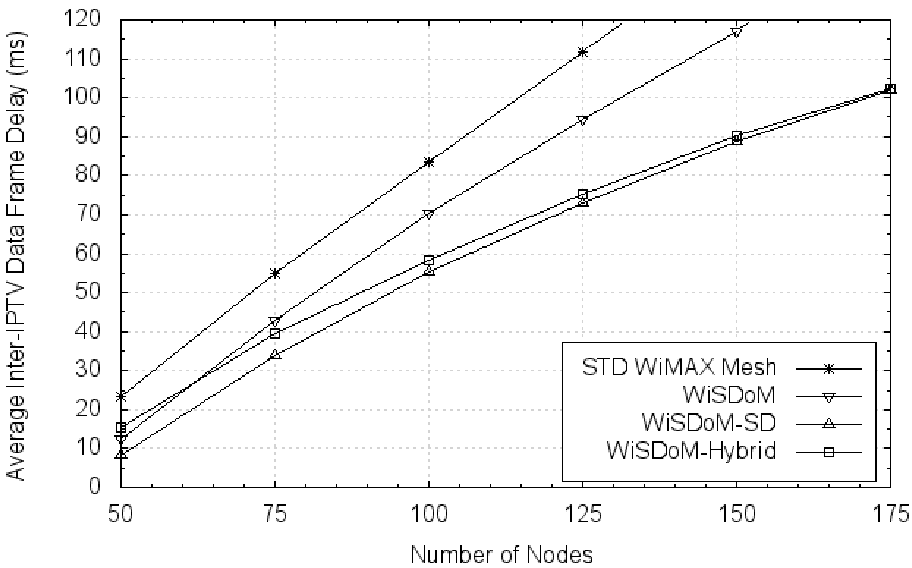

Figure 2.12. Average inter-IPTV data frame delay using uniform distribution of channel selection probability.

Table 2.5. Average inter-IPTV frame delay for uniform distribution of channel switching probability.

Model	Supported Users	Average Inter-frame Delay (milliseconds)
WiMAX Mesh Mode	77	57
WISDoM	98	71
WISDoM-Hybrid	128	77
WISDoM-SD	130	77

Relaxing the *no delay* policy increases the total number of subscribers without causing discomfort at the user side. Also, the average inter-frame delays for all WISDoM models and the WiMAX Mesh mode is below the allowed 100 milliseconds, with respect to average number of users receiving the service as shown in Figure 2.12. For WiMAX mesh mode supporting 77 users, the average delay is around 57 milliseconds, and for the WISDoM models, WISDoM, WISDoM-Hybrid, and WISDoM-SD supporting 98, 128, and 130 users each, the average inter-frame delay becomes 71, 77, and 77 milliseconds, respectively, as given in Table 2.5.

For lower number of users present in the network, it is possible to serve the users with more robust modulations having longer range and better penetration of obstacles, eliminating the need for relaying substantially. The WISDoM model exhibits lower average delays than the WISDoM-Hybrid model, for around 50 users, where the connectivity rate of WISDoM model is 90%, and the hybrid model serves approximately 10% more subscribers with the help of using more robust modulations, in the cost of a little more inter-frame delays. The results for the WISDoM-SD model are comparatively close to the results of the WISDoM-Hybrid model, with better utilization.

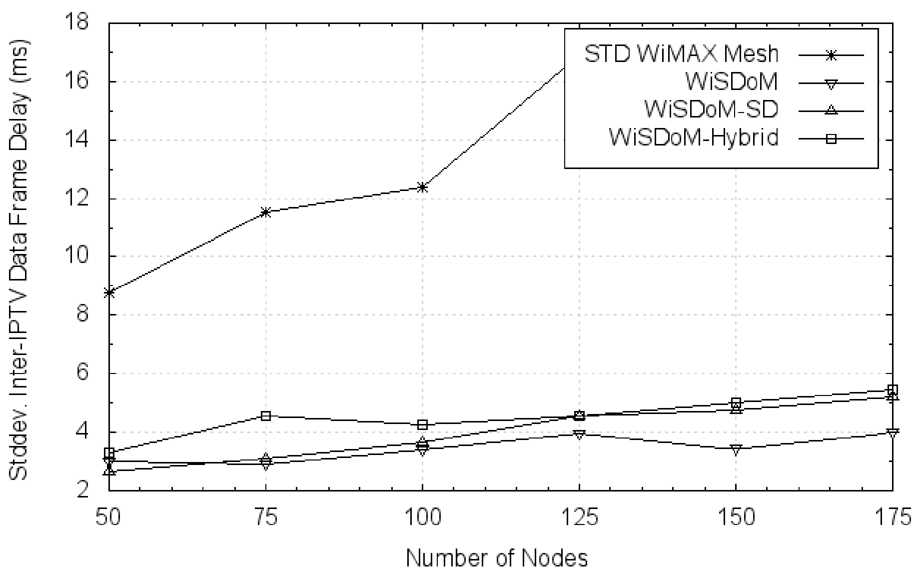

Figure 2.13. Standard deviation of inter-IPTV data frame delay using uniform distribution of channel selection probability.

All WISDoM models use QAM modulations requiring shorter transmission slots. This condition results in less variation in inter-IPTV frame delays, providing a more stable user experience independent of the number of users compared to WiMAX Mesh mode, where the modulation varies over time and the multicasting tree formation is not as fine tuned as the WISDoM models. Even for small number of users, the 100 millisecond delay boundary is easily exceeded in WiMAX mesh mode. The standard deviation of the inter-frame delay is given in Figure 2.13.

2.4.2.2. IPTV Channel Switching Using Normal Distribution. The popularity rating of each TV channel is different, either as a whole or in periods during the day. Depending on the rating values, the user behavior can be estimated beforehand for the selection of channels, and the IPTV network utilization can be adjusted accordingly.

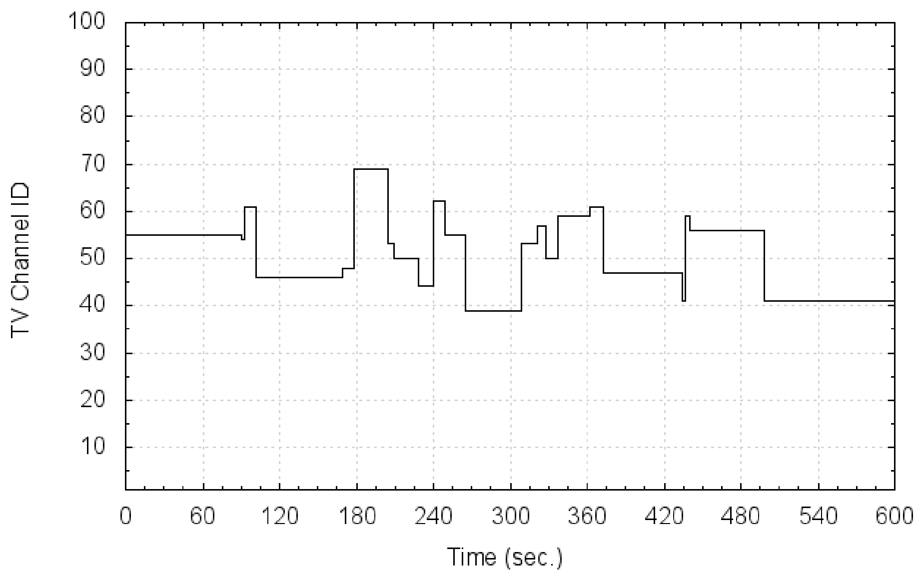

Figure 2.14. IPTV channel switching behavior over time, using normal distribution of channel selection probability.

In the previous simulation setup, we introduced a uniform probability distribution for each IPTV stream, to be selected by the users during the channel switching intervals. In this case, we utilize a normal distribution, where some of the IPTV channels are more popular than the others (favoring multicasting), and some are demanded less (favoring the unicasting). As we have 100 IPTV channels, the parameters of the normal distribution are selected such that channel number 50 is the most popular channel. In other words mean is channel number 50, and standard deviation is 20 channels. The simulation duration is 600 seconds, with 15 repetitions in each round.

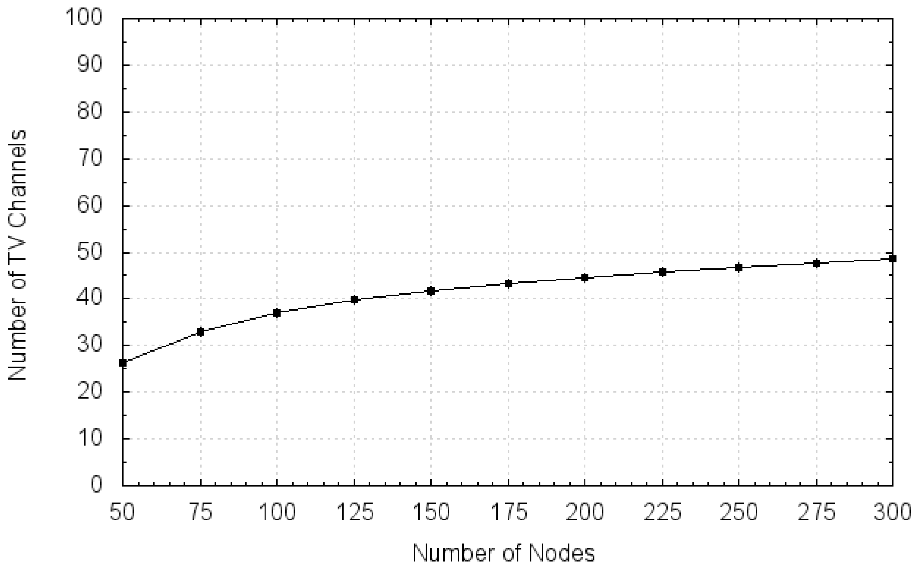

Figure 2.15. Average number of requested distinct IPTV channels using normal distribution of channel selection probability.

A sample plot of user behavior on channel selection is provided in Figure 2.14 with respect to normal distribution of channel selection probability. Users tend to select the channels around Channel 50 as expected from the normal distribution. The average number of distinct IPTV channels demanded by all subscribers is also below 50 as shown in Figure 2.15, consistent with the probability distribution, and lower than that of the uniform case with 80 channels requested on average.

The average number of transmitted IPTV data frames for each of the two-hop transmissions are shown in Figure 2.16. As the number of subscribers increases, the amount of second hop transmissions required increases relatively faster. Since most of the subscribers request the same channels due to normal distribution of channel switching probability, scheduling time required for the first hop is reduced, and a larger scheduling time for the second hop is available. Most of the traffic can be multicast in parallel at the second hop, reducing the overall bandwidth consumption significantly.

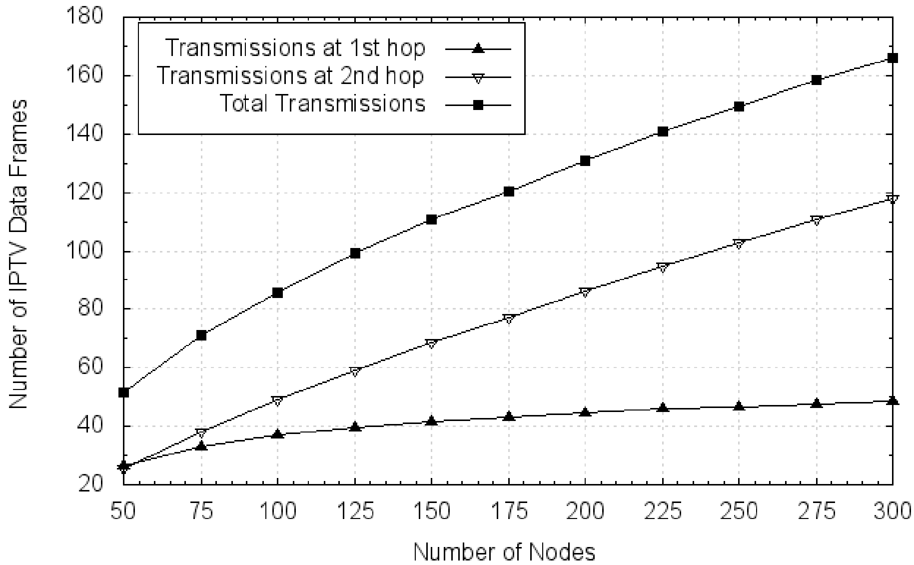

Figure 2.16. Average number of IPTV data frame transmissions in a scheduling round using normal distribution of channel selection probability.

The multicasting groups gets larger in terms of number of users, increasing the opportunity to deliver the content in parallel. As can be seen in Figure 2.17, the rate of parallel transmissions has a larger share compared to the case of the uniform distribution.

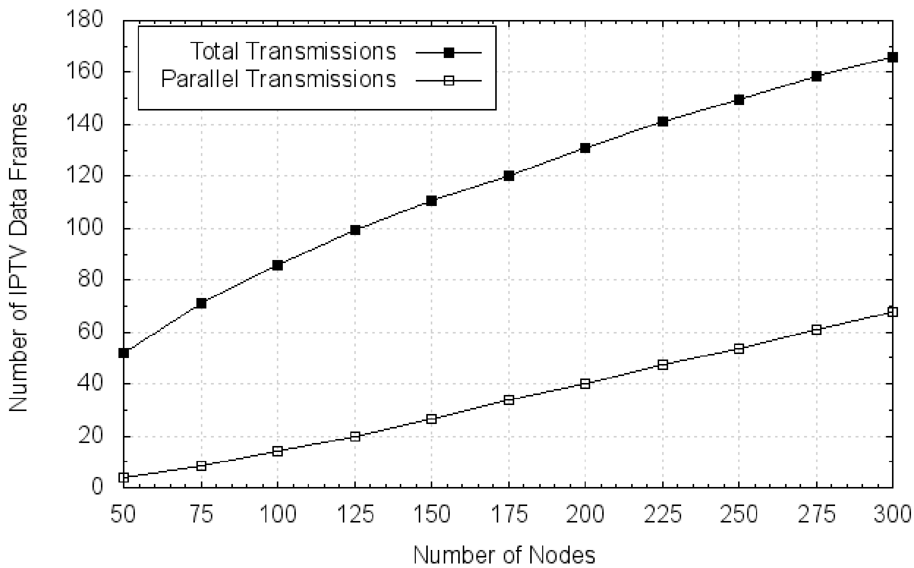

Figure 2.17. Average number of parallel IPTV data frame transmissions in a scheduling round using normal distribution of channel selection probability.

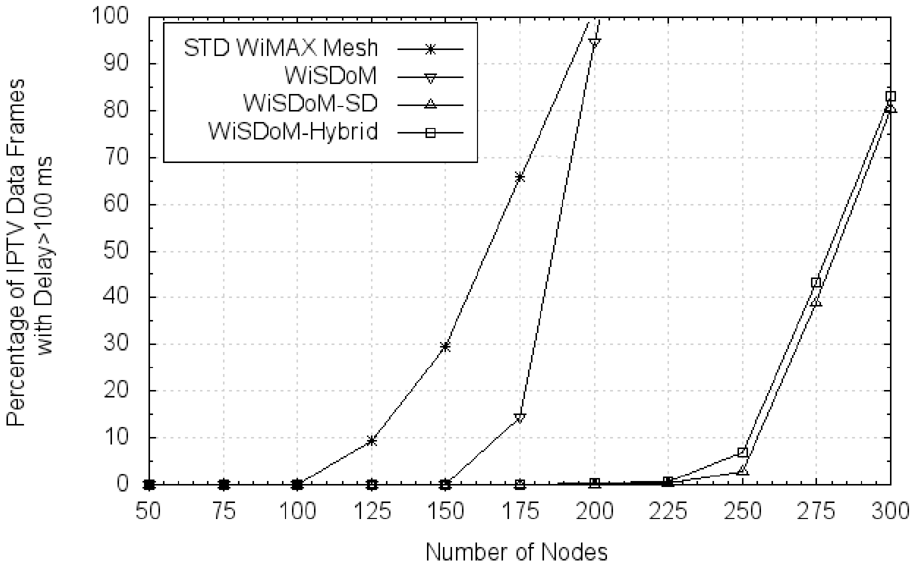

Figure 2.18. Percentage of IPTV data frames delayed more than 100 milliseconds using normal distribution of channel selection probability.

A similar comparison to the uniform distribution case in terms of the 100 milliseconds allowed inter-frame delay can be observed in Figure 2.18, where the WiMAX mesh mode can support up to 102 users without causing user dissatisfaction. WISDoM, WISDoM-Hybrid, and WISDoM-SD can support as much as 149, 225, and 228 users respectively, where the latter two use the parallel transmission scheduling approach considering the interference avoidance opportunities

In terms of average inter-frame delay considering all models, the delay values are 63, 78, 83, and 83 milliseconds for WiMAX mesh mode, WISDoM, WISDoM-Hybrid, and WISDoM-SD models respectively, supporting 102, 149, 225, and 228 users each, as shown in Figure 2.19 and Table 2.6.

For user density with 175 users per cell and higher, the WISDoM-SD model converges to the WISDoM-Hybrid model. On the other hand, for smaller number of nodes such as 50, the delay values are slightly higher than that of the WISDoM model. The connectivity rate of WISDoM is around 90% using more robust modulation, while it is approximately 99% for WISDoM-Hybrid and WISDoM-SD.

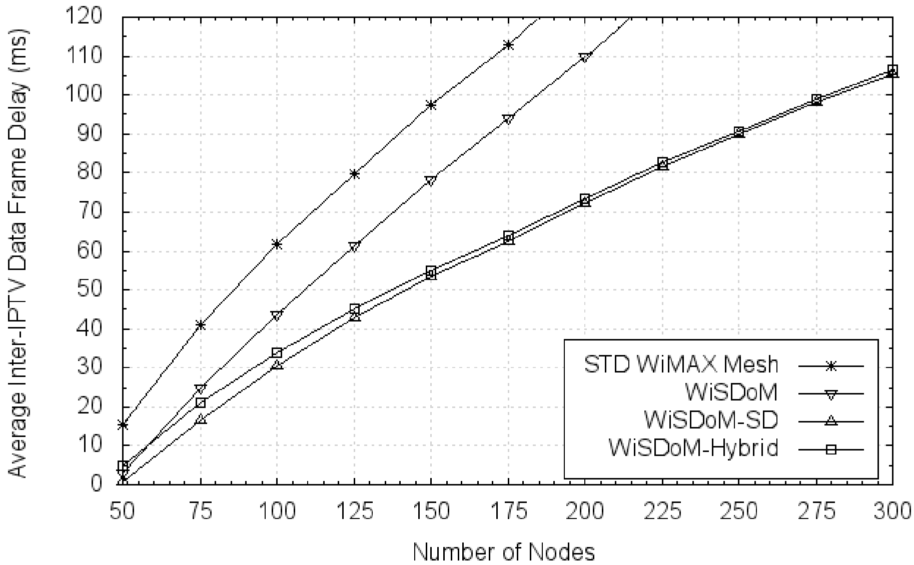

Figure 2.19. Average inter-IPTV data frame delay using normal distribution of channel selection probability.

Table 2.6. Average inter-IPTV frame delay for normal distribution of channel switching probability.

Model	Supported Users	Average Inter-Frame Delay (milliseconds)
WiMAX Mesh Mode	102	63
WISDoM	149	78
WISDoM-Hybrid	225	83
WISDoM-SD	228	83

With respect to the standard deviation results of the uniform channel switching probability simulations, the inter-IPTV frame delays in WiMAX mesh mode is again higher compared to the WISDoM models that utilize a single high capacity modulation. The WISDoM models increase stability in IPTV user experience by providing service to more subscribers with less fluctuations in traffic, as shown in Figure 2.20.

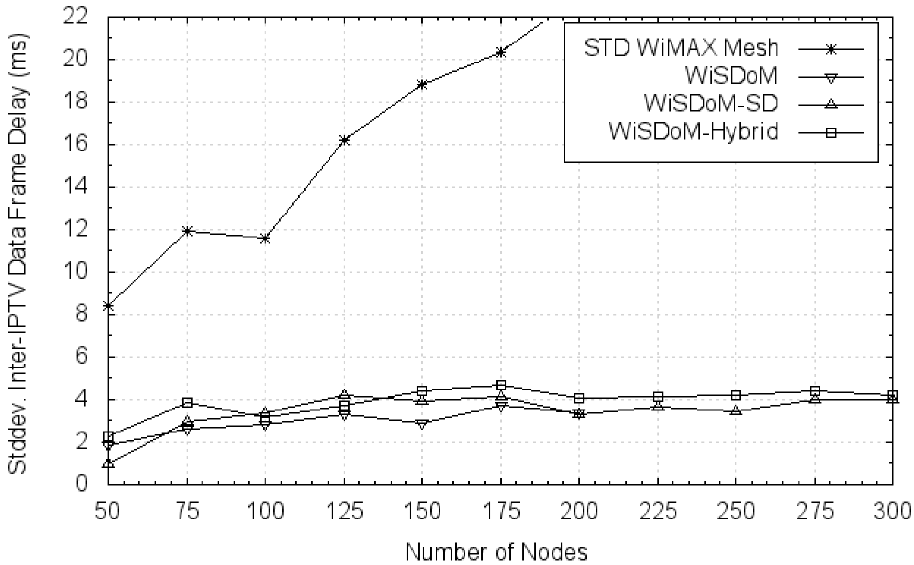

Figure 2.20. Standard deviation of inter-IPTV data frame delay using normal distribution of channel selection probability.

2.5. Closing Remarks

In this part of the thesis, we have proposed an alternative multicasting solution for delay sensitive applications like IPTV, and VoIP, based on an ad hoc capable mesh network, such as WiMAX mesh mode, where users may connect to other users if they cannot establish a direct communication link to the base station with sufficient capacity. The proposed model also includes a parallel transmission scheduling model minimizing the interference, and optimizing the spectrum utilization in different locations of the network coverage area. The amount of retransmissions have been reduced considerably by utilizing spatial diversity. The number of users who can receive IPTV service has been increased significantly compared to a regular WiMAX PMP mode. Also, the proposed model can serve more subscribers than the regular WiMAX mesh mode.

The results presented are based on OPNET simulations for two cases, where the former uses a uniform probability distribution for IPTV channel switching by the users, and the latter uses a normal distribution taking the subscriber ratings of each IPTV channel into account.

3. CELL PLANNING IN WIRELESS NETWORKS USING 3D MAPS

Figure 3.1. 3D city map.

Wireless mobile networks are the current modern commercial infrastructures that provide voice communication and data transfer services ubiquitously and remotely over-the-air. Mostly used by mobile phones and smart phones, the mobile networks require precise radio infrastructure planning in a limited area. After obtaining the license of operation from the regulation authorities, a telecommunication operator company needs to plan the deployment of radio access network transmitters (e.g. base stations) on the specified area. The essential resource in commercial wireless communication is the limited radio frequency spectrum ranges allocated for the operator, which can be used simultaneously by mobile devices. Therefore, mobile networks require strict frequency and base station planning in urban areas. Since the allocated radio frequency ranges are so scarce, the mobile network operators have to reuse the given set of frequencies at different locations, and also reuse the sub-band frequency sets.

Every new generation of mobile network roll-out is a major upgrade to existing infrastructure components, if not a full network deployment right from scratch. As the new wireless network technology penetration gradually spreads over different urban areas around the globe, there is an opportunity to reuse the information from previous deployments, and even older wireless transmission technologies.

3.1. Background Information

Mobile network operators work hard to minimize the post-deployment efforts by using efficient initial deployment plans and simulations. Frequent redeployment and reconfiguration of network components such as base stations is required after deployment of a mobile network, since the initial planning process cannot properly estimate the entire physical effects of the actual environmental conditions on electromagnetic signals before deployment.

Electromagnetic signal propagation is a three dimensional phenomenon. Although radio waves are more resilient to obstacles compared to the light due to their respective natures, physical phenomena that alter the course and properties of light, such as reflection, refraction, scattering, interference, diffraction, transmission through different materials, or absorption can also alter the radio signals. For a preliminary design of a mobile network, a radio transmission for each carrier wave can be roughly modeled using multipath ray tracing methods and detailed 3D models of the environment.

3.1.1. Ray Tracing

The straightforward multipath ray tracing methods require precise 3D models of the area, including the finest details like sharp corners, construction material (e.g. metal/glass/concrete surfaces, roughness of the surfaces), moving vehicles, and details of all vegetation in order to calculate the diminishing effects of the environment [84]. Many propagation models like the Two-Ray Ground-Reflection Model [18] partially make use of ray-tracing functions for LoS transmissions with dominant nLoS ground reflected radio wave components [85].

Ray tracing methods are similar to the recursive illumination operations in 3D rendering processes within computer generated imagery (CGI) applications. CGI is a highly advanced and successful technology, as long as the entire 3D data is available to the application. The unique architecture and geography of each city requires 3D models to be revised continuously to predict a better deployment plan, and it will be almost impossible to provide the complete input data set. Even if the 3D input data set is provided, the computational complexity of ray tracing makes it infeasible for practical use in wide deployment areas. Unfortunately, using ray tracing on real world objects for signal propagation modeling is not a practical approach, considering the current state of the computation technology,

Radio signals attenuate by distance, even in space with no obstacles. Attenuation is a path-loss, or loss of signal strength, which is a function of distance. If the transmission is line of sight, i.e. there are no obstacles in between the transmitter and the receiver except the air, it is called "free space path loss". Signals that are attenuated too much cannot be detected or the information they carry cannot be extracted at the location of receivers. The obstacles in the course of radio waves cause even more attenuation, and for short range transmissions, multiple reflected signals of a single transmission can be detected by a receiver with a time shift, causing a multipath fading effect, distorting the communication. Such loss of signal strength has been studied as "Rayleigh fading" effect at short range transmissions [86].

Increasing the signal power, and using specially designed antenna technologies helps with less attenuation, but is not a solution to frequency limitation. Although transmissions with higher signal power levels theoretically have better probability of success in longer trajectories, they are more likely to cause interference to other transmissions, reducing the number of possible concurrent mobile communications.

3.1.2. Cellular Networks

The coverage of a base station can be expressed as the area (often referred to as a *cell*) that mobile devices can successfully communicate with the base station for voice and data services. The shape of this coverage area depends on the transmission power, antenna type, and obstacles in the area. The type of the antenna allows the base stations to efficiently reuse the available radio frequency spectrum in the cell area. For urban areas, the cell coverage is mainly reduced by the obstacles, i.e. buildings and large objects in the area. The larger the distance between the mobile device and the base station, the more transmission power is necessary for both the base station transmitter and the mobile device. On the other hand, increasing the power level more than an optimum value causes interference with other cells, reduces the overall number of simultaneous communications and results in loss of revenue. Also, increased distance between the mobile device and the base station will also cause the limited battery of the mobile to discharge too early.

The optimum size of a cell is the maximum distance that a base station can provide a healthy wireless service with minimum interference to other base stations. In addition to the speed of radio waves, there are strict computational timing issues in the infrastructure regarding the two-way communication between the base station and the mobile equipment, which also limits the maximum range of a mobile cell.

Wireless cellular networks provide better quality of service by using smart planning algorithms for radio network infrastructure. Multiple cells can collaborate to cover the licensed service area for providing ubiquitous mobile access. The number and locations of required base stations in a mobile network depends on mobile device usage profiles. For urban areas with higher population compared to the rural areas, the number of wireless communication requests per meter square is also higher. This demand can be fulfilled by smaller cells using lower transmission powers to prevent interference.

In order to serve larger number of mobile users, the network planning teams have to determine the potential coordinates of base stations for efficiently reusing the scarce radio frequency bandwidth at multiple locations. Anticipating the performance of the network before installing the components is a cost effective step in network planning. Radio access network planning requires estimations on both spatial capacity demands and wireless signal fading patterns. In order to deploy the infrastructure components efficiently, mobile network planning requires precise signal measurements from test base stations and a well analyzed site survey. However, without fading estimation models, it is nearly impossible to anticipate the signal propagation characteristics in urban areas having no previous deployment of a specific wireless network technology.

Each mobile network has the tools to monitor the propagation characteristics of wireless signals instantaneously. The efficiency of any urban area mobile cellular network can actually be calculated after deploying the physical network and measuring the received signal power all over that area precisely. The networks are mostly prone to fine tuning after the deployment process, which is initially based on a rough cellular plan in the area, and built upon some mathematical urban area signal propagation models.

Radio signal propagation and fading characteristics of the environment is a crucial parameter in cell planning. Signal propagation has been deeply analyzed since the discovery of radio communication. In order to fulfill the increasing demand in mobile communications, scientists have come up with many sophisticated mathematical and empirical radio propagation models, especially for urban areas with higher population. These models are useful in predicting the path-loss, or loss of strength, in radio waves under different environmental circumstances. They are used to estimate the behavior of radio waves under various environmental conditions such as distance, transmission height, weather, frequency, architecture, vegetation, etc., to estimate the received signal power levels with respect to the potential radio transmitter locations.

3.2. Literature Survey

For many earlier propagation models that are still in use today, the carrier waves are either the signals of radio and television broadcasting, or wireless communication links. Propagation models like Egli [19], and Longley-Rice [20] have been proposed in late 1950s as point-to-point LoS outdoor irregular terrain path loss models mainly for television broadcasting. Egli model can also be applied to cellular communication networks where a higher fixed antenna and a mobile antenna is involved in a transmission. On the other hand ITU terrain loss model [21, 22] was developed for nLoS transmissions, having obstacles in between the transmitter and the receiver. Since the signal components are those diffracted around the obstacles, this model is also applicable to urban cellular communications.

In addition to analytical models, some preliminary measurements can be taken from a deployment site by transmitting at multiple locations using nomadic base stations if necessary. Models such as the Young model for cities with many tall structures like skyscrapers [87], Lee model for area-to-area communications, and Lee model for point-to-point communications are empirical propagation models based on such measurements [23]. The Okumura radio propagation model is a similar measurement-based empirical model for fitting a path loss function to urban area measurements in cities with fewer tall structures like skyscrapers [24]. An improved version of the Okumura model is named as the Hata model for urban areas, which aims to model the multipath effects of diffraction, reflection, and scattering in cities [25]. Both Okumura and the inheriting Hata model have been modified for suburban and open area transmissions. Further improvement to Hata model has been developed as COST-Hata/COST-231/Hata-PCS Extension model for urban communications to model a wider range of operating frequencies [26]. Probabilistic models like the Nakagami-m distribution have also been developed for cellular communications in large cities [27].

The unique architecture and geography of each city requires propagation models to be revised continuously for more efficient deployment planning. For the empirical

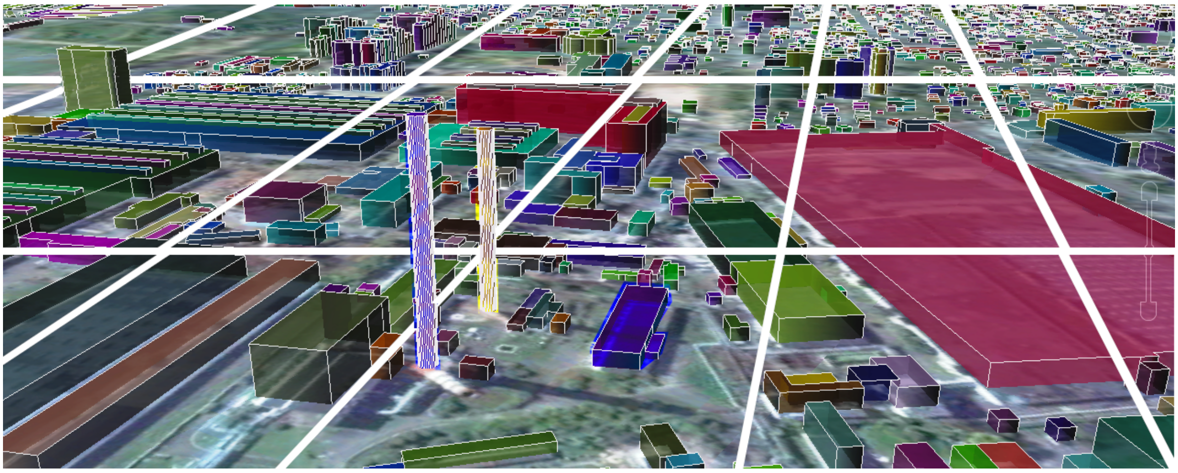

Figure 3.2. 3D city map data separated into local regions.

models, multiple rounds of signal measurement operations may have to be performed before deployment. However, this is a tedious, long, and costly process subject to legal constraints, such as the regulation for granting frequency allocation license when the planning team needs to operate on a frequency band that requires such a license [88]. Also, a long running measurement operation can compromise the business confidentiality of a planning process.

Many fading models assume homogeneous distribution of obstacles in between the transmitters and receivers. However, it is not possible to observe the same signal propagation conditions over an entire city area. There are local regions that have distinct characteristics based on the geographical and architectural structures like buildings, hills, lakes, rivers, parks, humidity, temperature, etc. Although any two cities are different in terms of architecture and overall signal propagation, there may be local regions that are somewhat similar to each other, exhibiting similar path loss characteristics.

3.3. MAPLE, Mixed Path Inspired Path Loss Estimation

In the second part of the thesis, we propose a model that can be used to generate local regions in urban areas, which can be used to estimate the signal propagation in other urban areas. The network coverage areas are divided into adjacent tile sections organized in a geographical grid (as shown in Figure 3.2 and Figure 3.9), including all

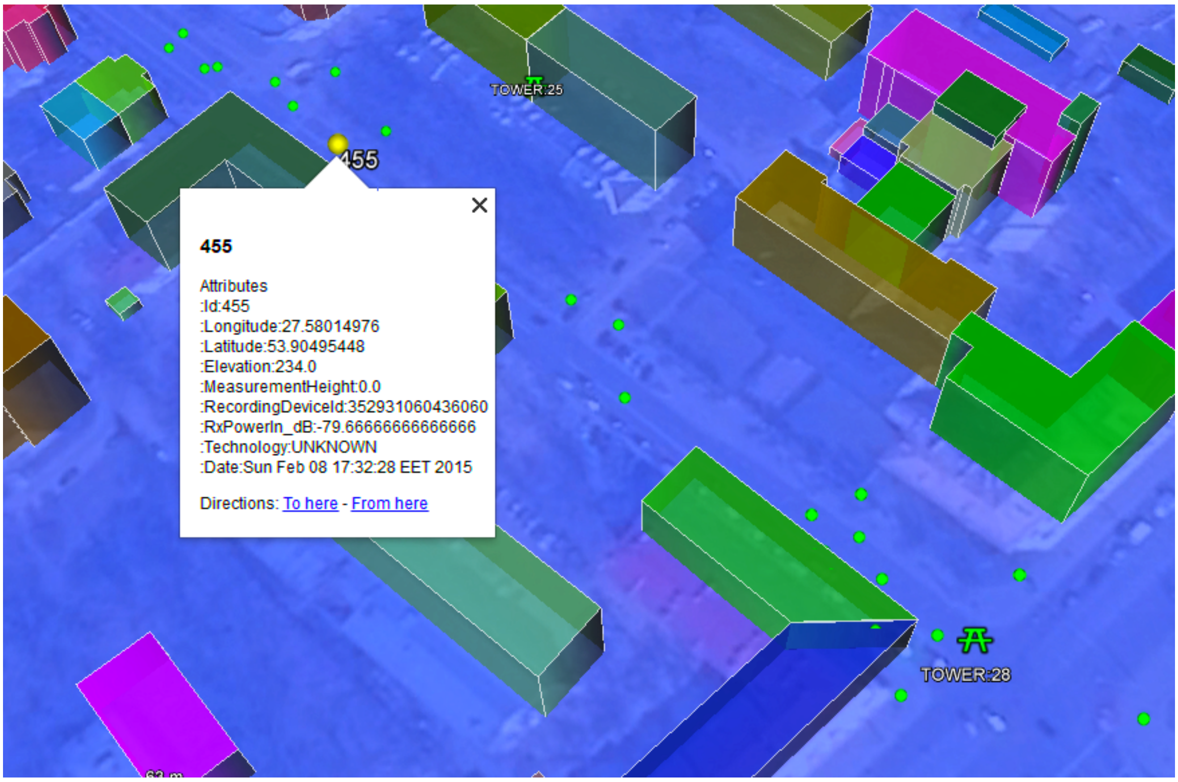

Figure 3.3. Towers and measurements on the 3D map.

3D structures on the tiles. Each tile section has a distinct set of physical properties that can be used to improve the precision of signal propagation models locally. The similarities between physical properties of section tiles are used to find out potential signal propagation models of future deployment areas, and to plan the locations of base stations more effectively, reducing the planning efforts and optimization costs.

The system is trained with signal measurements and propagation characteristics of multiple areas having similar cellular network technologies. Received power level at any signal measurement location is the result of a *mixed path* propagation that penetrates different artificial or natural structures, vegetation, and water bodies between the measurement point and the corresponding base station location. As a practical approach, it is simpler, cheaper, and more efficient to utilize a mixed-path LoS propagation approximation model and use the vast amounts of already available actual measured signal data from training areas having similar wireless mobile network technology that will be deployed to the new areas [28].

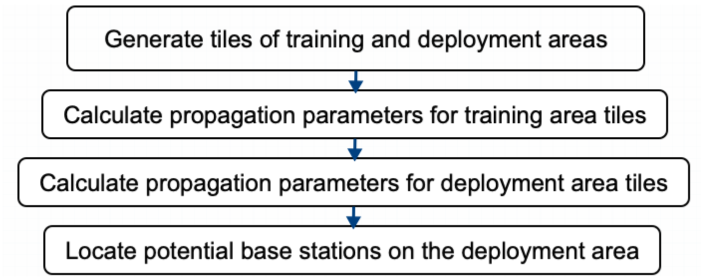

Figure 3.4. Main flow of MAPLE process.

The MAPLE process has four stages of execution as summarized in Figure 3.4.

The *first stage* generates the tiles of training and deployment areas, with the respective data set on physical properties (Section 3.3.1). A geographical grid structure, consisting of adjacent area tiles with equal longitudinal and latitudinal spans, is generated for the training and deployment areas. The flow in Figure 3.5 summarizes this step, and the details are provided with the flow in Figure 3.7.

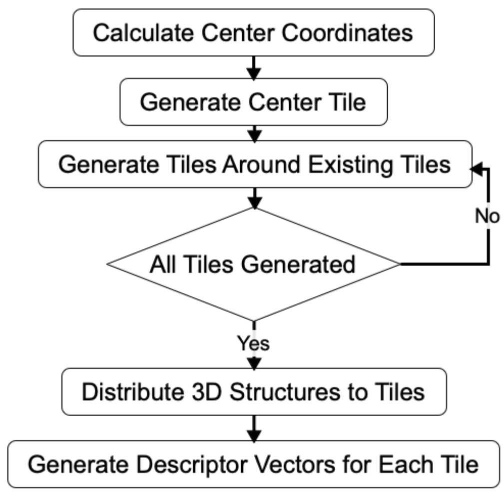

Figure 3.5. Tile generation flow of MAPLE process.

The *second stage* generates individual mixed path signal propagation parameters for the training area tiles ($\mathbb{T}_T$) using received signal power measurements of existing base stations, and the 3D map of the training area (Section 3.3.2). The tiles contain different 3D urban structures and have their own signal propagation characteristics. The signal propagation parameters of each tile are calculated with respect to the received signal level measurements at different locations on the grid. The LoS traces from all base stations to their measurements intersect one or more intermediate grid tiles, as shown in Figure 3.6. The measurements contribute to the calculation of signal propagation characteristics of all intermediate tiles by utilizing the proposed mixed path formulation.

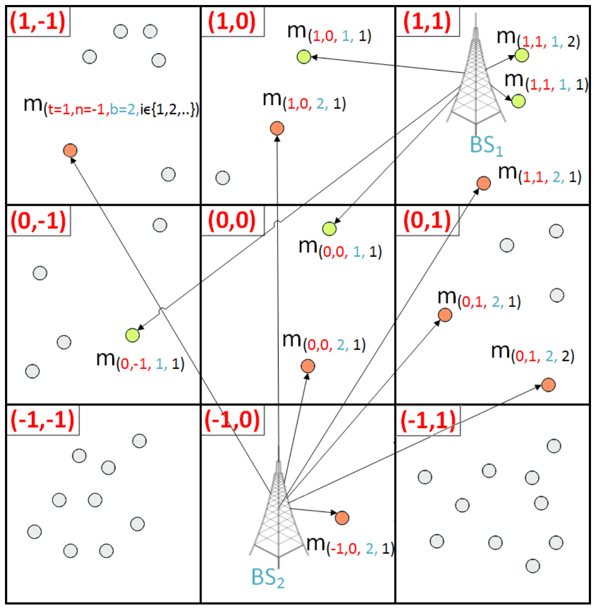

Figure 3.6. Base stations and measurements on the grid. Each measurement point is associated with the tile it is positioned in and the corresponding base station.

The *third stage* generates signal propagation parameters of the deployment area tiles ($\mathbb{T}_D$) as a weighted average of such parameters of the training area tiles (Section 3.3.3). The weights are calculated using a similarity function based on the structural and meteorological likeliness between the training and the deployment area tiles. The similarity of two tiles can be calculated as the reciprocal of the ℓ_2 norm of normalized descriptor parameter vectors of both tiles. The reference implementation of the proposed technique uses Log-Distance propagation model that can be applied to smaller cells using high frequency signals in crowded urban areas.

Given a set of high priority coverage points, and an optional set of existing base station locations at the deployment area, the *fourth stage* determines the locations of base stations in the deployment area, reusing the existing radio towers if available, and suggesting new tower locations if necessary (Section 3.3.4).

All operations can be repeated with modified input data to compare the effects of different situations such as a shifted base station location, additional high priority service point, modified tile size, and other parameters.

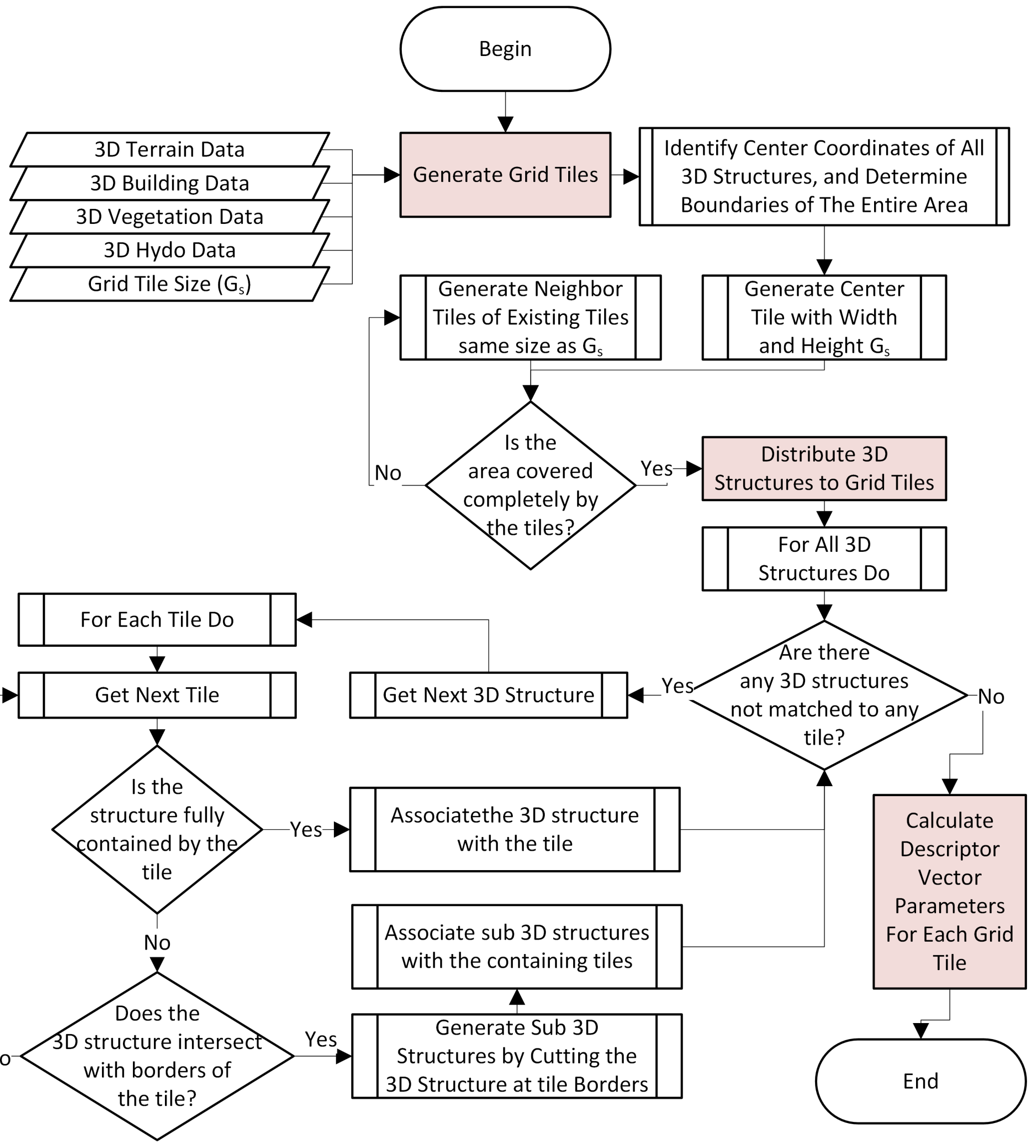

Figure 3.7. Generation details of grid tiles to cover the entire area of a mobile network.

3.3.1. Generating Tiles of 3D Maps

In order to help designing new wireless networks for deployment areas, the precision of propagation models approach can be improved by relating the 3D structural data with the signal measurements located at certain training areas, with existing cellular infrastructures. Locations of potential base stations at the deployment areas depend mainly on the 3D urban structures at the area and signal propagation characteristics of both training and deployment areas.

A set of input data such as tiles with 3D structures at the training and deployment areas, existing radio infrastructure information, and signal measurements of the training area is required for the proposed technique to operate as shown in Figure 3.7. Reusable tower locations at the deployment area can also be provided for more cost effective deployments. An application for Log-Distance propagation method has been implemented and tested with actual base stations measurement data [28].

3.3.1.1. Grid Structure. All training areas and deployment areas are bounded by individual convex polygons consisting of n corner points with spherical coordinates expressed as $C_i = (\varphi_i, \lambda_i)$ where $1 \leq i \leq n$, and $3 \leq n$. The variables φ_i and λ_i correspond to latitude and longitude values, respectively. The geographical center of the entire area, C_0, can be calculated as

$$C_0 = \{(\varphi_0, \lambda_0) | \varphi_0 = \frac{1}{n} \sum_{i=1}^{n} \varphi_i, \lambda_0 = \frac{1}{n} \sum_{i=1}^{n} \lambda_i\}. \tag{3.1}$$

Formation of the grid begins with the center tile $T_{(0,0)}$ (Figure 3.8) having its center coordinates located at $C_{(0,0)} = C_0$ of (3.1). The center coordinates of all tiles are calculated relative to $C_{(0,0)}$. The variable grid tile size G_s, measured in meters, is equal to the distance between north and south borders, and to the distance between east and west borders of $T_{(0,0)}$ across the center coordinates $C_{(0,0)}$. The number of tiles in the grid depends on the size of the area and G_s.

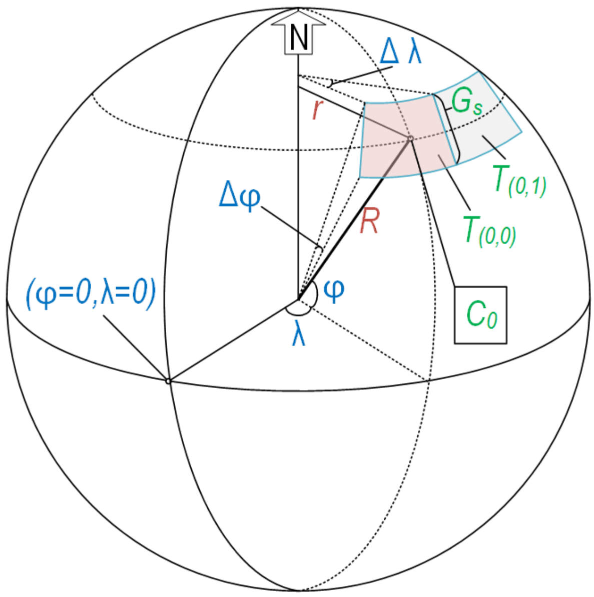

Figure 3.8. Tile positioning on the globe, showing the center tile $T_{(0,0)}$, and spherical coordinates corresponding to the middle of the center tile.

The north-south latitude span $\Delta\varphi$ and east-west longitude span $\Delta\lambda$ are calculated with respect to G_s on $T_{(0,0)}$. The values of $(\Delta\varphi, \Delta\lambda)$ are expressed in decimal degrees, e.g. (29.12345, 160.23455), and they are required for calculating the coordinates of all other tiles in the grid. Only tiles with the same size can be compared. The lengths of east and west borders of a tile are equal, but the lengths of north and south borders can differ especially in regions closer to the geographical poles.

The ratio of $\Delta\varphi$ to 1^o is equal to the ratio of G_s to the distance between each pair of successive major latitude arcs (3.2), which declines from 111,700 meters to 110,057 meters [89] while moving away from the equator towards both poles. Thereby, $\Delta\varphi$ can be calculated more precisely if that varying distance is included in the formula. Similarly, the ratio of $\Delta\lambda$ to 360^o is equal to the ratio of G_s to the perimeter of the latitudinal circle intersecting $C_{(0,0)}$, with a radius of $r = R\cos\varphi_0$, where R is the radius of the Earth (3.3).

$$\Delta\varphi = G_s/(111700 - (111700 - 110057)|\varphi_0|/90) \tag{3.2}$$

$$\Delta\lambda = G_s 360^o/(2\pi R\cos\varphi_0) \tag{3.3}$$

Equations 3.2 and 3.3 can also be used to calculate the change in latitude and longitude for a specific amount of displacement (e.g. G_s in this case) towards the poles or parallel to the Equator, respectively.

Each $T_{(t,n)}$ has four border arcs as east, west, north and south edges which can be represented as E_n, W_n, N_t, and S_t, respectively. The borders of any tile in the grid can be calculated using $\Delta\varphi, \Delta\lambda$, and tile neighborhood relation of the tile to the center tile.

$$N_t = \varphi_0 + t\Delta\varphi + \Delta\varphi/2 = \varphi_t + \Delta\varphi/2 \tag{3.4}$$

$$S_t = \varphi_0 + t\Delta\varphi - \Delta\varphi/2 = N_t - \Delta\varphi \tag{3.5}$$

$$E_n = \lambda_0 + n\Delta\lambda + \Delta\lambda/2 = \lambda_n + \Delta\lambda/2 \tag{3.6}$$

$$W_n = \lambda_0 + n\Delta\lambda - \Delta\lambda/2 = E_n - \Delta\lambda \tag{3.7}$$

Figure 3.9. Sample grid tile characteristics and propagation parameters.

3.3.1.2. Tile Neighborhood. The tiles in a grid are indexed as $T_{(t,n)}$ according to their relative position to $T_{(0,0)}$. Geographical center coordinates ($C_{(t,n)}$) of all $T_{(t,n)}$ can be calculated relative to the center tile as

$$C_{(t,n)} = \{(\varphi_t, \lambda_n) | \varphi_t = \varphi_0 + t\Delta\varphi, \lambda_n = \lambda_0 + n\Delta\lambda, t \in \mathbb{Z}, n \in \mathbb{Z}\}, \tag{3.8}$$

where the integers t and n stand for the latitudinal and longitudinal neighborhood stepping numbers in north-south and east-west directions, respectively. The ordering of the parameters is compliant with EPSG4326 [90] and ISO6709 [91] standards. $T_{(0,1)}$ is the eastern, $T_{(0,-1)}$ is the western, $T_{(1,0)}$ is the northern, and $T_{(-1,0)}$ is the southern adjacent neighbors of $T_{(0,0)}$, as shown in Table 3.1.

Table 3.1. Grid tile addressing (Northern tiles on top).

$T_{(3,-2)}$	$T_{(3,-1)}$	$T_{(3,0)}$	$T_{(3,1)}$	$T_{(3,2)}$
$T_{(2,-2)}$	$T_{(2,-1)}$	$T_{(2,0)}$	$T_{(2,1)}$	$T_{(2,2)}$
$T_{(1,-2)}$	$T_{(1,-1)}$	$T_{(1,0)}$	$T_{(1,1)}$	$T_{(1,2)}$
$T_{(0,-2)}$	$T_{(0,-1)}$	$\mathbf{T_{(0,0)}}$	$T_{(0,1)}$	$T_{(0,2)}$
$T_{(-1,-2)}$	$T_{(-1,-1)}$	$T_{(-1,0)}$	$T_{(-1,1)}$	$T_{(-1,2)}$
$T_{(-2,-2)}$	$T_{(-2,-1)}$	$T_{(-2,0)}$	$T_{(-2,1)}$	$T_{(-2,2)}$
$T_{(-3,-2)}$	$T_{(-3,-1)}$	$T_{(-3,0)}$	$T_{(-3,1)}$	$T_{(-3,2)}$

3.3.1.3. 3D Structures on Tiles. All buildings, vegetation areas, water areas, and elevation profiles are associated to the grid tiles that they overlap with. If a 3D structure does not fit inside a single tile, it is split into substructures at the borders of the adjacent tiles involved, and the substructures are associated with the corresponding tiles as shown in Figure 3.10 and Figure 3.11.

Figure 3.10. 3D structures associated with the bounding tiles.

3.3.1.4. Descriptor Vectors of Grid Tiles. For each tile $T_{(t,n)}$ in the grid, a specific data set $V_{(t,n)}$ (3.9) is populated with characteristic properties based on the elevation profile, associated 3D structures, climate, and atmospheric conditions. $V_{(t,n)}$ can be defined as

$$V_{(t,n)} = (v_1, ..., v_k), \tag{3.9}$$

where k is the descriptor vector length determined by the number of descriptor parameters to be considered and v_i is a real number between zero and one for $1 \leq i \leq k$. Each v_i corresponds to a physical or statistical property within $T_{(t,n)}$ such as:

- Mean and standard deviation of altitude for all terrain points
- Number of buildings between 5m to 10m, 10m to 30m, 30m to 60m, and more than 60m tall
- Mean and variance of the distances between the buildings
- Spacing between the buildings that are in LoS view of each other at 5m, 10m, 30m, and 60m or more meters from the ground
- Mean and standard deviation of base areas, heights, and volumes of buildings
- Percentages of the area of water bodies and vegetation
- Numbers of the water bodies and vegetation areas, etc.

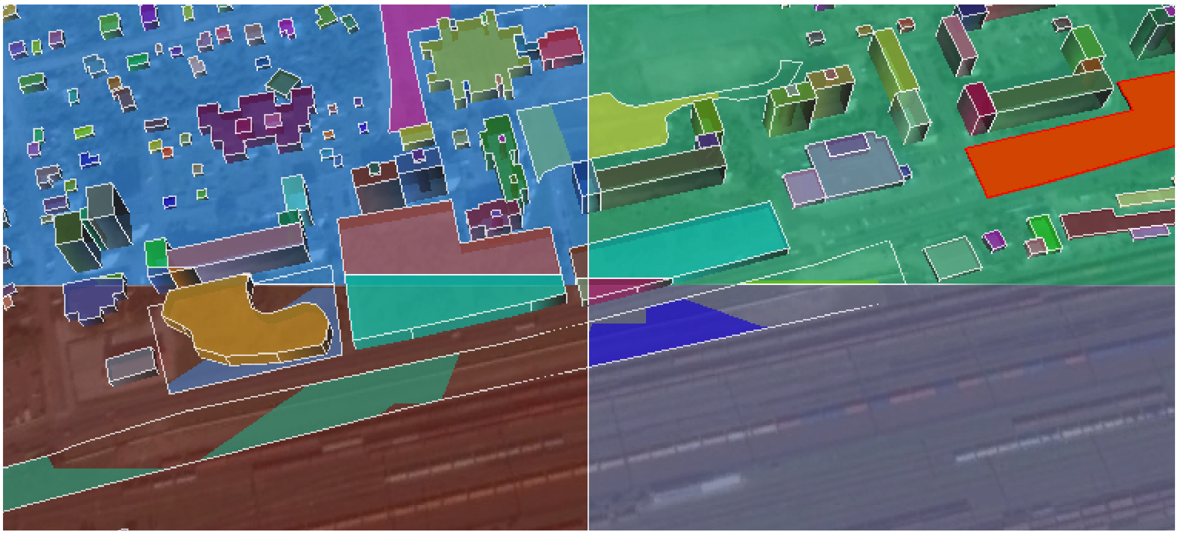

Figure 3.11. 3D structure splitting at tile borders, where any structure exceeding the boundary of any tile tile is split into sub structures that are positioned on the neighboring tiles.

All v_i values are normalized separately considering all tiles. $\mathbb{V}_T = \{V_{(t,n)} | T_{(t,n)} \in \mathbb{T}_T\}$ and $\mathbb{V}_D = \{V_{(t,n)} | T_{(t,n)} \in \mathbb{T}_D\}$ are the sets of descriptor vectors for corresponding tiles $T_{(t,n)}$ of training and deployment areas, respectively.

There are 116 distinct descriptors for each tile, and the entire list of descriptor vector fields are listed in APPENDIX A. Some of the major structural vector elements can be listed as follows: *tile area, lowest point above sea level, mean altitude of points above sea level, mean altitude of points above ground level, building base area ratio below 5 meters, building base area ratio between 5 to 10 meters, building base area ratio between 10 to 30 meters, building base area ratio between 30 to 60 meters, building base area ratio above 60 meters, building count below 5 meters, building count between 5 to 10 meters, building count between 10 to 30 meters, building count between 30 to 60 meters, building count above 60 meters, mean building base area, mean building height, mean building volume, building density, water body density, green space density, water body area percentage, water body count, vegetation area percentage, vegetation area count.* A sample group of descriptor vectors is provided in Table 3.2, where each value corresponds to the share of each item on the surface area.

Table 3.2. Sample descriptor vectors for different tiles, showing normalized values of total surface share for each type of obstacles in the given environment.

Tile Details	Tall Buildings	Short Buildings	Parks	Lakes, Pools
City Center	0.87	0.10	0.02	0.01
Suburbs	0.02	0.61	0.30	0.07
Industrial Area	0.03	0.70	0.20	0.07
Green Areas	0.00	0.13	0.67	0.20

3.3.1.5. Similarity of Grid Tiles. The ℓ_2 norm distance calculation between two tiles T and $T^{'}$, based on their individual descriptor vectors, is

$$\ell_2(V, V^{'}) = ||V - V^{'}||_2 = \sqrt{\sum_{i=1}^{|V|} (v_i - v_i^{'})^2}. \tag{3.10}$$

If an ℓ_2 calculation is required for multiple sets of V_j within any tile comparison process, then all v_i corresponding to a specific property at position i of the vectors are normalized, i.e. $\forall(i, V_j)$ each $v_i \in V_j$ is scaled into $[0, 1]$ with respect to the maximum value of v_i in all vectors V_j for all tiles involved.

After evaluating descriptors of the tiles, the similarity of two tiles, T and $T^{'}$, is denoted by $s(T, T^{'})$ and evaluated as

$$s(T, T^{'}) = 1/\ell_2(V, V^{'}) = \frac{1}{\sqrt{\sum_{i=1}^{|V|} (v_i - v_i^{'})^2}} \tag{3.11}$$

where V and $V^{'}$ stand for the normalized descriptor vectors of the tiles T and $T^{'}$, respectively, and $\ell_2(\cdot, \cdot)$ is the ℓ_2-norm.

3.3.1.6. Base Stations and Signal Measurements. The proposed model analyzes the received signal power levels of the set of base stations B in the areas involved, where $B = \{b|b$ is a base station located at $(\varphi_b, \lambda_b)\}$. Several measurements throughout the grid for a base station b are required by the model to operate properly.

The set of all base stations located inside a tile segment $T_{(t,n)}$ centered at (φ_t, λ_n), is $B_{T_{(t,n)}} = \{b|b$ is a base station located at (φ_b, λ_b), where $\varphi_t - \Delta\varphi/2 < \varphi_b \leq \varphi_t + \Delta\varphi/2$, and $\lambda_n - \Delta\lambda/2 < \lambda_b \leq \lambda_n + \Delta\lambda/2\}$.

The set of all measurements located inside $T_{(t,n)}$ associated with a base station b is $M_{(T_{(t,n)},b)} = \{m_{(T_{(t,n)},b,i)}|m$ is the i^{th} signal measurement inside $T_{(t,n)}$ associated with b located at (φ_m, λ_m), where $\varphi_t - \Delta\varphi/2 < \varphi_m \leq \varphi_t + \Delta\varphi/2$, and $\lambda_n - \Delta\lambda/2 < \lambda_m \leq \lambda_n + \Delta\lambda/2$ $\}$.

Additionally, $B = \bigcup_{T_{(t,n)}} (B_{T_{(t,n)}})$, $M_b = \bigcup_{T_{(t,n)}} (M_{(T_{(t,n)},b)})$, and $M_{T_{(t,n)}} = \bigcup_{b \in B} (M_{(T_{(t,n)},b)})$, where M_b is the set of all measurements in the entire network area associated with a base station b.

The similarity between the 3D structures of intermediate grid tiles and signal attenuation over the course of LoS trace is a key factor for determining the propagation parameters of the selected path loss model for all $T_{(t,n)}$. Using several measurements of each base station around its radial axis within practical maximum transmission range, it is possible to estimate propagation parameters for the tiles that lie between the measurements and their corresponding base stations. Only the training area regions are required to contain base stations and their measurements.

3.3.1.7. Signal Paths at Training Areas and Deployment Areas. Instead of using the same set of propagation parameters throughout the entire area, isolated individual parameters are evaluated by utilizing mixed-path model and the tile properties for each tile, thereby increasing the precision of the selected propagation model. As part of the approximation model, the LoS path of each measurement may span more than

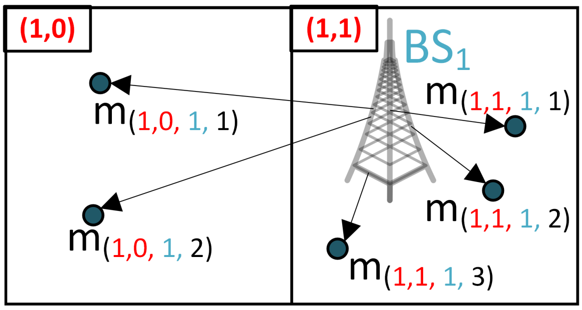

Figure 3.12. Measurements of a base station, indexed according to the tile and the BS.

one tile, depending on tile size G_s, and the locations of the base station and the measurement point. Each actual measurement at the training site contributes to the calculation of the signal propagation parameters of all tiles intersected by the LoS path between the measurement location and the corresponding base station location. The actual nLoS paths of the measurements are implicitly approximated by the calculations of the remaining measurements and tile propagation parameters.

Tile propagation parameters can be calculated by making use of every single measurement that has a signal path crossing that specific tile. Therefore, the tile parameters are dependent on parameters of other tiles as well. For a signal originating from a base station in a certain tile, the received power at the measurement point in another tile is a result of gradual attenuation at varying levels according to the individual propagation parameters (γ, P_{L_0}) of each intermediate tile.

<u>3.3.1.8. Log-Distance Propagation Model.</u> The Log-Distance propagation model has been used in the reference implementation of the MAPLE model, since it is an adjustable propagation model that can be applied both to indoor and crowded outdoor environments requiring smaller cells for with frequency signals in urban areas [29]. The Log-Distance model requires a pair of γ and P_{L_0} parameters as the path-loss exponent and the path-loss at reference distance, respectively. Instead of using a single pair of parameters for the entire city, the proposed MAPLE model calculates γ and P_{L_0} parameters for each tile and the base station pair by using the transmit power of the

given base station (P_{Tx}), the received signal power levels ($P_{Rx,i}$) from n distinct measurement locations in the given tile (each with a distance of d_i to the base station), and the mixed path calculation given in Section 3.3.2.

If we focus only on a single base station and the measurements without considering the tile structures, the resulting measurements exhibit Log-Distance propagation model, and the approximate $P_{Rx,i}$ is given as

$$P_{Rx_{dBm},i} \approx P_{Tx_{dBm}} - P_{L_0} - 10\gamma \log_{10} d_i \, . \tag{3.12}$$

The terms in (3.12) can be rearranged into a matrix form for n measurements as given in (3.13):

$$\overbrace{\begin{bmatrix} P_{Tx_{dBm}} - P_{Rx_{dBm},1} & -1 \\ P_{Tx_{dBm}} - P_{Rx_{dBm},2} & -1 \\ \vdots & \vdots \\ P_{Tx_{dBm}} - P_{Rx_{dBm},n} & -1 \end{bmatrix}}^{A_{n\times 2}} \overbrace{\begin{bmatrix} \frac{1}{10\gamma} \\ \frac{1}{10\gamma} P_{L_0} \end{bmatrix}}^{\theta_{2\times 1}} \approx \overbrace{\begin{bmatrix} log_{10} d_1 \\ log_{10} d_2 \\ \vdots \\ log_{10} d_n \end{bmatrix}}^{D_{n\times 1}} \tag{3.13}$$

In order to solve (3.13) for θ, the least squares method $\min_\theta ||A\theta - D||_2$ is used as a best-fit solution. The solution that minimizes the sum of squared errors becomes $\hat{\theta} = A^+ D$, where A^+ is the Moore-Penrose pseudo-inverse of A [92].

3.3.2. Mixed Path Calculation at a Training Site

Propagation parameters of each training area tile T and a base station b are calculated in three steps. The ultimate goal is to isolate the propagation parameters that are specific to the given T. The first and second steps generate prime (γ', P'_{L_0}) and double prime (γ'', P''_{L_0}) parameters, respectively. The third step generates the hat parameters $(\hat{\gamma}, \hat{P}_{L_0})$ as a weighted average of double prime parameters of that tile. The received power of a signal is estimated by the mixed path attenuation model and the propagation parameters of the intermediate tiles that are evaluated in three steps.

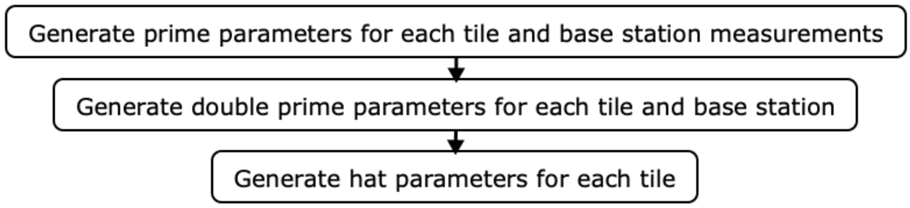

Figure 3.13. Propagation parameters calculation of training area tiles.

3.3.2.1. First Step. The *first step* assumes that the entire area has the same channel parameters with the tile of measurement while solving (3.13) for a given tile T and the base station b that has measurements in T. To solve (3.13) for a given T and b, we use the least squares method since we assume the entire area has the same channel parameters with T. The solution yields to $(\gamma'_{(T,b)}, P'_{L0(T,b)})$ for each T and b. However, the signaling path passes through some intermediate tiles in some cases.

3.3.2.2. Second Step. The *second step* aims to isolate the effect of intermediate tiles and find the tile-specific channel parameters by using mixed path formulation in a novel way. The received signal level is a result of mixed path propagation that penetrate different artificial or natural structures, organisms, and vehicles. The MAPLE method divides the service area with all its 3D structures (Fig. 1.2) into a group of regular adjacent grid tiles and identifies the signal propagation characteristics of each tile area with respect to all base stations and corresponding signal measurements. These propagation characteristics can then be used to improve the precision of signal propagation models at the site of a new network.

While evaluating double prime parameters of a given T and b, if the tile of b is same with T, then the solution in *first step* is exactly the tile-specific parameters and there is no need to consider mixed path model since there are no intermediate tiles on the signal path (i.e., the signal path is within a single tile). Therefore, the tiles are

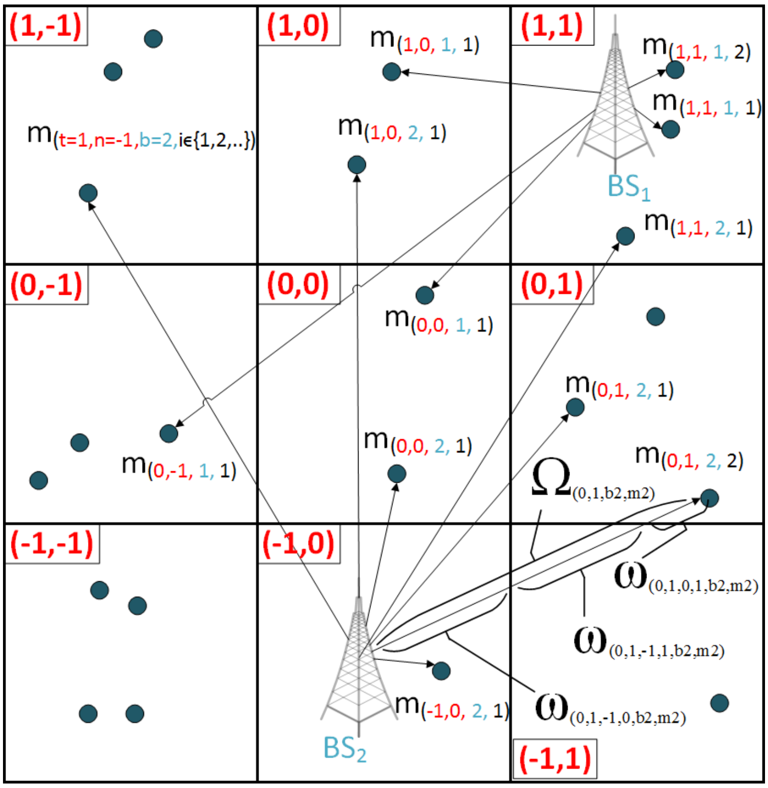

Figure 3.14. Base stations and measurements on the grid. LoS paths are divided into path segments intersecting different tiles, to be used for estimating the tile specific channel parameters based on mixed path propagation. Example path between a measurement point m in tile T and base station b ($\Omega_{(T,b,m)}$) and path segments ($\omega_{(T,T_i,b,m)}$) passing from intermediate tiles are also shown.

ordered according to their distances to b, and (γ'', P''_{L0}) parameters of the closer tiles are calculated before the others. In Figure 3.15 and Table 3.3, an example sequence of tiles is shown where the tile marked with 1 is the tile of b.

To evaluate the $(\gamma''_{(T_i,b)}, P''_{L0(T_i,b)})$ parameters, the mixed path-inspired relationship between the parameters $(\gamma'_{(T,b)}, P'_{L0(T,b)})$ and $(\gamma''_{(T_i,b)}, P''_{L0(T_i,b)})$ is given as

$$\begin{bmatrix} \gamma'_{(T,b)} \\ P'_{L0(T,b)} \end{bmatrix} = \sum_{T_i} \left(W_{(T,T_i,b)} \begin{bmatrix} \gamma''_{(T_i,b)} \\ P''_{L0(T_i,b)} \end{bmatrix} \right) \tag{3.14}$$

where T_i represents an intermediate tile between the signaling path from b to tile T, and $W_{(T_i,b)}$ represents the weight for the double prime parameters. The weights are calculated with the idea of mixed path model [21] as

$$W_{(T,T_i,b)} = \frac{\sum\limits_{m \in M_{(T,b)}} |\omega_{(T,T_i,b,m)}|}{\sum\limits_{m \in M_{(T,b)}} |\Omega_{(T,b,m)}|} \tag{3.15}$$

where $|\cdot|$, $M_{(T,b)}$, $\Omega_{(T,b,m)}$, and $\omega_{(T,T_i,b,m)}$ represent the length operator, the set of measurement points in tile T associated with the base station b, path between a measurement point m in tile T and base station b, and the path segment passing through the intermediate tile T_i (Figure 3.14), respectively.

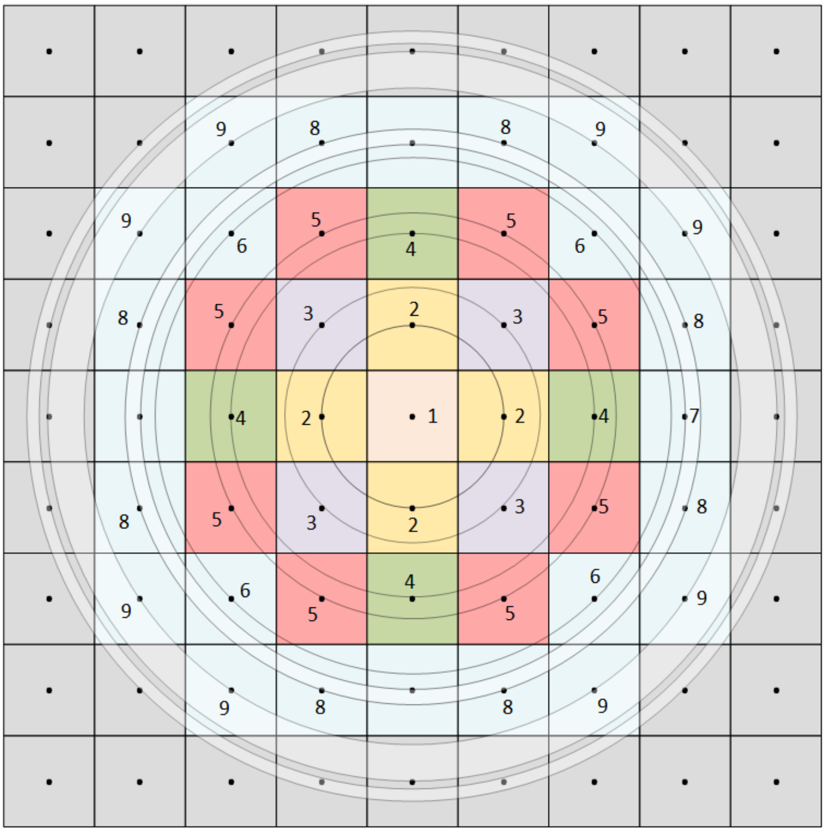

Figure 3.15. Radial grid tile visiting order starting from the tile of b (center tile). For the second step calculations and for the given base station b, the calculation order starts with the tile marked with 1 (i.e., the tile of b) and then continues with the tiles that are marked with 2 and so on.

Since the double prime parameters of tiles are calculated in an order with respect to the distance to b, we start with the tile of b, and there are no intermediate tiles in this case. Therefore, $(\gamma''_{(T,b)}, P''_{L0(T,b)}) = (\gamma'_{(T,b)}, P'_{L0(T,b)})$ for the tile of b. For the next tile, the intermediate tiles can be a subset of tiles from the previously evaluated ones (i.e., if the distance based order is followed, the required double prime parameters would be already evaluated for the intermediate tiles).

Table 3.3. Tile ordering for parameter calculation, the tile marked with "1" is a tile where a base station is located. The ordering sequence is regenerated during individual parameter generation process of each tile.

				10				
	11	9	8	7	8	9	11	
	9	6	5	4	5	6	9	
	8	5	3	2	3	5	8	
10	7	4	2	1	2	4	7	10
	8	5	3	2	3	5	8	
	9	6	5	4	5	6	9	
	11	9	8	7	8	9	11	
				10				

At this step, we reach a parameter set $(\gamma''_{(T,b)}, P''_{L0(T,b)})$ for each tile and base station pair. The main goal of the next step is to average the base station effect out and reach the tile-specific channel parameters $(\widehat{\gamma}_{(T)}, \widehat{P}_{L0(T)})$.

3.3.2.3. Third Step. Any LoS path $\Omega_{(T,b,m)}$ may span multiple intermediate tiles T_i having (γ'', P''_{L_0}) parameters calculated for b at the second step (Figure 3.14). A secondary received power $P''_{Rx(T_i,b,m)}$ can be calculated by (3.16) at the location of each $m_{(T,b,i)}$ (the i^{th} measurement of base station b, located in tile T), as if the entire LoS path of length $|\Omega_{(T,b,m)}| = d_{(b,m)}$ were crossing an area with propagation parameters equal to those of the intermediate tile T_i.

$$P''_{Rx(T_i,b,m)} = P_{Tx(b)} - P''_{L0(T_i,b)} - 10\gamma''_{(T_i,b)} \log_{10} d_{(b,m)} \tag{3.16}$$

We model the received power ($\widehat{P}_{Rx(b,m)}$) at a measurement point as the weighted sum (3.17) of all calculations from (3.16) proportional to the ratio of length of the path segment $\omega_{(T,T_i,b,m)}$ to the length of the total path, $\Omega_{(T,b,m)}$.

$$\widehat{P}_{Rx(b,m)} = \sum_{T_i} \left(\frac{|\omega_{(T,T_i,b,m)}|}{|\Omega_{(T,b,m)}|} P''_{Rx(T_i,b,m)} \right) \tag{3.17}$$

A mean squared error for each tile T with respect to any b can be calculated as the average of the sum of squares of differences between actual ($P_{Rx(b,m)}$) measurement values and the calculated ($\widehat{P}_{Rx(b,m)}$) values, as in (3.18):

$$\varepsilon_{(T,b)} = \frac{1}{|M_{(T,b)}|} \sum_{m \in M_{(T,b)}} \left(P_{Rx(b,m)} - \widehat{P}_{Rx(b,m)} \right)^2 \tag{3.18}$$

Hat parameters ($\widehat{\gamma}_{(T)}$, $\widehat{P}_{L0(T)}$) are weighted averages of all double prime parameters at a tile T, which were calculated for multiple base stations. Within the training data, the weight for double prime parameters is considered to be inversely proportional to the error factor of the corresponding base station, on that specific tile. Therefore, ($\widehat{\gamma}_{(T)}$, $\widehat{P}_{L0(T)}$) can be calculated as

$$\begin{bmatrix} \widehat{\gamma}_{(T)} \\ \widehat{P}_{L0(T)} \end{bmatrix} = \frac{\sum_b \left(\frac{1}{\varepsilon_{(T,b)}} \begin{bmatrix} \gamma''_{(T,b)} \\ P''_{L0(T,b)} \end{bmatrix} \right)}{\sum_b \frac{1}{\varepsilon_{(T,b)}}}. \tag{3.19}$$

3.3.3. Mixed Path Calculation at a Deployment Site

For any deployment area tile $T_D \in \mathbb{T}_D$, propagation parameters $(\tilde{\gamma}_{(T_D)}, \tilde{P}_{L0(T_D)})$ can be calculated as a weighted average of hat parameters of training area tiles $T_T \in \mathbb{T}_T$. The similarity values in (3.11) are the weights for $\widehat{\gamma}_{(T_T)}, \widehat{P}_{L0(T_T)}$, as in

$$\begin{bmatrix} \tilde{\gamma}_{(T_D)} \\ \tilde{P}_{L0(T_D)} \end{bmatrix} = \frac{\sum\limits_{V_{T_T} \in \mathbb{V}_T} \left(s(V_{T_T}, V_{T_D}) \begin{bmatrix} \widehat{\gamma}_{(T_T)} \\ \widehat{P}_{L0(T_T)} \end{bmatrix} \right)}{\sum\limits_{V_{T_T} \in \mathbb{V}_T} s(V_{T_T}, V_{T_D})} \tag{3.20}$$

where V_{T_D} and V_{T_T} are the descriptor vectors of the tiles T_D in the deployment area and T_T in the training area, respectively.

3.3.4. Base Station Location Estimation at a Deployment Site

The deployment area radio transmitter locations are determined based on the received signal level at the high priority coverage points $P = \{p_{(\varphi,\lambda)} | p$ is a point located at $(\varphi_p, \lambda_p)\}$ identified by the planners for better coverage to serve the platinum customers, i.e., the subscribers who are expected to adopt the newly deployed technology earlier. A point $p_{(\varphi,\lambda)}$ corresponds to any location that has to be covered by a potential new deployment at the deployment area. In order to minimize the cost of new cellular networks, operators can determine certain coordinates based on population, time of day, customer segmentation, etc. Deployment area signal propagation parameters and existing base station locations can be used to enhance the planning process if available.

In order to start covering the desired locations with a minimum received signal level constraint, the median location for all points is determined. If any existing base station can provide coverage with minimum allowed power level at that the point closest to the median, then that base station location is selected as a potential site with power, infrastructure, and legal agreements, etc. for the new network plan, and all other high priority points that can be covered by that base station are marked as covered. The process is repeated as long as either there are no uncovered high priority points left, or no other existing base stations can be found, or no other existing base stations can provide strong enough coverage at remaining high priority points.

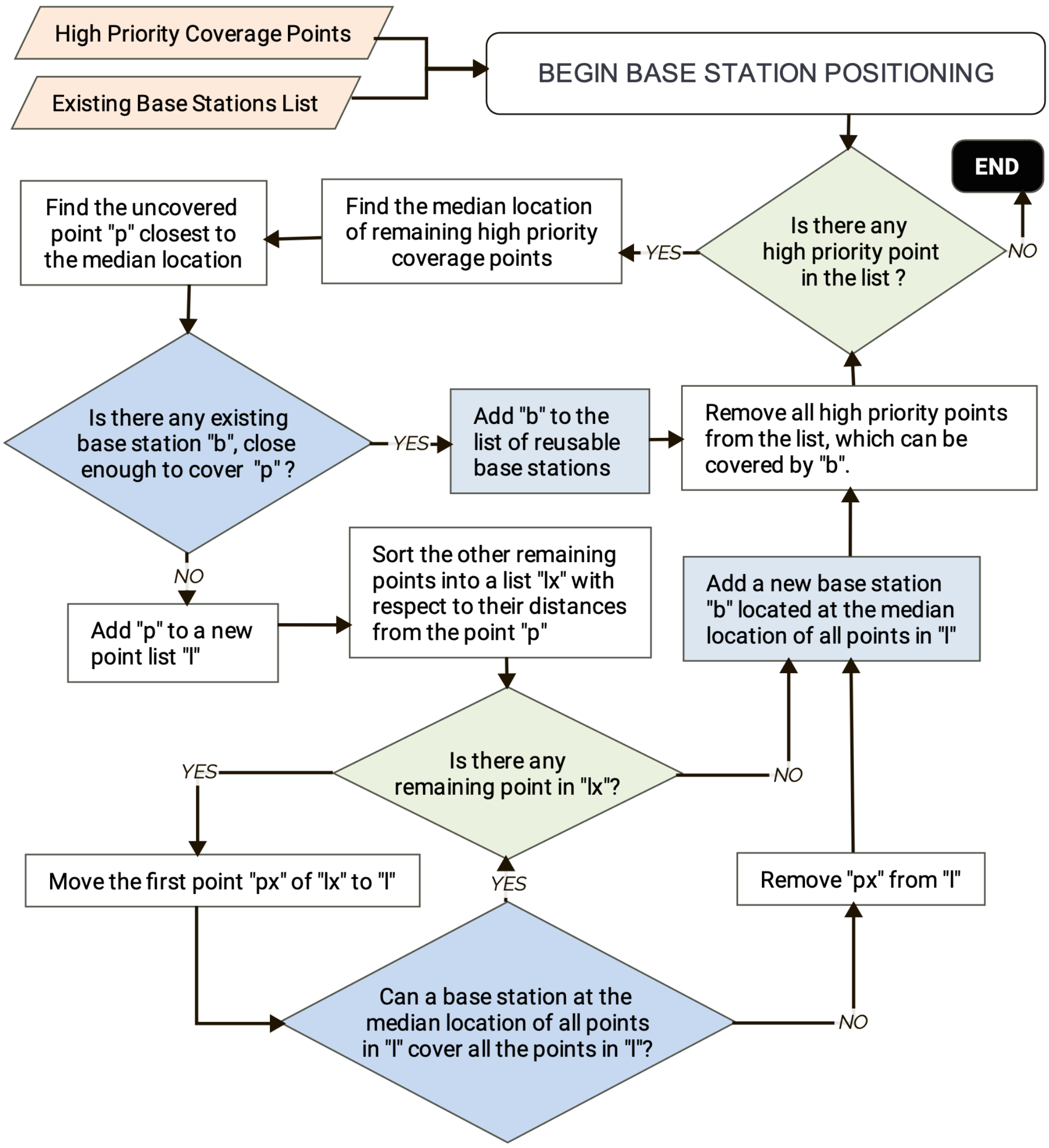

Figure 3.16. Reuse of existing base stations, and addition of new base stations in the deployment area.

If there are any high priority points left uncovered, then the process starts adding new base stations at the median location of all points it can provide strong enough signal coverage, starting with the coverage point closest to the median of all uncovered high priority points. The detailed flow of the algorithm is given in Figure 3.16.

3.4. Experiments and Results

The research presented in this part of the thesis has been funded by a private telecommunications company, and the proposed method has been tested with actual 3D maps and signal measurements of two cities in Europe. The cities are named as B and M in short, and they are 300 km apart from each other. Obtaining such a set of actual measurements is a costly process and requires permission from the network operator. A subset of the actual network data has been used for testing purposes since all installed base stations as well as signal measurement data are limited and commercially confidential, containing information such as the coverage status of the current operator.

The validation is performed with respect to actual real life signal measurement values, rather than a mathematical distribution. In order to validate the results of the method entirely with actual signal values, two major test setups have been prepared. In the first setup, city B has been used as the training area and city M as the deployment area, where the actual measurements of the deployment area are used as high priority coverage points in order to validate the calculated signal power levels at those locations. In the second setup, city M has been used as the training area and city B as the deployment area. Similarly, the measurements of city B are used for validation.

In addition to the major test scenarios where the entire set of real signal measurements have been used for training, 10 more secondary training areas are generated using cross-validation. Each one of the secondary training areas is generated by discarding a different set of training area measurements consisting of 20% of all training area measurements. The entire set of actual measurements of the deployment cities have been used for validation in each one of the 12 cases. The results in this section indicate the average values of all 12 test and validation cases. Also each one of the 12 cities has been tested against tile sizes of 1000, 800, 600, 400, 300, and 200 meters, providing a total of 72 different test cases.

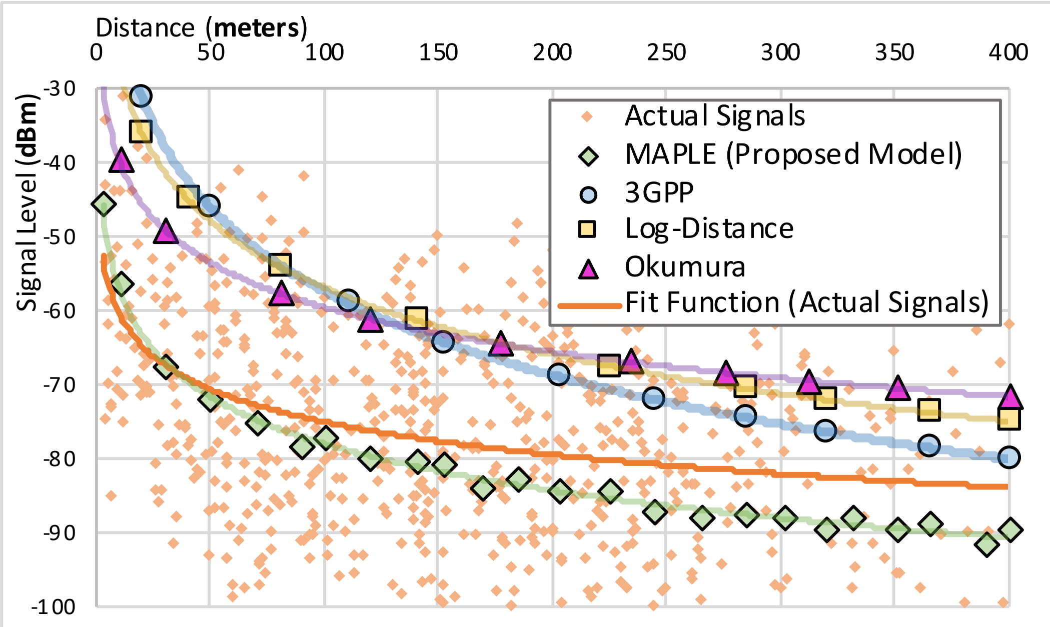

Figure 3.17. Signal level estimation at the deployment area with $G_s = 200m$.

Figure 3.17 shows the signal estimation on the deployment cities, as dBm vs distance(m), for tile size of 200m. The fit function of actual measurements is $y = -6.39 \ln(x) - 45.72$.

For providing a fair and reasonable evaluation, the pair of regular Log-Distance parameters yielding the least Root Mean Squared Error (RMSE) [93] with respect to actual measurements on the training area has been selected. The set of parameters used is given as $\{(\gamma, P_{L_0}) | 1.5 \leq \gamma \leq 3, \text{and } 0 \leq P_{L_0} \leq 30\}$, where the parameter values in the set converge to actual measurements. Then, the selected pair is applied to the deployment area, and the calculated signal level results are compared to that of the results of the proposed MAPLE method. At each test setup, the RMSE and Normalized Mean Squared Error (NMSE) between the actual signal levels and the calculated signal levels of MAPLE method have been compared to the RMSE and NMSE values of regular Log-Distance, 3GPP, and Okumura propagation models. Calculations for all measurement points in the deployment site, and Log-Distance Best Fit Parameters are provided in Table B.2 of APPENDIX B.

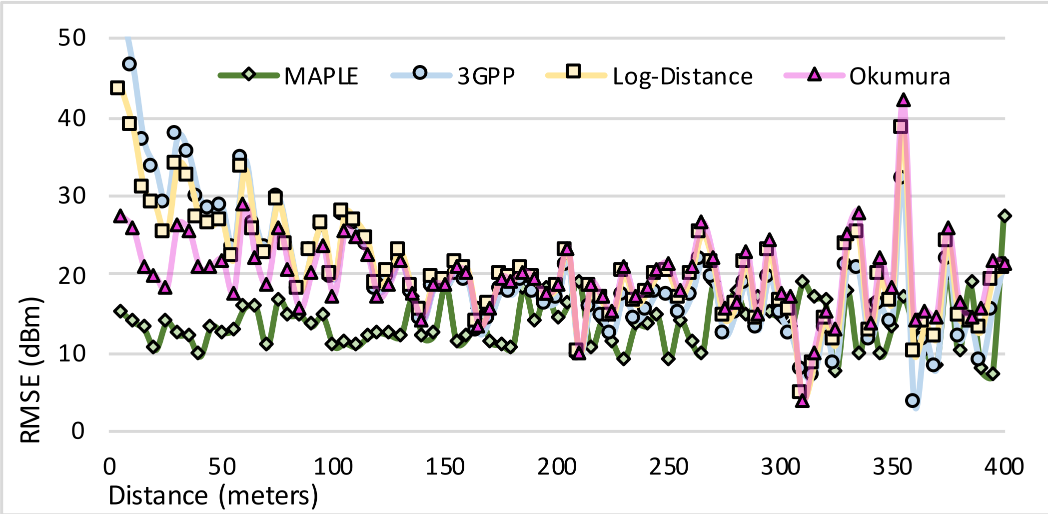

Figure 3.18. Average RMSE with respect to actual signal levels.

All propagation models have been also tested against the fitting curve of the actual measurements to eliminate the fluctuation of measurements at similar distances. Figure 3.18 and Figure 3.19 show the RMSE values of the propagation models with respect to the actual signal measurements, and the logarithmic fit function of the actual measurements, respectively. The MAPLE model performs significantly better compared to the generic propagation models including Log-Distance model, considering the average trendline of actual measurements. The tile size used in the plots is 200 meters, which is the smallest size that can be used to generate reasonable tiles depending on the distribution of the current set of actual measurements.

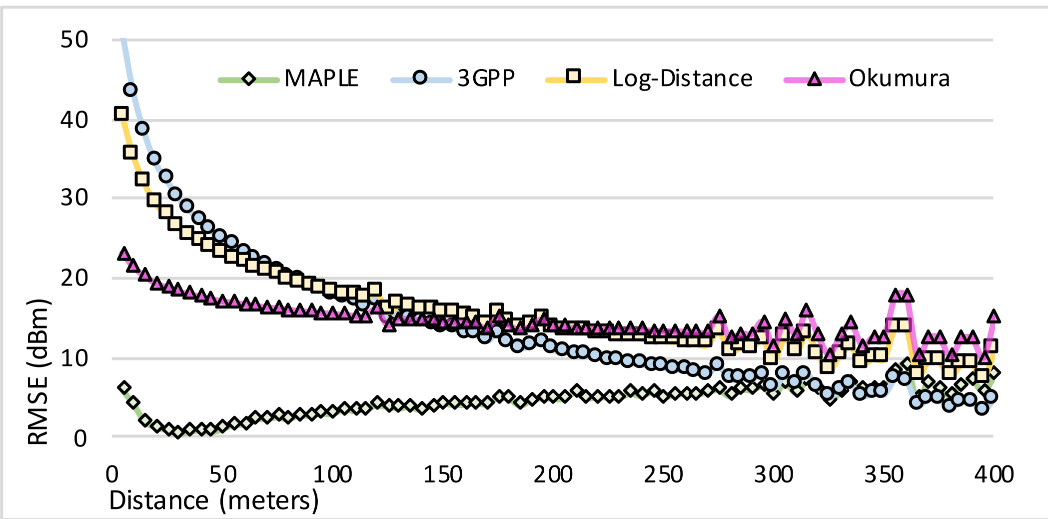

Figure 3.19. Average RMSE with respect to fit function of actual signal levels.

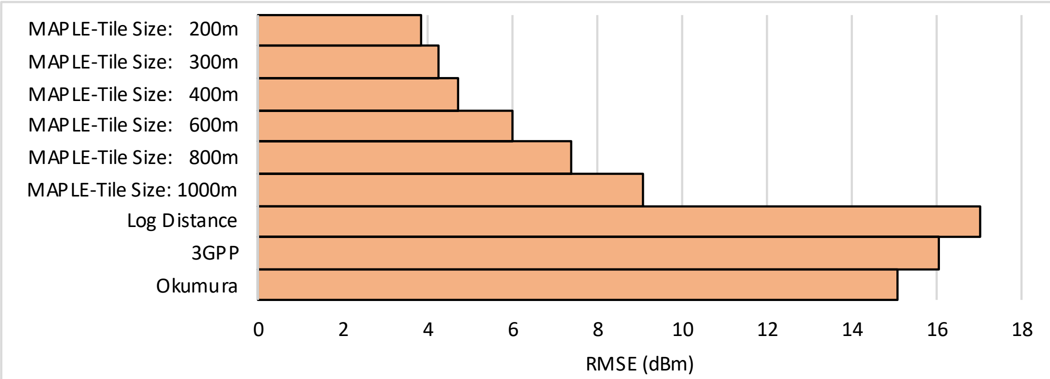

Figure 3.20. Average RMSE with respect to fit function and tile size.

The average RMSE of the model is 9.06 dBm for a tile size of 1000 meters, and 3.8 dBm for a tile size of 200 meters. However, with the best-fitting parameters of training area, the Log-Distance model achieves an average of 17.01 dBm of RMSE, the 3GPP model achieves as much as 16.02 dBm of average RMSE, and the Okumura model can achieve an average of 15.04 dBm RMSE. Increased tile size results in larger RMSE with respect to the trendline, such as 4.24, 4.68, 5.98, 7.35, and 9.06 dBm for tile sizes of 300, 400, 600, 800, and 1000 meters, respectively, as given in Figure 3.20 and Table 3.4. The results of larger tiles converge to the results of the Log-Distance model, as expected, since the Log-Distance model is a special case of the MAPLE model, where the entire area is covered by a single large tile. The list of RMSE (in dBm) and NMSE for all measurement points in the deployment site with respect to all 72 cases are presented in Table B.3 and Table B.4 of APPENDIX B, respectively.

Table 3.4. Average test results for all measurement points in the deployment site (L.D.: Log-Distance, Oku.:Okumura).

				MAPLE with tile size:					
	L.D.	Oku.	3GPP	1000m	800m	600m	400m	300m	200m
RMSE(dBm)	17.01	15.04	16.02	9.06	7.35	5.98	4.68	4.24	3.80
NMSE	0.21	0.19	0.20	0.12	0.10	0.08	0.06	0.06	0.05
Variance	95.00	42.45	153.69	62.54	59.73	54.55	50.02	41.68	39.76
stdDev(dBm)	9.75	6.52	12.40	7.91	7.73	7.39	7.07	6.46	6.30

Each of the descriptor vectors consist of 116 different numeric values. The 3D maps for the city centers of these cities are 5×5 km^2 in size. There are a total of $625 + 625 = 1250$ tiles generated for the two cities with a tile size of 200 meters. In order to provide an insight on how the descriptor vectors can be related to the propagation parameters, we classified the tiles depending on the most significant structural properties such as mean building base area, mean building height, and mean building volume. Table 3.5 shows the relation between tile descriptor vectors and the magnitudes of the propagation parameters. Instead of listing the entire list of tiles, the table shows sample tiles with respect to the most significant descriptor properties. As can be seen from the sample tiles, the path loss exponent and the reference path loss values are dependent on the sizes of the buildings on the tiles. A more detailed version of the list is provided in Table B.1 of APPENDIX B as reference.

Table 3.5. Relations between tile descriptor vectors and propagation parameters. Each line corresponds to a sample tile.

Tile	Mean Building Base Area (m^2)	Mean Building Height (m)	Mean Building Volume (m^3)	γ	P_{L_0}
1	240	7	1790	2.11	21
2	264	9	2543	2.18	22
3	238	11	2727	2.47	25
4	406	16	6281	2.58	25
5	472	19	7893	2.83	28
6	451	22	9235	2.88	29

3.4.1. RMSE Results for Different Distance Clusters

Both MAPLE other methods it has been compared to utilize logarithmic path-loss functions in their calculations as a general practice. However, when comparing the results of logarithmic functions, there is a fast deterioration for measurement closer to the base station, which causes the RMSE values, with respect to the fit function of the actual measurements, for all propagation values to rise dramatically. Despite the overall negative effects on the RMSE, only a fraction of the measurements (i.e. users) are located within the closer proximity to the base station, as seen in Figure 3.17.

The algorithms have also been tested for users having a distances of at least 50, 100, and 150 meters to their respective base stations, in order to evaluate the performance of the algorithms considering majority of users and eliminating the fast deterioration effects of the logarithmic path-loss functions. With these additional three setups, the total number of test cases that use the actual signal measurements becomes 288. Figure 3.21 shows the RMSE results for all measurements, Figure 3.22, Figure 3.23, and Figure 3.24 show the RMSE results for all users that are at least 50, 100, and 150 meters away from the corresponding base stations, respectively. A combined graph of these RMSE values is provided as Table B.1 of APPENDIX B. Similarly additional graphs regarding NMSE, variance of RMSE, and standard deviation of RMSE for each of the above cases are also provided for your reference in Table B.2, Table B.3, Table B.4 of APPENDIX B, respectively.

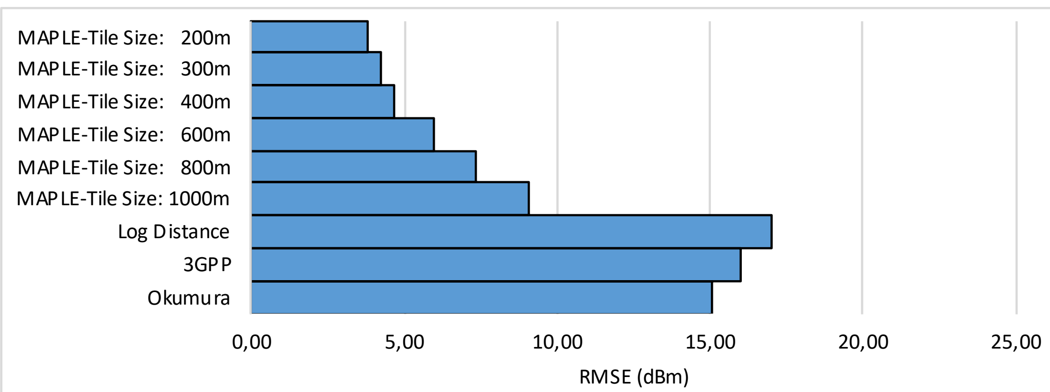

Figure 3.21. Average RMSE for all measurements.

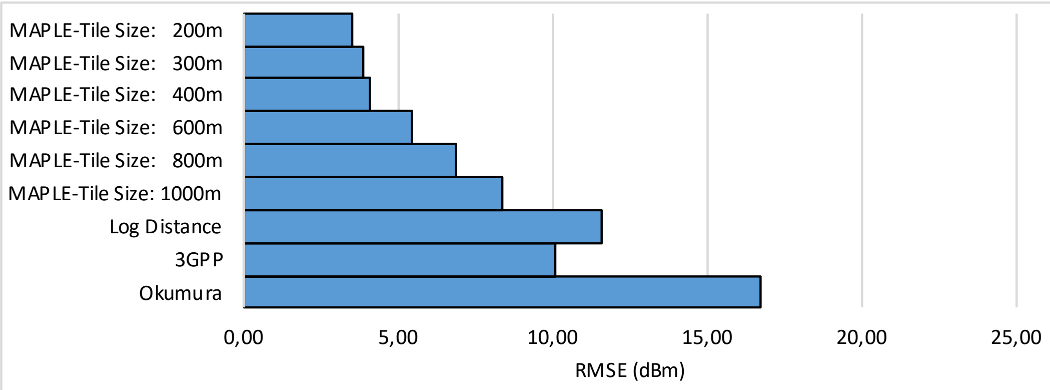

Figure 3.22. Average RMSE for measurements at least 50m away from base stations.

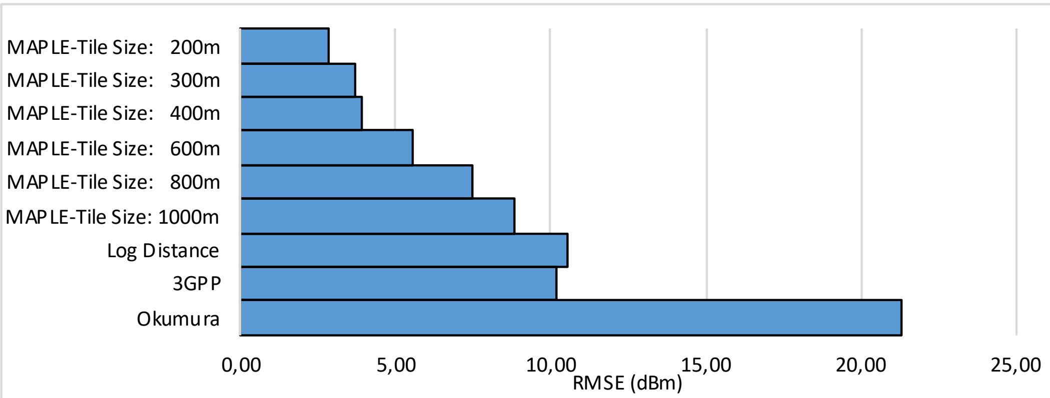

Figure 3.23. Average RMSE for measurements at least 100m away from base stations.

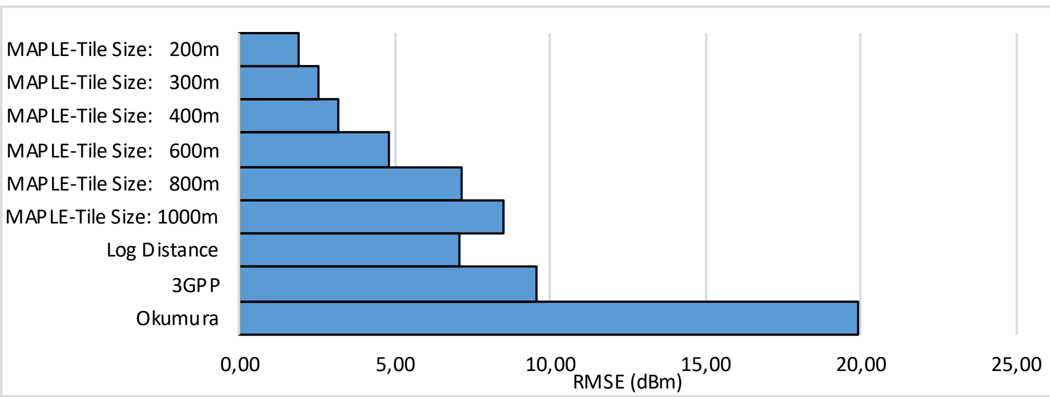

Figure 3.24. Average RMSE for measurements at least 150m away from base stations.

3.4.2. Additional Base Station Positioning

Another comparative result set has been presented in this section regarding the additional base station positioning on the deployment area. In order to provide a fair and reasonable evaluation of the similarity-based MAPLE channel estimation scheme for the deployment area, the results presented in this section demonstrate the estimated received signal strengths from existing base stations, before the deployment of any additional base stations. The results obtained with additional base station are even more promising in both tests, but not included in this thesis since those additional base stations were not deployed and actual measurements for comparison were not taken during the lifetime of the project.

Table 3.6. Average percentage of additional base stations for all measurement points in the deployment site.

Minimum	MAPLE with tile size:					
Expected SNR	1000m	800m	600m	400m	300m	200m
-90 dBm	9.98	9.43	9.17	8.35	8.66	7.30
-80 dBm	17.67	16.83	16.27	15.62	14.14	13.28
-70 dBm	22.98	22.15	21.10	20.74	19.86	18.57
-60 dBm	24.84	24.92	23.73	22.45	21.82	21.02
-50 dBm	29.45	29.23	29.11	28.72	27.14	26.97

Table 3.6 shows the percentage of additional base stations required at different levels of wireless QoS in the network area, with a lower bound on the allowed SNR.

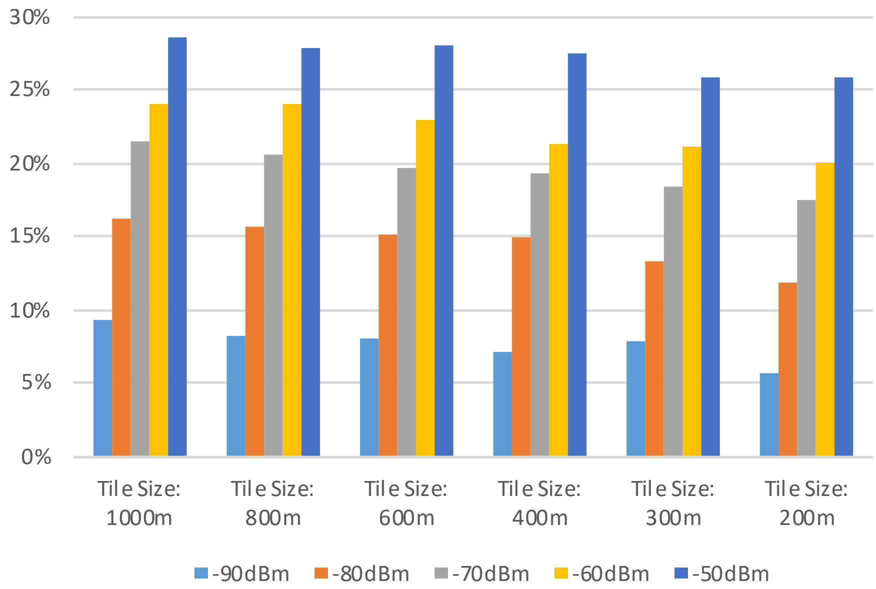

Figure 3.25. Additional base stations with respect to tile size and minimum allowed SNR.

Figure 3.25 is a representation of Table 3.6, grouping with respect to the tile size. Similarly Figure 3.26 provides a grouping on minimum allowed SNR.

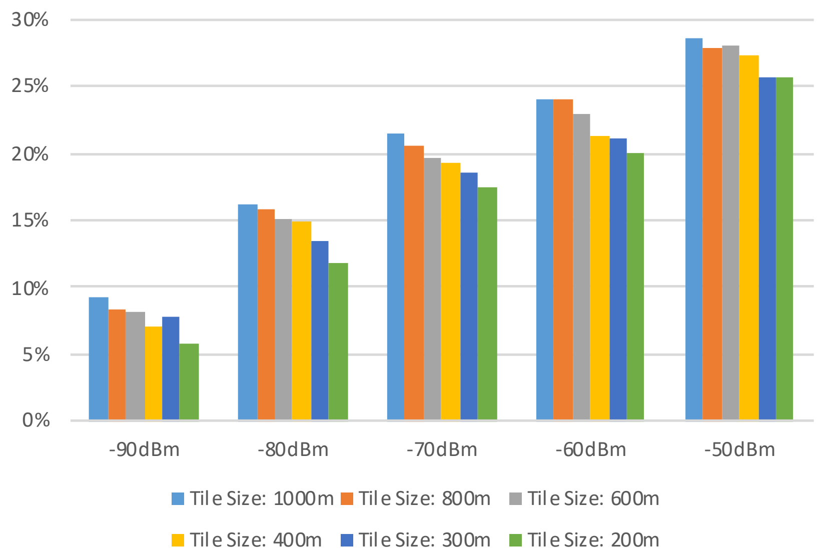

Figure 3.26. Additional base stations with respect to minimum allowed SNR and tile size.

3.4.3. Runtime Performance

The performance of the algorithms have been tested on two different computers having i5 and i7 processors. The major four stages of the MAPLE model have been analyzed under different tile sizes. The first stage generates the tiles of both training and deployment areas with their corresponding descriptor vectors of physical properties. Figure 3.27 shows the average duration (in milliseconds) of generating a single tile with tile sizes of 200, 300, 400, 600, 800, and 1000 meters for both cities. The tiles with smaller sizes require relatively more processing time compared to larger tiles because of the search required for 3D structures to be allocated on each tile. Also smaller tiles are more likely to split more 3D structures on the boundaries, whereas most of the 3D structures can be located on larger tile as a whole, without the need to split at the tile edges.

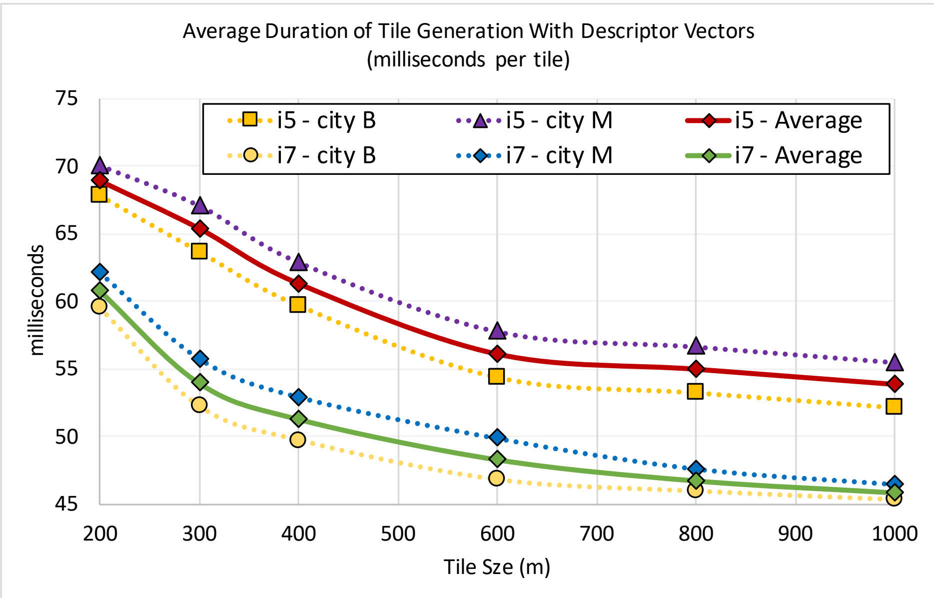

Figure 3.27. Average duration of tile generation with descriptor vectors (milliseconds per tile). Smaller tiles require relatively more processing time due to the 3D structure search, split and assignment procedure.

Larger tiles will handle more 3D structures, leaving fewer items to be searched by the remaining tiles to process. On the other hand, smaller tiles will only remove a fraction of the overall 3D structures compared to the larger tiles. The amount of time required for generating each tile is between 70 and 50 milliseconds on an i5 processor, for tiles sizes of 200 and 1000 meters respectively. The same process takes between 60 and 45 milliseconds on an i7 processor. All performance values shown in this and following stages are pure calculation results, excluding any IO regarding processing of data source files, or and database access.

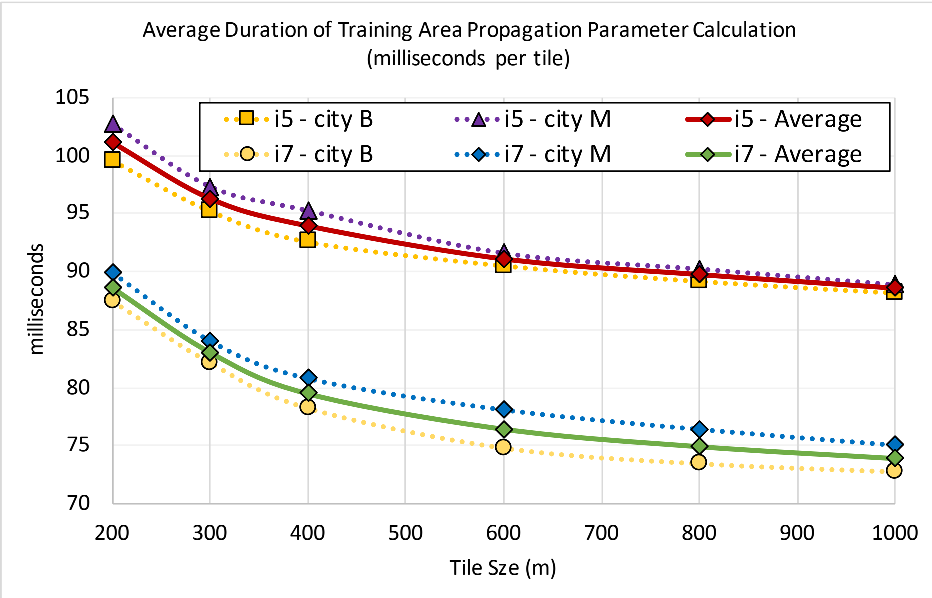

Figure 3.28. Average duration of training area propagation parameter calculation (milliseconds per tile). Smaller tiles generate more path segments from the measurements to the corresponding base stations, which in turn increases the amount of processing compared to the larger tiles.

The second stage generates the propagation characteristics of each training area tile, where smaller tiles introduce more path segments of measurements to process compared to larger tiles, which cause less number of path segments to be generated. Figure 3.28 shows the average duration (in milliseconds) of generating propagation parameters of each tile in the training areas with tile sizes of 200, 300, 400, 600, 800, and 1000 meters. The amount of time required to generate the descriptor vectors of each tile in a training area is between 85 and 105 milliseconds on an i5 processor, for tile sizes of 1000 and 200 meters respectively. The same process takes between 70 and 90 milliseconds on an i7 processor.

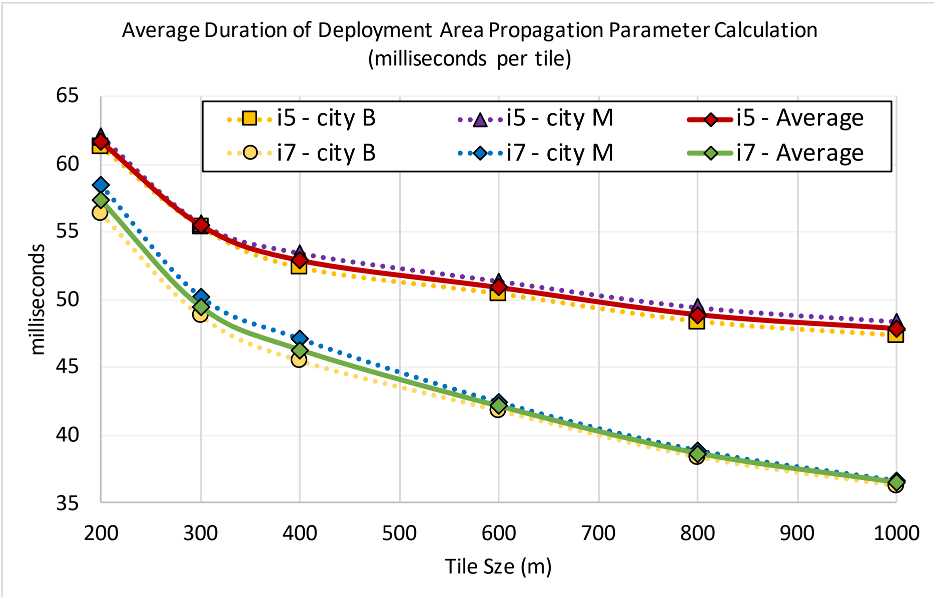

Figure 3.29. Average duration of deployment area propagation parameter calculation (milliseconds per tile). In a fixed sized area, the number of small tiles is more than larger tiles. Deployment area propagation parameters are calculated using the entire set of existing training area tiles of the same size, thereby increasing the processing time of smaller tiles.

The third stage generates the propagation parameters of deployment area tiles. Both cities consist of a $5 \times 5\text{km}^2$ area each. The number of tiles is inversely proportional to the square of tile size. In order to calculate the propagation parameters of deployment area tiles, all tiles of the training area are used in a similarity function. Therefore, as shown in Figure 3.29, the number of tiles contributing to calculation of the propagation parameters in a deployment area requires a significant processing time. The amount of time required to generate propagation parameters of deployment areas tiles is between 45 and 65 milliseconds on an i5 processor, for tile sizes of 1000 and 200 meters respectively. The same process takes between 35 and 60 milliseconds on an i7 processor.

The fourth and final stage is used to calculate base station positions at the deployment area based on the propagation parameters of the deployment area tiles. The duration of the process also depends on the tile size, which determines the number of path segments, and the amount of calculations necessary for the base station coverage

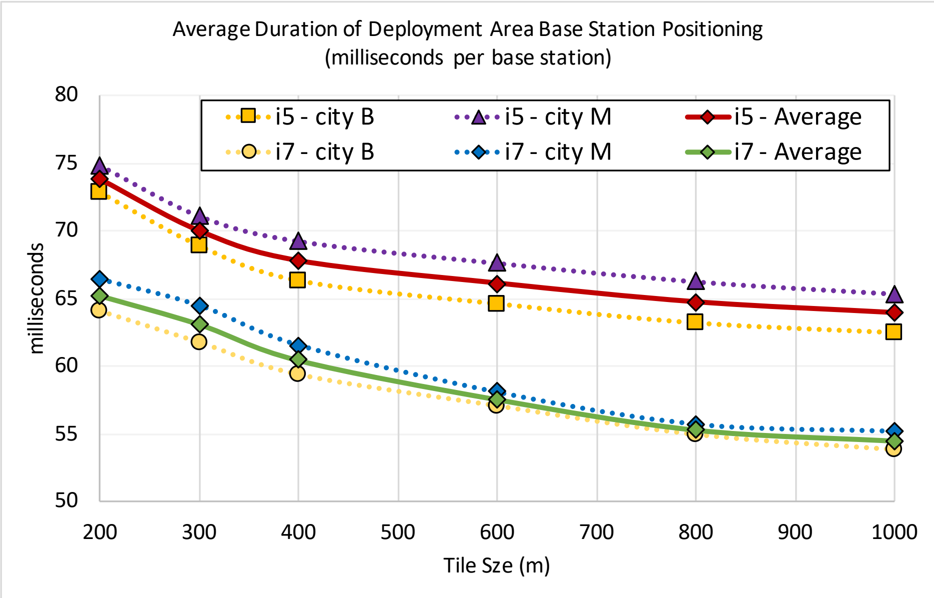

Figure 3.30. Average duration of deployment area base station positioning (milliseconds per base station).

calculations with respect to the tile propagation parameters. As shown in Figure 3.30, the location estimation process

The amount of time required to estimate the location of each base station in a deployment area is between 65 and 75 milliseconds on an i5 processor, for tile sizes of 1000 and 200 meters respectively. The same process takes between 55 and 65 milliseconds on an i7 processor.

3.5. Closing Remarks

The proposed MAPLE model for Log-Distance propagation model has been implemented and tested with actual signal measurement data from two different cities in Europe, for a total of 288 test setups. The MAPLE model isolates and learns the terrain specific propagation parameters by utilizing a three-step mixed path-inspired model and associates the propagation parameters with 3D map features of tile structures. The proposed model can be used to plan the base station locations of new cellular networks, by utilizing existing signal quality measurements and 3D city map data from other cities.

The main purpose of MAPLE is to improve the precision of Log-Distance propagation model by taking the obstacles of different local regions into account. As the primary outcome, the signal level estimation process results in significantly better RMSE values and better average signal levels with respect to distance, compared to the other propagation models mentioned in the thesis such as 3GPP and Okumura as well. Learning terrain specific propagation parameters has a potential to improve path loss and coverage estimations with a cost of acquiring and storing data for learning phase.

When using larger tiles, the results of MAPLE model converge to the results of the underlying Log-Distance propagation model as shown in the results. Tiles with smaller size are more effective in terms of signal propagation estimation. The execution time depends on the size and number of tiles to be processed. Given sufficient amount of measurement, the MAPLE model responds in reasonable time, with an output of potential base station locations in the deployment area.

4. CONCLUSIONS

In this thesis, we propose an alternative wireless multicast scheduling model (WISDoM-SD) for streaming bandwidth hungry multimedia content over cooperative mesh networks. Increasing number of users overloads the available bandwidth very easily in case of unicast transmissions. However, depending on popularity of different streaming channels, users can be associated with multicast groups and parallel transmissions can take place in different parts of the base station coverage area so as to serve a higher number of users than the unicasting model. The model utilizes the relay capability of mesh networks for extending high quality data rate coverage of the base stations to the local areas with poor connections. The simulation results indicate that the users with stronger connections can share their bandwidth with other wireless users efficiently, improving the overall throughput of the network.

As a complementary study, we have also proposed a signal propagation estimation model named MAPLE to estimate the potential locations of base stations, by exploiting physical similarities between local regions in different areas. The model can be trained to use 3D city maps and actual signal measurements to adapt signal propagation characteristics at local regions of existing networks to new deployment areas. MAPLE has been tested in two cities in Europe, and the model improves the Log-Distance model with the help of actual signal measurements at many distinct locations. Using high number of measurements is essential in generating smaller tiles for more precise signal level estimation. On the other hand, larger tiles cause MAPLE to behave similar to the Log-Distance propagation model, which is a special case of MAPLE having one large tile covering the entire area. The main purpose of MAPLE model was to improve the accuracy of the Log-Distance propagation model and it is achieved with a significantly less RMSE. Moreover, MAPLE performed significantly better than 3GPP and Okumura models as well, in terms of signal level estimations.

For future work, the WISDoM-SD model can be extended to support live streaming applications other than IPTV which has predefined set of channels. It can be improved to transmit data to secondary users from multiple relay nodes at the same time reducing the overhead at the relay node. Also, the model can be enhanced to relay from fixed line connections to wireless in local neighborhood. As a final improvement to WISDoM-SD, the scheduling algorithm can be optimized further to allow transmission of relay nodes during the first hop transmissions from the MBS to the user devices as well. This process may require consideration of the interference avoiding opportunities, checking if the relay node will not cause destructive transmission, and whether the relay can transmit and receive simultaneously or not.

The MAPLE model can be further improved to yield results on 5G networks. The performance can be enhanced by using parallel algorithms that can be executed on GPU clusters. MAPLE is a learning based model and it employs straightforward learning methods, on the other hand, the learning process can be enhanced by machine learning techniques for dynamic adaptation to additional regions. We have initiated a statistical data generation technique to be able to run the model for areas where sufficient number of measurements cannot be obtained. We have briefly discussed the steps of this future work in Appendix C.

REFERENCES

1. Choi, J., A. S. Reaz and B. Mukherjee, "A Survey of User Behavior in VoD Service and Bandwidth-Saving Multicast Streaming Schemes", *IEEE Communications Surveys Tutorials*, Vol. 14, No. 1, pp. 156–169, 2012.

2. Lin, F. Y. ., "Optimal real-time admission control algorithms for the video-on-demand (VOD) service", *IEEE Transactions on Broadcasting*, Vol. 44, No. 4, pp. 402–408, Dec 1998.

3. Woo, H. and C.-k. Kim, "Multicast Scheduling for VOD Services.", *Multimedia Tools Appl.*, Vol. 2, pp. 157–171, 03 1996.

4. Zhou, Y., T. Z. J. Fu and D. M. Chiu, "On replication algorithm in P2P VoD", *Networking, IEEE/ACM Transactions on*, Vol. 21, pp. 233–243, 02 2013.

5. Zhou, Y., T. Z. J. Fu and D. M. Chiu, "Server-assisted adaptive video replication for P2P VoD", *Signal Processing: Image Communication*, Vol. 27, p. 484–495, 05 2012.

6. Roberts, L. G. and B. D. Wessler, "Computer Network Development to Achieve Resource Sharing", *Proceedings of the May 5-7, 1970, Spring Joint Computer Conference*, AFIPS '70 (Spring), pp. 543–549, ACM, New York, NY, USA, 1970, `http://doi.acm.org/10.1145/1476936.1477020`.

7. Budiarjo, I., H. Nikookar and L. Ligthart, "Cognitive Radio Modulation Techniques", *Signal Processing Magazine, IEEE*, Vol. 25, pp. 24 – 34, 12 2008.

8. Kuran, M. and T. Tugcu, "A survey on emerging broadband wireless access technologies", *Computer Networks*, pp. 3013–3046, 08 2007.

9. Abichar, Z., Yanlin Peng and J. M. Chang, "WiMax: The Emergence of Wireless

Broadband", *IT Professional*, Vol. 8, No. 4, pp. 44–48, July 2006.

10. Ozyurt, M., S. Ulug and T. Tugcu, "Utilizing WiMAX mesh mode for efficient IPTV transmission", *Proceedings of the 13th International Symposium on Modeling Analysis and Simulation of Wireless and Mobile Systems, MSWiM 2010, Bodrum, Turkey, October 17-21, 2010*, pp. 23–30, 2010, https://doi.org/10.1145/1868521.1868527.

11. Ulug, S., M. Ozyurt and T. Tugcu, "WISDoM-SD: Wireless IPTV service distribution over mesh mode via space diversity"", *Ad Hoc Networks*, Vol. 12, pp. 178 – 192, 2014, http://www.sciencedirect.com/science/article/pii/S1570870511001909.

12. Kuran, M. S., B. Yilmaz, F. Alagoz and T. Tugcu, "Quality of Service in Mesh Mode IEEE 802.16 Networks", *2006 International Conference on Software in Telecommunications and Computer Networks*, pp. 107–111, Sep. 2006.

13. Valenzuela, R., "A ray tracing approach to predicting indoor wireless transmission", *IEEE 43rd Vehicular Technology Conference*, pp. 214–218, May 1993.

14. Geok, T., F. Hossain, M. Kamaruddin, N. Z. Abd Rahman, S. Thiagarajah, A. Chiat, J. Hossen and C. Liew, "A Comprehensive Review of Efficient Ray-Tracing Techniques for Wireless Communication", *International Journal on Communications Antenna and Propagation (IRECAP)*, Vol. 8, p. 123, 04 2018.

15. Corucci, A., P. Usai, A. Monorchio and G. Manara, *Wireless Propagation Modeling by Using Ray-Tracing*, pp. 575–618, 01 2014.

16. Chen, J., O. Esrafilian, D. Gesbert and U. Mitra, "Efficient Algorithms for Air-to-Ground Channel Reconstruction in UAV-Aided Communications", *2017 IEEE Globecom Workshops (GC Wkshps)*, pp. 1–6, Dec 2017.

17. Esrafilian, O., R. Gangula and D. Gesbert, "Learning to Communicate in UAV-

Aided Wireless Networks: Map-Based Approaches", *IEEE Internet of Things Journal*, Vol. 6, No. 2, pp. 1791–1802, April 2019.

18. Jaeckel, S., L. Raschkowski, S. Wu, L. Thiele and W. Keusgen, "An Explicit Ground Reflection Model for mm-Wave Channels", *2017 IEEE Wireless Communications and Networking Conference Workshops (WCNCW)*, pp. 1–5, March 2017.

19. Joshi, G. G., C. B. Dietrich, C. R. Anderson, W. G. Newhall, W. A. Davis, J. Isaacs and G. Barnett, "Near-ground channel measurements over line-of-sight and forested paths", *IEE Proceedings - Microwaves, Antennas and Propagation*, Vol. 152, No. 6, pp. 589–596, Dec 2005.

20. Chamberlin, K. and R. Luebbers, "An evaluation of Longley-Rice and GTD propagation models", *IEEE Transactions on Antennas and Propagation*, Vol. 30, No. 6, pp. 1093–1098, Nov 1982.

21. "ITU-R P.1546-4:Method for point-to-area predictions for terrestrial services in the frequency range 30 MHz to 3 000 MHz", , Oct. 2009.

22. Ostlin, E., H. M. Zepernick and H. Suzuki, "Evaluation of the new semi-terrain based propagation model recommendation ITU-R P.1546", *2003 IEEE 58th Vehicular Technology Conference. VTC 2003-Fall (IEEE Cat. No.03CH37484)*, Vol. 1, pp. 114–118 Vol.1, Oct 2003.

23. Galvan-Tejada, G. M. and E. Q. Duarte-Reynoso, "A study based on the Lee propagation model for a wireless sensor network on a non-uniform vegetation environment", *2012 IEEE Latin-America Conference on Communications*, pp. 1–6, Nov 2012.

24. Medeisis, A. and A. Kajackas, "On the use of the universal Okumura-Hata propagation prediction model in rural areas", *VTC2000-Spring. 2000 IEEE 51st Vehicular*

Technology Conference Proceedings (Cat. No.00CH37026), Vol. 3, pp. 1815–1818 vol.3, 2000.

25. Hata, M., "Empirical formula for propagation loss in land mobile radio services", *IEEE Transactions on Vehicular Technology*, Vol. 29, No. 3, pp. 317–325, Aug 1980.

26. Acar, T., F. Çalışkan and E. Aydın, "Comparison of computer-based propagation models with experimental data collected in an urban area at 1800 MHz", *2015 IEEE 16th Annual Wireless and Microwave Technology Conference (WAMICON)*, pp. 1–6, April 2015.

27. Hasna, M. O. and M. S. Alouini, "Outage probability of multihop transmission over Nakagami fading channels", *IEEE Communications Letters*, Vol. 7, No. 5, pp. 216–218, May 2003.

28. Ozyurt, M., H. B. Yilmaz and T. Tugcu, "MAPLE: Mixed Path Calculation In Tile-Based 3D Maps", *IEEE Communications Letters*, pp. 1–1, 2019.

29. Hekmat, R. and P. Van Mieghem, "Connectivity in wireless ad-hoc networks with a log-normal radio model", *Mobile networks and applications*, Vol. 11, No. 3, pp. 351–360, 2006.

30. Xiao, Y., X. Du, J. Zhang, F. Hu and S. Guizani, "Internet Protocol Television (IPTV): The Killer Application for the Next-Generation Internet", *Communications Magazine, IEEE*, Vol. 45, No. 11, pp. 126–134, 2007, `http://ieeexplore.ieee.org/xpls/abs_all.jsp?arnumber=4378332`.

31. Yarali, A. and A. Cherry, "Internet protocol television (IPTV)", pp. 1 – 6, 12 2005.

32. She, J., F. Hou, P.-H. Ho and L.-L. Xie, "IPTV over WiMAX: Key Success Factors, Challenges, and Solutions [Advances in Mobile Multimedia]", *Communications Magazine, IEEE*, Vol. 45, No. 8, pp. 87 –93, august 2007.

33. Li, Q., X. Lin, J. Zhang and W. Roh, “Advancement of MIMO technology in WiMAX: from IEEE 802.16d/e/j to 802.16m”, *Communications Magazine, IEEE*, Vol. 47, No. 6, pp. 100 –107, june 2009.

34. Ghosh, A., D. Wolter, J. Andrews and R. Chen, “Broadband Wireless Access with WiMax/802.16: Current Performance Benchmarks and Future Potential”, *IEEE Communications Magazine - IEEE Commun. Mag.*, Vol. 43, pp. 129–136, 02 2005.

35. Sedoyeka, E., Z. Hunaiti, M. Al Nabhan and W. Balachandran, “WiMAX Mesh networks for underserved areas”, *Computer Systems and Applications, 2008. AICCSA 2008. IEEE/ACS International Conference on*, pp. 1070 –1075, march 2008.

36. “IEEE 802.11-Wireless LAN Medium Access Control (MAC) and Physical Layer (PHY) Specifications”, IEEE Standard for Information technology.

37. Retnasothie, F., M. Ozdemir, T. Yucek, H. Celebi, J. Zhang and R. Muththaiah, “Wireless IPTV over WiMAX: Challenges and Applications”, *Wireless and Microwave Technology Conference, 2006. WAMICON ’06. IEEE Annual*, pp. 1 –5, 4-5 2006.

38. Alim, O. and A. El Naggary, “Coverage Vs throughput challenges in Mobile WiMAX”, *Radio Science Conference, 2009. NRSC 2009. National*, pp. 1 –9, 17-19 2009.

39. Jian Tao, Fuqiang Liu, Zhihui Zeng and Zhangxi Lin, “Throughput enhancement in WiMax mesh networks using concurrent transmission”, *Proceedings. 2005 International Conference on Wireless Communications, Networking and Mobile Computing, 2005.*, Vol. 2, pp. 871–874, Sep. 2005.

40. Chen, J. and K. Wang, “Reliable WiMAX Multicast Applications”, *2008 IEEE 8th International Conference on Computer and Information Technology Workshops*,

pp. 182–187, July 2008.

41. She, J., X. Yu, P.-H. Ho and E.-H. Yang, “A cross-layer design framework for robust IPTV services over IEEE 802.16 networks”, *IEEE Journal on Selected Areas in Communications*, Vol. 27, pp. 235–245, 02 2009.

42. Goyal, V., “Multiple descriptive coding: Compression meets the network”, *IEEE Signal Process. Mag.*, Vol. 18, pp. 73–93, 01 2001.

43. Tse, D. and P. Viswanath, *Fundamentals of Wireless Communications 12*, Cambridge University Press, 01 2010.

44. Azgin, A. and Y. Altunbasak, “A cooperative error recovery framework for IPTV over WiMAX”, pp. 616 – 621, 02 2011.

45. Hou, F., L. Cai, J. She, P.-H. Ho, X. Shen and J. Zhang, “Cooperative Multicast Scheduling Scheme for IPTV Service over IEEE 802.16 Networks”, pp. 2566 – 2570, 06 2008.

46. Cudak, M., “IEEE 802.16m System Requirements”, IEEE 802.16 Broadband Wireless Access Working Group, 2010, `http://ieee802.org/16/tgm/docs/80216m-07_002r10.pdf`.

47. Paulraj, A., D. Gore, R. Nabar and H. Bolcskei, “An overview of MIMO communications - a key to gigabit wireless”, *Proceedings of the IEEE*, Vol. 92, No. 2, pp. 198 – 218, feb 2004.

48. Shatila, H., M. Khedr and J. H. Reed, “Adaptive modulation and coding for WiMAX systems with vague channel state information using cognitive radio”, *Proceedings of the 2010 International Symposium on Performance Evaluation of Computer and Telecommunication Systems (SPECTS ’10)*, pp. 405–409, July 2010.

49. Muquet, B., E. Biglieri and H. Sari, “MIMO Link Adaptation in Mobile WiMAX

Systems", *2007 IEEE Wireless Communications and Networking Conference*, pp. 1810–1813, March 2007.

50. Chen, J., N. Liao, Y. Shi and J. Li, "Link Adaptation for Video Multicasting in Mobile WiMAX Network", *2009 6th IEEE Consumer Communications and Networking Conference*, pp. 1–6, Jan 2009.

51. Wang Hai, Wan Lei and Liao Min, "HSDPA link adaptation based on novel quality model", *2005 IEEE 61st Vehicular Technology Conference*, Vol. 1, pp. 334–338 Vol. 1, May 2005.

52. Ramamurthi, V. and W. Chen, "Mobility Based MIMO Link Adaptation in LTE-Advanced Cellular Networks", *2010 International Conference on Broadband, Wireless Computing, Communication and Applications*, pp. 235–241, Nov 2010.

53. Jensen, T., S. Kant, J. Wehinger and B. Fleury, "Fast link adaptation for MIMO OFDM", *Vehicular Technology, IEEE Transactions on*, Vol. 59, pp. 3766 – 3778, 11 2010.

54. Jang, Y., Y. Kim, S. Park and S. Choi, "Link adaptation strategies for IEEE 802.15.4 WPANs: Protocol design and performance evaluation", *Journal of Communications and Networks*, Vol. PP, pp. 1–9, 05 2019.

55. Wang, X., G. Su, Y. Hao and L. Luo, "Design a Link Adaptive Management Algorithm for BLE Device", J. C. Hung, N. Y. Yen and L. Hui (Editors), *Frontier Computing*, pp. 1355–1364, Springer Singapore, Singapore, 2019.

56. Jun Xin, Ming-Ting Sun, Byung-Sun Choi and Kang-Wook Chun, "An HDTV-to-SDTV spatial transcoder", *IEEE Transactions on Circuits and Systems for Video Technology*, Vol. 12, No. 11, pp. 998–1008, Nov 2002.

57. "Summarization of MPEG Compressed Video Sequences", *Advanced Science Letters*, Vol. 4, No. 11-12, 2011.

58. Mohamed, M. A., M. Zubair and H. M. Ibrahim, “QoS Based IPTV Over Mobile WiMAX Networks”, *Wireless Personal Communications*, Vol. 96, No. 2, pp. 1711–1740, Sep 2017, `https://doi.org/10.1007/s11277-017-4264-6`.

59. Jianfeng Chen, Ning Liao, Yntao Shi and Jun Li, “Dynamic region based modulation for video multicasting in mobile WiMAX network”, *2008 11th IEEE Singapore International Conference on Communication Systems*, pp. 1668–1673, Nov 2008.

60. Ioan Vlad Uilecan, Chi Zhou and G. E. Atkin, “Framework for delivering IPTV services over WiMAX wireless networks”, *2007 IEEE International Conference on Electro/Information Technology*, pp. 470–475, May 2007.

61. Kuo, W., W. Liao and T. Liu, “Adaptive Resource Allocation for Layer-Encoded IPTV Multicasting in IEEE 802.16 WiMAX Wireless Networks”, *IEEE Transactions on Multimedia*, Vol. 13, No. 1, pp. 116–124, Feb 2011.

62. Kuo, W. ., T. Liu and W. Liao, “Utility-Based Resource Allocation for Layer-Encoded IPTV Multicast in IEEE 802.16 (WiMAX) Wireless Networks”, *2007 IEEE International Conference on Communications*, pp. 1754–1759, June 2007.

63. Pinola, J. and K. Pentikousis, “IPTV over WiMAX with MIPv6 Handovers”, *VTC Spring 2009 - IEEE 69th Vehicular Technology Conference*, pp. 1–5, April 2009.

64. Jong Min Lee, Hyo-Jin Park, Seong Gon Choi and Jun Kyun Choi, “Adaptive Hybrid Transmission Mechanism for On-Demand Mobile IPTV Over WiMAX”, *IEEE Transactions on Broadcasting*, Vol. 55, No. 2, pp. 468–477, June 2009.

65. Lee, K. S., S. W. Rhee and H. Y. Youn, “A MAC Layer Multicasting Approach for WiMAX Access Networks”, *2008 Sixth Annual IEEE International Conference on Pervasive Computing and Communications (PerCom)*, pp. 348–353, March 2008.

66. Howon Lee and Dong-Ho Cho, “Reliable multicast services using CDMA codes in IEEE 802.16 OFDMA system”, *2005 IEEE 61st Vehicular Technology Conference*,

Vol. 4, pp. 2349–2353 Vol. 4, May 2005.

67. Ge, W., J. Zhang and S. Shen, "A Cross-Layer Design Approach to Multicast in Wireless Networks", *IEEE Transactions on Wireless Communications*, Vol. 6, No. 3, pp. 1063–1071, March 2007.

68. Deb, S., S. Jaiswal and K. Nagaraj, "Real-Time Video Multicast in WiMAX Networks", *IEEE INFOCOM 2008 - The 27th Conference on Computer Communications*, pp. 1579–1587, April 2008.

69. Chen, J., W. Jiao, P. Jiang and Q. Guo, "A Multicast Mechanism in WiMax Mesh Network", *2006 Asia-Pacific Conference on Communications*, pp. 1–5, Aug 2006.

70. Xergias, S., N. Passas and A. K. Salkintzis, "Centralized Resource Allocation for Multimedia Traffic in IEEE 802.16 Mesh Networks", *Proceedings of the IEEE*, Vol. 96, No. 1, pp. 54–63, Jan 2008.

71. Wei, H.-y., S. Ganguly, R. Izmailov and H. Zygmunt, "Interference-aware IEEE 802.16 WiMax mesh networks", Vol. 5, pp. 3102 – 3106 Vol. 5, 01 2005.

72. Song Guo and O. Yang, "A dynamic multicast tree reconstruction algorithm for minimum-energy multicasting in wireless ad hoc networks", *IEEE International Conference on Performance, Computing, and Communications, 2004*, pp. 637–642, April 2004.

73. Kuo, W. and J. Lee, "Recipient Maximization Multicast Scheme in IEEE 802.16j WiMAX Relay Networks", *2010 IEEE 71st Vehicular Technology Conference*, pp. 1–5, May 2010.

74. Ballardie, T., P. Francis and J. Crowcroft, "Core Based Trees (CBT)", *Conference Proceedings on Communications Architectures, Protocols and Applications*, SIGCOMM '93, pp. 85–95, ACM, New York, NY, USA, 1993, `http://doi.acm.org/10.1145/166237.166246`.

75. Chaporkar, P. and S. Sarkar, "Wireless multicast: theory and approaches", *IEEE Transactions on Information Theory*, Vol. 51, No. 6, pp. 1954–1972, June 2005.

76. Byers, J. W., M. Luby and M. Mitzenmacher, "A digital fountain approach to asynchronous reliable multicast", *IEEE Journal on Selected Areas in Communications*, Vol. 20, No. 8, pp. 1528–1540, Oct 2002.

77. Feng, d., W. Sun, Y. Jin, W. Hu and W. Guo, "Stability oriented multicast routing algorithm", *Proceedings of SPIE - The International Society for Optical Engineering*, Vol. 6354, 10 2006.

78. Yingjiu Guo, Chuang Lin, Hao Yin and Zhang Zhao, "Design and analysis of IPTV digital copyright management security protocol", *2007 International Symposium on Intelligent Signal Processing and Communication Systems*, pp. 554–557, Nov 2007.

79. Moon, J. S. and I. Lee, "Multicast Key Management in Multimedia Broadcasting Service Environment", *Proceedings of the 4th International Conference on Ubiquitous Information Technologies Applications*, pp. 1–6, Dec 2009.

80. Pinto, A. and M. Ricardo, "Secure multicast in IPTV services", *Computer Networks*, Vol. 54, No. 10, pp. 1531 – 1542, 2010, `http://www.sciencedirect.com/science/article/pii/S1389128609003909`.

81. "IEEE 802.16-Wireless Metropolitan Area Networks", IEEE Standard for Information technology.

82. Digham, F., M.-S. Alouini and M. Simon, "On the Energy Detection of Unknown Signals Over Fading Channels", *IEEE Transactions on Communications*, Vol. 55, pp. 21–24, 02 2007.

83. Shah, A., D. Staddon, I. Rubin and A. Ratkovic, "Multimedia over FDDI", *Local Computer Networks. Proceedings, 17th Conference on*, pp. 110 –124, 13-16 1992.

84. Chuah, C.-N., D. N. C. Tse, J. M. Kahn and R. A. Valenzuela, “Capacity scaling in MIMO wireless systems under correlated fading”, *IEEE Transactions on Information Theory*, Vol. 48, No. 3, pp. 637–650, Mar 2002.

85. Uchida, K., J. Honda, T. Tamaki and M. Takematsu, “Handover Simulation Based on a Two-Rays Ground Reflection Model”, *2011 International Conference on Complex, Intelligent, and Software Intensive Systems*, pp. 414–419, June 2011.

86. Mesleh, R. Y., H. Haas, S. Sinanovic, C. W. Ahn and S. Yun, “Spatial Modulation”, *IEEE Transactions on Vehicular Technology*, Vol. 57, No. 4, pp. 2228–2241, July 2008.

87. Jensen, M. A. and J. W. Wallace, “A review of antennas and propagation for MIMO wireless communications”, *IEEE Transactions on Antennas and Propagation*, Vol. 52, No. 11, pp. 2810–2824, Nov 2004.

88. Ren, Z., S. Stańczak, M. Shabeeb, P. Ferii and L. Thiele, “A distributed algorithm for energy saving in nomadic relaying networks”, *2014 48th Asilomar Conference on Signals, Systems and Computers*, pp. 1791–1795, Nov 2014.

89. Snyder, J. P., *Map projections–A working manual*, Vol. 1395, US Government Printing Office, 1987.

90. Jain, S. and T. Barclay, “Adding the EPSG: 4326 Geographic Longitude-Latitude Projection to TerraServer”, , 2003.

91. Kresse, W., D. M. Danko and K. Fadaie, “Standardization”, *Springer Handbook of Geographic Information*, pp. 245–271, Springer, 2011.

92. Albert, A., *Regression and the Moore-Penrose pseudoinverse*, Elsevier, 1972.

93. Chai, T. and R. R. Draxler, “Root mean square error (RMSE) or mean absolute error (MAE)?–Arguments against avoiding RMSE in the literature”, *Geoscientific*

Model Development, Vol. 7, No. 3, pp. 1247–1250, 2014.

94. Wang, S., W. Guo and M. D. McDonnell, "Distance distributions for real cellular networks", *2014 IEEE Conference on Computer Communications Workshops (INFOCOM WKSHPS)*, pp. 181–182, April 2014.

APPENDIX A: LIST OF DESCRIPTOR VECTOR FIELDS

The fields of descriptor vector are listed as follows:

- Tile area,
- Lowest point above sea level,
- Mean altitude of points above sea level,
- Standard deviation of altitude of points above sea level,
- Mean altitude of points above ground level,
- Standard deviation of altitude of points above ground level,
- Building base area ratio below 5 meters,
- Building base area ratio between 5 to 10 meters,
- Building base area ratio between 10 to 30 meters,
- Building base area ratio between 30 to 60 meters,
- Building base area ratio above 60 meters,
- Building count below 5 meters,
- Building count between 5 to 10 meters,
- Building count between 10 to 30 meters,
- Building count between 30 to 60 meters,
- Building count above 60 meters,
- Mean building base area
- Standard deviation of building base area,
- Mean building height,
- Standard deviation of building height,
- Mean building volume,
- Standard deviation of building volume,
- Building density,
- Water body density,
- Green space density,
- For a plane parallel to the ground at 5 meters of height:

  - Number of buildings intersected by the plane,
  - Mean distance between buildings intersected by the plane,
  - Standard deviation of distance between buildings intersected by the plane,
- For a plane parallel to the ground at 10 meters of height:
  - Number of buildings intersected by the plane,
  - Mean distance between buildings intersected by the plane,
  - Standard deviation of distance between buildings intersected by the plane,
- For a plane parallel to the ground at 30 meters of height:
  - Number of buildings intersected by the plane,
  - Mean distance between buildings intersected by the plane,
  - Standard deviation of distance between buildings intersected by the plane,
- For a plane parallel to the ground at 60 meters of height:
  - Number of buildings intersected by the plane,
  - Mean distance between buildings intersected by the plane,
  - Standard deviation of distance between buildings intersected by the plane,
- For a plane parallel to the ground at 100 meters of height:
  - Number of buildings intersected by the plane,
  - Mean distance between buildings intersected by the plane,
  - Standard deviation of distance between buildings intersected by the plane,
- Water body area percentage,
- Water body count,
- Vegetation area percentage,
- Vegetation area count.
- Average monthly temperatures in Celsius for each month,
- Standard deviation of temperatures in Celsius for each month,
- Average monthly humidity percentage for each month,
- Standard deviation of humidity percentage for each month,
- Average monthly precipitation in grams per square meter for each month,
- Standard deviation of precipitation in grams per square meter for each month,

APPENDIX B: COMPLEMENTARY TABLES AND FIGURES

Table B.1. Summary of relations between tile descriptor vectors and propagation parameters. Each line corresponds to a collection of tile clusters. Clusters are formed based on building area, building height, building volume, and number of buildings per m^2.

Mean Building Base Area (m^2)		Mean Building Height (m)		Mean Building Volume (m^3)		Mean Building Density ($1/m^2$)		Mean	Mean
Min	Max	Min	Max	Min	Max	Min	Max	γ	P_{L_0}
97	137	6	10	524	1297	0.0064	0.0062	2.17	24
93	126	12	19	982	2216	0.0070	0.0065	2.23	27
87	148	21	26	1793	3757	0.0060	0.0058	2.48	32
142	218	5	12	721	2854	0.0040	0.0039	2.27	26
138	207	13	20	1834	4362	0.0042	0.0041	2.38	29
155	218	22	29	3208	4172	0.0040	0.0039	2.54	33
236	361	8	14	1689	4884	0.0024	0.0023	2.19	29
248	384	16	23	4125	9104	0.0023	0.0022	2.34	27
267	398	25	32	6893	13742	0.0022	0.0020	2.52	32
392	524	8	13	3453	6634	0.0016	0.0014	2.32	24
401	549	16	19	7234	12506	0.0016	0.0012	2.45	32
418	536	23	29	10326	13684	0.0016	0.0013	2.63	28
584	763	5	12	3254	9375	0.0011	0.0010	2.36	23
572	794	14	18	7852	17493	0.0011	0.0010	2.68	27
609	782	29	24	18403	19438	0.0011	0.0010	2.77	34

Table B.2. Statistics for all measurement points in the deployment site, and Log-Distance best fit parameters (γ, PL_0) at training site.

	Training Site				Deployment Site	
		Measurement	Best-Fit			Measurement
Case	City	Count	γ	PL_0	City	Count
1	City 1.0	426	2.99	30	City 2.0	567
2	City 1.1	349	2.84	27		
3	City 1.2	374	2.69	30		
4	City 1.3	353	2.84	24		
5	City 1.4	364	2.99	30		
6	City 1.5	345	2.84	27		
7	City 2.0	567	2.54	24	City 1.0	426
8	City 2.1	454	2.69	30		
9	City 2.2	463	2.84	27		
10	City 2.3	448	2.99	30		
11	City 2.4	453	2.84	24		
12	City 2.5	489	2.99	30		

Table B.3. RMSE (in dBm) for all measurement points in the deployment site.

Case	Log-Distance	Okumura	3GPP	MAPLE with tile size:					
				1000m	800m	600m	400m	300m	200m
1	13.97	17.78	13.62	9.57	7.76	6.08	4.66	4.14	3.79
2	13.42	16.72	14.01	9.43	7.34	6.14	4.48	4.49	3.59
3	15.27	17.43	13.15	9.27	7.57	6.34	4.51	4.53	3.43
4	14.36	19.71	14.45	9.02	7.41	6.51	4.42	4.35	3.06
5	13.97	18.94	15.07	9.19	7.72	6.24	5.03	4.62	3.84
6	13.21	17.52	13.37	9.78	7.34	5.62	4.84	4.51	3.39
7	12.01	16.49	11.77	8.81	7.21	5.86	4.97	4.78	4.67
8	12.42	17.03	12.34	8.72	7.34	6.09	4.74	4.73	4.81
9	12.58	16.45	12.82	8.77	7.32	5.27	4.53	4.42	4.71
10	12.44	18.12	12.17	8.98	6.71	6.03	4.64	4.63	4.02
11	13.46	19.54	11.03	8.52	7.24	6.19	4.72	4.58	4.48
12	12.47	17.67	12.52	8.68	7.19	5.43	4.56	4.74	4.26

Table B.4. NMSE for all measurement points in the deployment site.

Case	Log-Distance	Okumura	3GPP	MAPLE with tile size: 1000m	800m	600m	400m	300m	200m
1	0.172	0.228	0.172	0.125	0.102	0.081	0.061	0.054	0.049
2	0.166	0.214	0.177	0.124	0.096	0.082	0.059	0.058	0.047
3	0.189	0.223	0.166	0.121	0.099	0.084	0.059	0.059	0.045
4	0.177	0.253	0.183	0.118	0.097	0.087	0.058	0.057	0.040
5	0.172	0.243	0.191	0.120	0.101	0.083	0.066	0.060	0.050
6	0.163	0.225	0.169	0.128	0.096	0.075	0.064	0.059	0.044
7	0.148	0.211	0.149	0.115	0.094	0.078	0.066	0.062	0.061
8	0.153	0.218	0.156	0.114	0.096	0.081	0.062	0.062	0.062
9	0.155	0.211	0.162	0.115	0.096	0.070	0.060	0.057	0.061
10	0.154	0.232	0.154	0.118	0.088	0.080	0.061	0.060	0.052
11	0.166	0.251	0.140	0.112	0.095	0.082	0.062	0.060	0.058
12	0.154	0.227	0.158	0.114	0.094	0.072	0.060	0.062	0.055

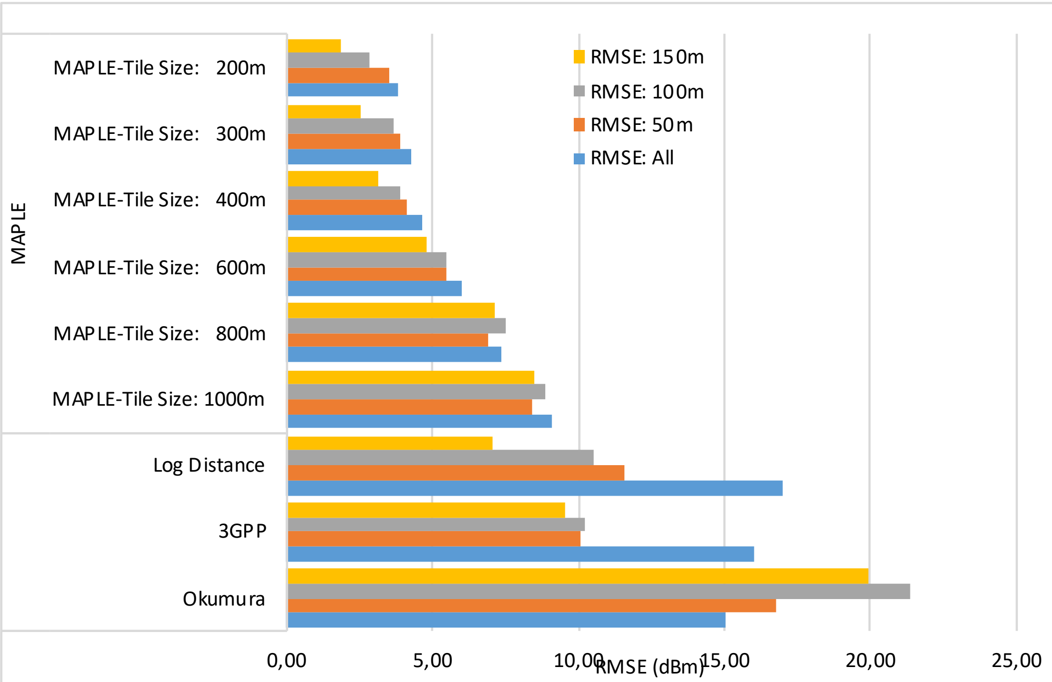

Figure B.1. Average RMSE for measurements.

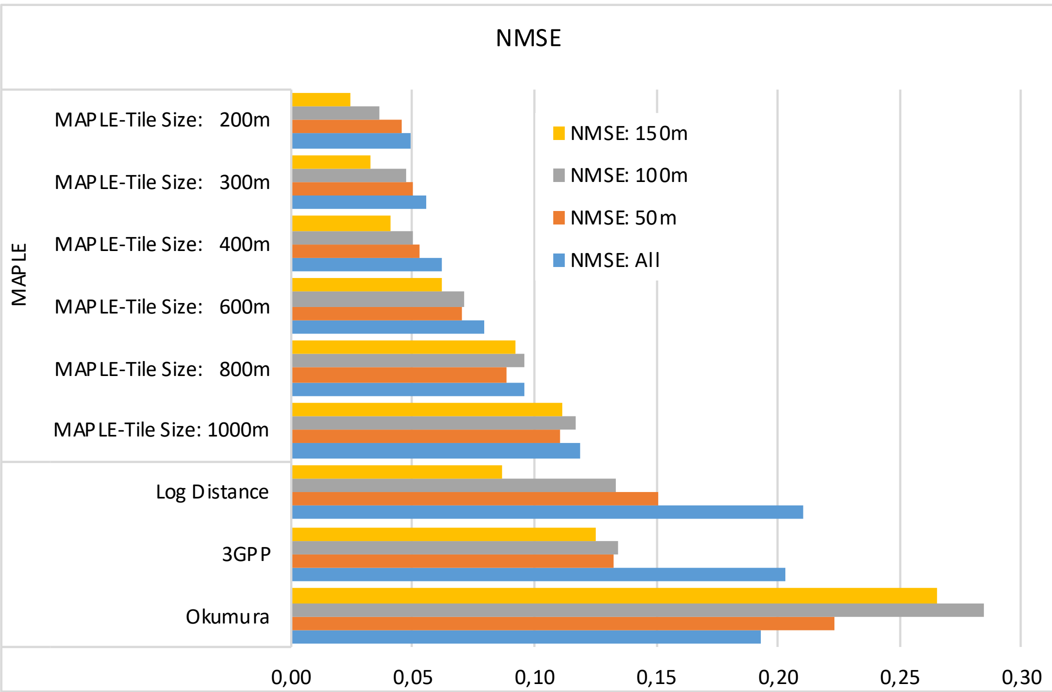

Figure B.2. Average NMSE for measurements.

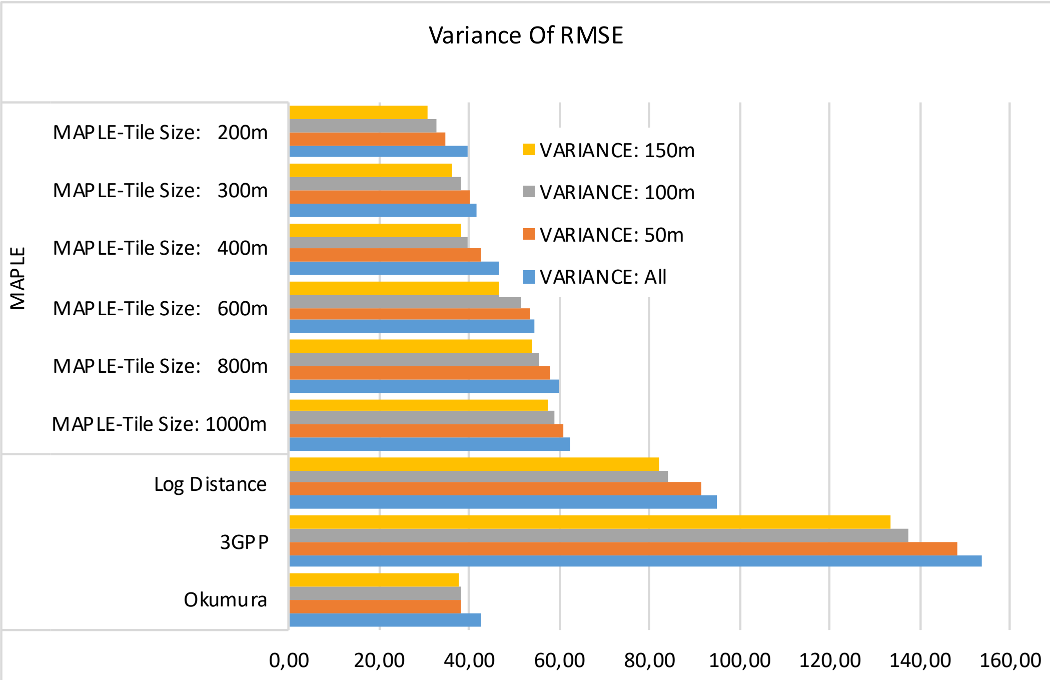

Figure B.3. Average variance of RMSE for measurements.

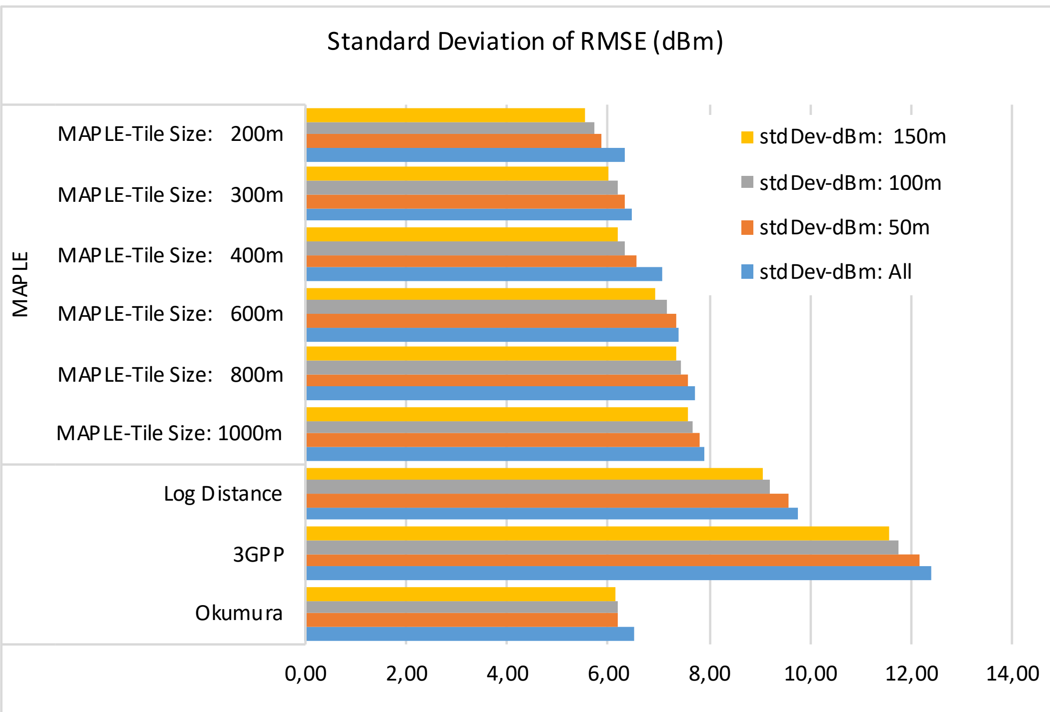

Figure B.4. Average standard deviation of RMSE for measurements.

APPENDIX C: FUTURE WORK: MACHINE LEARNING AND STATISTICAL DATA GENERATION

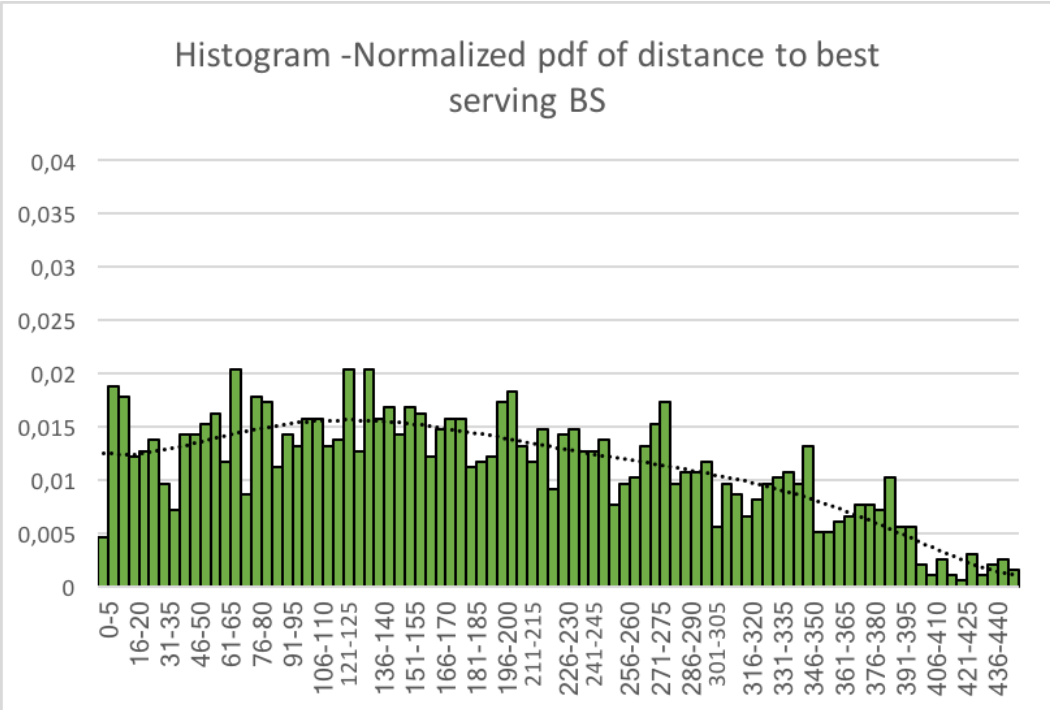

Figure C.1. Distribution of mobile users with respect to the best serving base stations.

We have analyzed our signal measurement set as shown in Figure C.1 and observed the similarity of the distribution of mobile user data to the previous study *Distance distributions for real cellular networks* [94]. Considering to the statistical concerns, the user population can be widened by adding quasi-random signal measurements based on actual user distribution statistics in the two cities and in similar European cities such as London, to generate simulations using the validated user distribution. However, we avoided the use of simulation data in this thesis especially to provide the validation of results on actual real world measurements. Although we observed better RMSE values in such setups, introducing simulated results has no benefit to the performance of MAPLE in the context of this thesis.

Alternatively many interpolated data can be added to the environment using Nakagami-m distributions as a control group. Generating the interpolated measure-

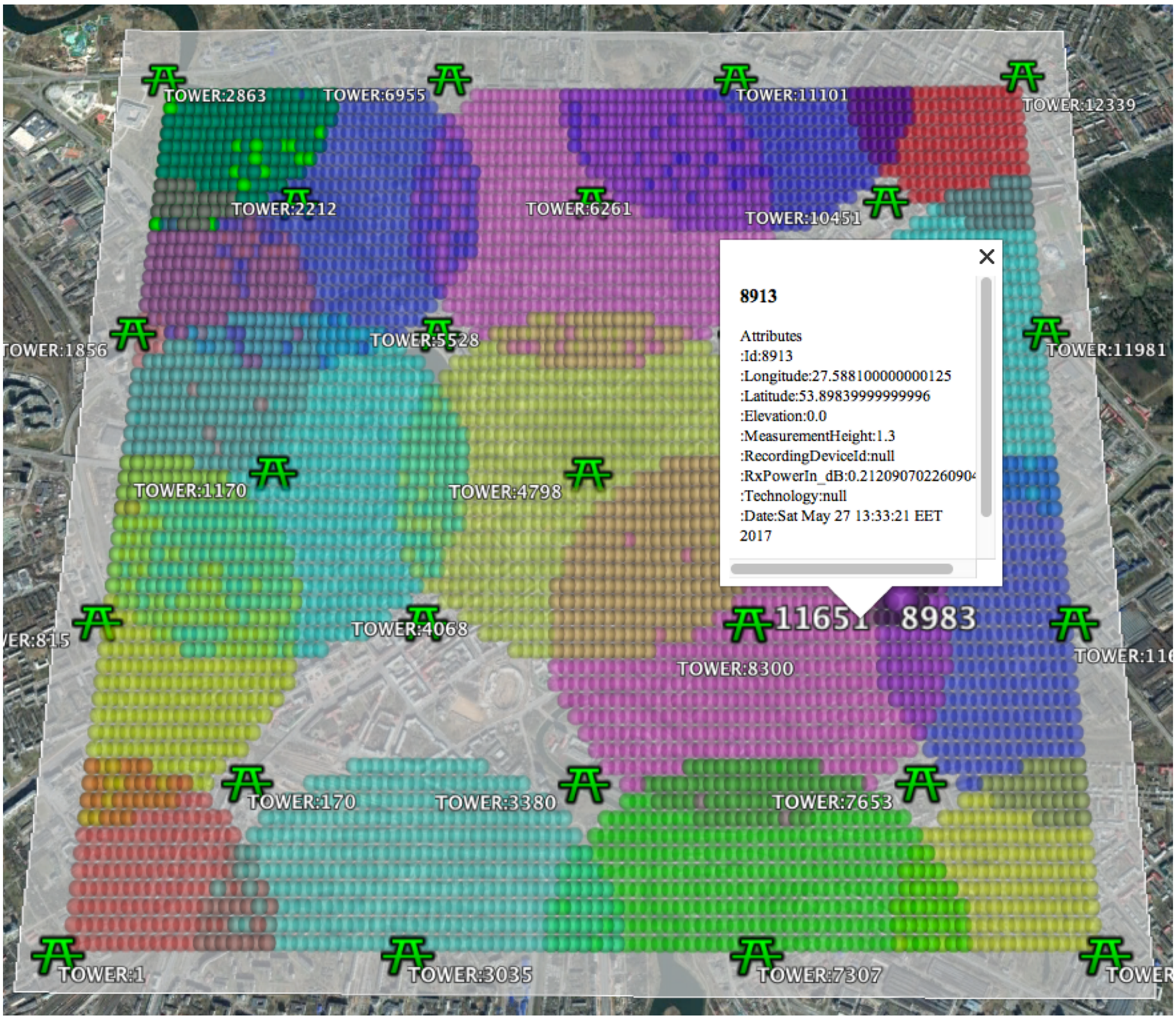

Figure C.2. Sample base stations and measurements, n=4.

ments with a different propagation model helps simulating the effects of 3D structures. If the auxiliary measurements are generated using the Log-Distance model in the first place, then comparing it with the MAPLE model will not be reasonable since Log-Distance model is always 100% accurate with itself. The difference between a measurement generated by Log-Distance model and another measurement generated by Nakagami-m distribution at the same location for the same base station is treated as the simulated effect of 3D structures on the LoS path.

Test area similarly consists of approximately a $5 \times 5 = 25km^2$ city central with 50 meters distance between two successive measurements. In order to cover the area with different number of cells, the base stations are distributed with equal spacing in a honeycomb grid formation as shown in Figure C.2. All the cells are assumed to be round and they are located on the area in such a way that four of the cells are centered at the corners of the area. If n base stations are placed on the north edge of the area, there are $n^2 + (n-1)^2$ base stations aligned on the grid including a total of $(n-1)^2$ additional base stations placed in the centers of every four neighboring cells, to cover the central portions of the four-cell groups. The number of measurements per base station depends on cell size, which is inversely proportional to the base station count. The coverage overlaps are essential for tile propagation parameter calculations.